NASA Technical Memorandum 83271

Effect of Nacelles on Aerodynamic Characteristics of an Executive-Jet Model With Simulated, Partial-Chord, Laminar-Flow-Control Wing Glove

Richard L. Campbell

APRIL 1982

NASA

NASA Technical Memorandum 83271

Effect of Nacelles on Aerodynamic Characteristics of an Executive-Jet Model With Simulated, Partial-Chord, Laminar-Flow-Control Wing Glove

Richard L. Campbell
Langley Research Center
Hampton, Virginia

National Aeronautics
and Space Administration

**Scientific and Technical
Information Branch**

1982

SUMMARY

Tests were conducted in the Langley High-Speed 7- by 10-Foot Tunnel using a 1/10-scale model of an executive jet to examine the effects of nacelles on wing pressures and model longitudinal aerodynamic characteristics. For the present investigation, each wing panel was modified with a simulated, partial-chord, laminar-flow-control glove. Horizontal-tail effects were also briefly examined. The tests covered a range of Mach numbers M from 0.40 to 0.82 and lift coefficients from 0.20 to 0.55. Oil-flow photographs of the wing at selected conditions are included.

The test results indicate that for a constant angle of attack, the addition of the nacelles caused a reduction in lift coefficient. This reduction varied from about 0.07 to about 0.17, depending on Mach number and angle of attack. The loss in lift resulted from a reduction in the induced velocities over the wing; consequently, for a constant angle of attack, the pressure coefficients were generally more positive over the forward portion of the glove when the nacelles were present, and wing shocks were moved forward and weakened. At a constant lift coefficient, the pressure coefficients over the forward portion of the glove were more negative with the nacelles on the model. These results indicate that the effect of the nacelles should be considered in any future modifications to the glove design.

At a lift coefficient of approximately 0.40, the nacelles caused a significant increase in the compressibility drag of the model. This increment in drag coefficient reached a maximum of about 0.0025 between $M = 0.75$ and 0.80.

The horizontal tail had a negligible effect on the pressure distributions.

INTRODUCTION

The rapidly rising cost of fuel, as well as its limited supply, has brought about an increased interest in making aircraft more fuel efficient. One concept that promises significant fuel savings for future aircraft is laminar flow control (LFC) as described in reference 1. The technique involves using suction to remove a portion of the boundary layer over various aircraft surfaces (in particular, the wings) in order to keep the boundary layer over that surface from transitioning to turbulent flow. Therefore, LFC would reduce the skin-friction coefficient for a particular surface and as a result the airplane would have less total cruise drag.

This concept has been flight-tested with some success (refs. 2 and 3), but the cost of developing and operating an effective LFC system for a commmercial transport has outweighed the benefit of reduced fuel consumption. However, the dramatic increase in fuel prices in 1973 made LFC economically attractive, so NASA and industry began to study some of the operational problems associated with maintaining LFC. The problems included keeping the wing leading edge free from ice and insect remains (which would cause premature transition of the boundary layer), finding a wing surface material that would provide for suction and be relatively easy to manufacture, and designing a suction system with as little weight and cost penalty as possible.

In order to evaluate some of the proposed solutions to these problems, NASA has planned flight tests using an executive jet, modified with a partial-chord LFC glove on each wing panel. On this jet aircraft, the engines are mounted on the fuselage, with the forward parts of the engine nacelles overhanging the wing trailing edge near the root. A mutual aerodynamic interference results when the nacelles are relatively close to the wing; therefore, this effect should be taken into account when trying to design a suitable LFC wing glove. This aerodynamic interference is especially important in the transonic speed regime, where the tests are to be made, since it could have an influence on the formation and location of shock waves on the wing.

In an effort to provide some insight into the effect of nacelles on wing pressures in the vicinity of the glove, tests were conducted in the Langley High-Speed 7- by 10-Foot Tunnel. A 1/10-scale model of an executive jet, modified with wing gloves to simulate one of the preliminary designs for the LFC gloves for the flight tests, was used in this investigation. The partial-chord gloves on the model had no suction capability; therefore, only the wing contours were simulated.

SYMBOLS

The International System of Units (SI), with the U.S. Customary Units given in parentheses, is used for the physical quantities in this report (see ref. 4). The measurements and calculations were made in U.S. Customary Units. Symbols in parentheses are used in computer-generated figures.

b	(B)	wing span, 162.96 cm (64.16 in.)
c		local streamwise chord, cm (in.)
$\bar{c}$		wing mean aerodynamic chord, 32.99 cm (12.99 in.)
C_D		drag coefficient, Drag/qS
C_L		lift coefficient, Lift/qS
C_m	(C_M)	pitching-moment coefficient, Pitching moment/$q\bar{S}\bar{c}$
C_p		pressure coefficient, $(p - p_\infty)/q_\infty$
M		Mach number
p		static pressure, Pa (psi)
q		dynamic pressure, Pa (psi)
S		wing reference area, 5009.34 cm^2 (776.45 in^2)
x/c	(X/C)	airfoil abscissa divided by local wing chord
y	(Y)	spanwise distance, cm (in.)
z/c	(Z/C)	airfoil ordinate divided by local wing chord

α model angle of attack, referenced to fuselage center line, deg

η (2Y/B) wing semispan station

Subscript:

∞ free-stream conditions

MODEL DESCRIPTION

The tests were conducted using a 1/10-scale model of an executive jet. The model was sting-mounted in the tunnel using an internal, six-component, strain-gage balance to measure forces and moments. (See fig. 1.) Model dimensions are given on the drawing in figure 2 and are included with other model descriptive data in table I.

The model consisted of the modified wing, fuselage, vertical tail, horizontal tail, and fuselage-mounted, twin-engine, flow-through nacelles. The nacelles were mounted on each side of the fuselage, to the rear of and slightly higher than the wings. The horizontal tail was set to an incidence of -2° and remained fixed for all the tail-on runs. The basic wing had a span of 162.96 cm (64.16 in.), an aspect ratio of 5.30, and an NACA 63A112 airfoil section at the root which changed to a modified NACA 63A309 at the tip. The wing had a leading-edge sweep of 34° inboard of the glove, 30° in the glove region, and 35° outboard of the glove.

The model originally had an external fuel tank mounted on each wing panel between a wing semispan station η of 0.42 and 0.54. These tanks were removed to allow the partial-chord wing gloves to be added. The gloves extended from $\eta = 0.38$ to $\eta = 0.64$, with an inboard fairing to $\eta = 0.33$ and an outboard fairing reaching $\eta = 0.68$. The gloves extended from the leading edge back to about $x/c = 0.35$ on the upper surface and to about $x/c = 0.12$ on the lower surface, and were installed with a higher angle of incidence than the basic wing. This change in airfoil section is the reason for the pronounced vertical discontinuity in the leading-edge location between the glove and outboard wing regions. (See fig. 1.)

The left wing had 50 pressure orifices installed in 3 chordwise rows, which were located at $\eta = 0.447$, 0.515, and 0.579. The orifices located ahead of $x/c = 0.35$ were mounted flush with the surface by using tubes embedded within the wing. Because of constraints on model modification, a different technique was used for the orifice installation at or aft of $x/c = 0.35$. In this region, several 0.5-mm (0.020-in.) outside-diameter tubes were mounted side by side along the surface at each of the three semispan stations. A fairing was used to minimize the effect on pressure distributions of the change in airfoil shape which resulted from the addition of the tubes. Then, a 0.25-mm (0.010-in.) diameter orifice was drilled in each tube at the desired location. The pressure orifice installation method resulted in slight offsets of the orifice locations from the given semispan stations. A photograph of the pressure orifices on the wing is included as figure 3. Measured airfoil coordinates from the glove region of the wing are given in table II, with the surface-mounted tubes included in the coordinates for $\eta = 0.515$.

The model was loaned to NASA at no charge by the Lockheed-Georgia Company. Since wing modifications and wind-tunnel testing did not involve Lockheed personnel, this company was not responsible for the acquisition or analysis of the data presented in this report.

APPARATUS, TESTS, AND CORRECTIONS

The tests were conducted in the Langley High-Speed 7- by 10-Foot Tunnel using the solid-wall test-section configuration. This is a continuous-flow, atmospheric wind tunnel capable of testing at speeds in the lower transonic regime. A description of the tunnel and its data system is given in reference 5.

The model was mounted on a sting in the tunnel using an internal, six-component, strain-gage balance. Force, moment, and pressure data were taken for every condition, with surface oil-flow photographs also being obtained for selected cases. Tests were made over a range of Mach numbers from 0.40 to 0.82, with Reynolds number varying from 2.9×10^6 to 4.8×10^6, based on the mean aerodynamic chord of 32.99 cm (12.99 in.).

The complete model configuration runs were made by adjusting the model angle of attack until values for the lift coefficient C_L of 0.20, 0.25, 0.30, 0.35, and 0.40 were obtained. The angles set for these values at each Mach number were then matched in the corresponding runs for the horizontal-tail-off and the nacelles-off configurations. The angle-of-attack schedule was utilized so that experimental pressures could be correlated with analytical results already obtained; this resulted in angles of attack from 2.92° to 5.58° and values of C_L from 0.20 to 0.55. The nacelles-off and nacelles-on cases were run with the horizontal tail off to match more closely the present transonic computer code modeling capability. The horizontal-tail-off and horizontal-tail-on cases were run with the nacelles on.

Transition strips were sized and located on the model using the criteria of reference 6. The strips were 0.16-cm (0.06-in.) wide bands of No. 120 carborundum grains located 1.68 cm (0.66 in.) behind the leading edges (on both upper and lower surfaces) of the wing and of the horizontal and vertical tails. Similar transition strips were applied to the fuselage and external surfaces of the nacelles.

Jet-boundary corrections were determined by using the methods of reference 7. These corrections were applied to the force data as follows:

$$\alpha_{corrected} = \alpha + 0.5566C_L$$

$$C_{D,corrected} = C_D + 0.0097C_L^2$$

The pitching-moment data were not corrected for jet-boundary effects. The drag was corrected for base drag by adjusting the model chamber pressure to free-stream static pressure. Blockage corrections were calculated by using the computer program described in reference 8, which was modified to take into account compressibility effects based on references 9 and 10. The method makes use of measured tunnel-wall pressures to determine the blockage corrections and should increase the accuracy for larger models. The largest Mach number increment calculated was 0.015.

PRESENTATION OF RESULTS

The wing pressures and longitudinal force and moment data obtained during this investigation have been converted to coefficient form and are presented, along with some wing oil-flow photographs, in the following figures:

DISCUSSION OF RESULTS

Wing Pressure Distributions

For a given Mach number and angle of attack, the local induced velocities over the front half of the wing were reduced by the addition of the nacelles which resulted in a significant loss of lift. This loss of lift can be observed in the pressure distributions by the more positive pressure coefficients over the front half of the wing. The effect was most noticeable over the glove region (leading edge to $x/c = 0.35$) for Mach numbers up to 0.80. As shown in figures 5 through 7, the shock that formed in this area of the wing moved forward and weakened for the nacelles-on configuration.

At the glove design Mach number of 0.80, pressures over the first half of the glove region were similar for both nacelles-off and nacelles-on configurations. (See fig. 8.) The major difference in pressure distributions occurred between $x/c = 0.25$ and 0.50. The difference was especially noticeable for $\eta = 0.515$, where the nacelles-off cases had a region of more negative pressure coefficient beginning at $x/c = 0.30$ and terminating with a shock between $x/c = 0.40$ and 0.50. The nacelles-on cases do not begin to show this peak until an angle of attack of over 4° is reached. (See fig. 8(e).) Pressure distributions at $M = 0.82$ had a similar peak, which was probably caused by several factors. First, the glove design pressure distribution had a slight peak just aft of $x/c = 0.30$. Second, the fairing of the glove to the original wing occurs here and may result in slight discontinuities in surface slope and curvature. Finally, the pressure orifice installation method required aft of $x/c = 0.30$ (surface-mounted tubes) would tend to make these pressure coefficients more negative.

For Mach numbers less than 0.80, pressures over the rear third of the wing showed little change with the addition of the nacelles to the model. At $M = 0.80$, however, the nacelles-off cases began to have more negative pressure coefficients over the rear third of the wing for the inboard and middle rows of orifices. (See figs. 8(c) to 8(e).) This indicates that the flow may be starting to separate over the rear part of the wing as a result of the boundary layer interacting with the shock located at about midchord. The separated region extends to the outboard row of orifices for the $M = 0.82$ cases.

The wing oil-flow photographs shown in figures 35 and 36 illustrate further the separation that occurs for the nacelles-off cases at $M = 0.80$. At an angle of attack of 2.9°, a shock is apparent just aft of midchord and extending out to the middle row of orifices; a region of separated flow behind the shock is also observed. However, the nacelles-on case for the same angle of attack (2.9°) shows no evidence of a shock or separated flow. At an angle of attack of 3.8°, the shock has moved forward and extends farther outboard for the nacelles-off case, and there is considerable reverse flow behind the shock. This correlates well with the trends seen by comparing figures 8(a) and 8(d). A shock is evident for the nacelles-on case at this angle of attack (3.8°), but it is farther forward and weaker than the one in the nacelles-off case, and it does not cause the boundary layer to separate. It should be emphasized again that these comparisons are made at a constant angle of attack; as a result, there is a significant difference (>0.15) in the lift coefficients for nacelles-off and nacelles-on cases.

It should be noted that the shock position in the oil-flow photographs is farther aft than in the pressure plots. This may be because the oil-flow pictures were taken after the transition strips were removed from the glove (the strips were removed for some tests involving transition location, the results of which are not included in this report). From the photographs, it appears that transition (laminar separation with turbulent attachment) occurs at about $x/c = 0.10$ to 0.20, whereas the pressure data were taken with transition fixed at about $x/c = 0.05$. This would result in a thinner boundary layer and consequently a more aft shock location for the oil-flow pictures.

As noted previously, the comparisons of data shown thus far have been made for the nacelles-off and nacelles-on configurations at the same angle of attack. Pressure distributions for the two configurations at about the same lift coefficient, $C_L \approx 0.4$, are shown in figures 10 through 15. At $M = 0.40$ and 0.60, there was little difference in the pressures for the two configurations. For $M = 0.70$ and 0.75, the nacelles-on cases had more negative pressure coefficients over the first 15 to 25 percent of the chord and less negative pressure coefficients from there to $x/c = 0.60$. At $M = 0.80$ and 0.82, the region of more negative pressure coefficients for the nacelles-on case covered the entire glove (leading edge to $x/c = 0.35$) with less negative values from there to $x/c = 0.60$. Pressures over the last third of the chord were the same at a given Mach number except for $M = 0.82$, at which separation is probably present for the nacelles-off cases.

As mentioned previously, the partial-chord glove shape used in this investigation was a preliminary design for the gloves for the LFC flight tests. Since pressures over the glove were significantly affected by the presence of the nacelles, it is clear that any future modifications to this design should take into account the effect of the nacelles on the flow over the wing.

The effect of the horizontal tail on the pressure distributions was negligible, as seen in figures 16 through 21.

Longitudinal Aerodynamic Characteristics

The effect of nacelles on the longitudinal aerodynamic characteristics of the model is presented in figures 22 through 27. For the range of conditions tested, adding the nacelles to the model always resulted in a loss in lift at a given angle of attack. The reduction, in terms of lift coefficient, varied from about 0.07 to about 0.17, depending on Mach number and angle of attack. The reason for the loss in lift is that the flow over the wing is slowed down as it approaches the nacelles, which results in more positive upper-surface pressures and lower section lift coefficients for the inboard and middle sections of the wing. The nonlinearity of the lift curve for the nacelles-off cases at $M = 0.80$ and 0.82 was not present for the nacelles-on cases, probably because the test range for the latter configuration did not reach lift coefficients at which extensive shock-induced separation was present.

For a given Mach number, the model drag coefficient at a given lift coefficient increased when the nacelles were added to the model. Analysis of the drag polars indicated that this increment in drag coefficient did not result from a change in induced drag but was most likely caused by the drag of the nacelles themselves.

Figure 28 shows the increase in drag coefficient (over the value at $M = 0.40$ for each configuration) with increasing Mach number for a lift coefficient of approximately 0.4. This value of lift coefficient is higher than the design lift coefficient of 0.3, but it was chosen so that no extrapolation of the data would be required and so that the values of drag coefficient would correspond roughly to the pressure comparisons in figures 10 through 15. The figure shows that the nacelles cause a significant increase in compressibility drag; this increment in drag coefficient reaches a maximum of about 0.0025 between $M = 0.75$ and 0.80. The increase in compressibility drag could result from shocks forming on the nacelles themselves or from an unfavorable interference of the nacelles with the supercritical flow over the wing and/or fuselage. Also, shocks on the outer portion of the wing are probably stronger for the nacelles-on cases since a higher angle of attack was required to achieve the same lift coefficient.

The addition of the nacelles made the model slightly more stable in pitch. At the higher Mach numbers, the nacelles-on cases had a more positive pitching-moment coefficient at a given lift coefficient. In order for the lift coefficient of the nacelles-on cases to match the lift coefficient of the nacelles-off cases, a higher angle of attack was required which may have resulted in wing stall in the tip region; therefore, the model would have a higher pitching moment.

As seen in figures 29 through 34, the addition of the horizontal tail resulted in a loss in lift, an increase in drag, and an increase in model pitch stability. These results were expected for the $-2°$ tail incidence at which the tests were run.

SUMMARY OF RESULTS

Tests were conducted in the Langley High-Speed 7- by 10-Foot Tunnel using a 1/10-scale model of an executive jet to examine the effects of nacelles on wing pressures and model longitudinal aerodynamic characteristics. For the present investigation, each wing panel was modified with a simulated, partial-chord, laminar-flow-control glove. Horizontal-tail effects were also briefly examined. The tests covered a range of Mach numbers M from 0.40 to 0.82 and lift coefficients from 0.20 to 0.55. The following results were obtained from these tests:

1. For a constant angle of attack, the addition of the nacelles resulted in a reduction in lift coefficient; this reduction varied from about 0.07 to about 0.17, depending on Mach number and angle of attack.

2. The loss in lift associated with the presence of the nacelles was the result of a reduction in the induced velocities over the wing. Consequently, for a constant angle of attack, the upper-surface pressure coefficients were generally more positive over the forward portion of the glove when the nacelles were present, and wing shocks were moved forward and weakened. For a constant lift coefficient, the pressure coefficients over the forward portion of the glove were more negative for the nacelles-on cases. These results indicate that the effect of the nacelles should be considered in any future modifications to the glove design.

3. At a lift coefficient of approximately 0.40, the nacelles caused a significant increase in the compressibility drag of the model; this increment in drag coefficient reached a maximum of about 0.0025 between $M = 0.75$ and 0.80.

4. The horizontal tail had a negligible effect on the wing pressure distributions.

Langley Research Center
National Aeronautics and Space Administration
Hampton, VA 23665
March 17, 1982

REFERENCES

1. Aircraft Fuel Conservation Technology - Task Force Report. OAST, NASA, Sept. 10, 1975. (Available as NASA TM X-74295.)

2. Pfenninger, W.; and Groth, E.: Low Drag Boundary Layer Suction Experiments in Flight on a Wing Glove of an F-94A Airplane With Suction Through a Large Number of Fine Slots. Boundary Layer and Flow Control, Volume 2, G. V. Lachmann, ed., Pergamon Press, 1961, pp. 981-999.

3. Whites, R. C.; Sudderth, R. W.; and Wheldon, W. G.: Laminar Flow Control on the X-21. Astronaut. & Aeronaut., vol. 4, no. 7, July 1966, pp. 38-43.

4. Standard for Metric Practice. E 380-79, American Soc. Testing & Mater., c.1980.

5. Fox, Charles H., Jr.; and Huffman, Jarrett K.: Calibration and Test Capabilities of the Langley 7- by 10-Foot High Speed Tunnel. NASA TM X-74027, 1977.

6. Braslow, Albert L.; and Knox, Eugene C.: Simplified Method for Determination of Critical Height of Distributed Roughness Particles for Boundary-Layer Transition at Mach Numbers From 0 to 5. NACA TN 4363, 1958.

7. Gillis, Clarence L.; Polhamus, Edward C.; and Gray, Joseph L., Jr.: Charts for Determining Jet-Boundary Corrections for Complete Models in 7- by 10-Foot Closed Rectangular Wind Tunnels. NACA WR L-123, 1945. (Formerly NACA ARR L5G31.)

8. Hackett, J. E.; Wilsden, D. J.; and Lilley, D. E.: Estimation of Tunnel Blockage From Wall Pressure Signatures: A Review and Data Correlation. NASA CR-152241, 1979.

9. Shapiro, Ascher H.: The Dynamics and Thermodynamics of Compressible Fluid Flow. Volume I. Ronald Press Co., c.1953.

10. Herriot, John G.: Blockage Corrections for Three-Dimensional-Flow Closed-Throat Wind Tunnels, With Consideration of the Effect of Compressibility. NACA Rep. 995, 1950. (Supersedes NACA RM A7B28.)

TABLE I.- GEOMETRIC CHARACTERISTICS OF MODEL

Body:	
Length, cm (in.)	169.57 (66.76)
Maximum diameter cm (in.)	21.59 (8.50)
Wing:	
Span, cm (in.)	162.96 (64.16)
Area, cm^2 (in^2)	5009.34 (776.45)
Mean aerodynamic chord $\bar{c}$, cm (in.)	32.99 (12.99)
Spanwise location of $\bar{c}$, cm (in.)	33.66 (13.25)
Moment reference center (0.25$\bar{c}$), cm (in.)	97.51 (38.39) aft of nose
Aspect ratio	5.30
Taper ratio	0.33
Dihedral, deg	2.89
Airfoil at root	NACA 63A112
Root airfoil leading edge, cm (in.)	67.34 (26.51) aft of nose
Incidence at root, deg	1.09
Airfoil at tip	NACA 63A309 (modified)
Twist, deg	-2.16
Leading-edge sweep, deg	
Inboard of glove	34
Glove	30
Outboard of glove	35
Horizontal tail:	
Span, cm (in.)	74.68 (29.40)
Area, cm^2 (in^2)	1384.63 (214.62)
Mean aerodynamic chord, cm (in.)	20.13 (7.93)
Streamwise location of 0.25 of mean aerodynamic chord, cm (in.)	164.58 (64.80) aft of nose
Spanwise location of mean aerodynamic chord, cm (in.)	15.52 (6.11)
Aspect ratio	4.03
Taper ratio	0.33
Incidence, deg	-2.00
Vertical tail:	
Span, cm (in.)	37.85 (14.90)
Area, cm^2 (in^2)	1023.80 (158.69)
Mean aerodynamic chord, cm (in.)	28.92 (11.39)
Streamwise location of 0.25 of mean aerodynamic chord, cm (in.)	157.98 (62.20) aft of nose
Aspect ratio	1.40
Taper ratio	0.37
Nacelles:	
Length, cm (in.)	31.50 (12.40)
Internal diameter, cm (in.)	4.01 (1.58)
Incidence, deg	-1.22
Spanwise location of nacelle center line, cm (in.)	
Inboard nacelle	17.02 (6.70)
Outboard nacelle	24.13 (9.50)

TABLE II.- MEASURED AIRFOIL COORDINATES

(a) $\eta = 0.381$; c = 33.7108 cm (13.2720 in.)

Upper surface				Lower surface			
x/c	z/c	x/c	z/c	x/c	z/c	x/c	z/c
0.0000	0.0000	.1658	.0540	0.0000	0.0000	.1733	-.0458
.0007	.0055	.1733	.0547	.0015	-.0077	.1809	-.0463
.0015	.0076	.1808	.0555	.0023	-.0095	.1884	-.0467
.0023	.0094	.1884	.0562	.0031	-.0110	.1959	-.0472
.0031	.0104	.1959	.0568	.0038	-.0120	.2035	-.0476
.0037	.0113	.2034	.0574	.0045	-.0129	.2110	-.0480
.0045	.0127	.2110	.0580	.0053	-.0138	.2186	-.0485
.0052	.0132	.2185	.0586	.0061	-.0146	.2260	-.0488
.0061	.0143	.2261	.0592	.0068	-.0152	.2336	-.0492
.0068	.0152	.2336	.0597	.0076	-.0159	.2411	-.0494
.0075	.0159	.2411	.0602	.0083	-.0165	.2637	-.0502
.0083	.0166	.2487	.0607	.0091	-.0171	.3014	-.0514
.0091	.0172	.2562	.0612	.0099	-.0176	.3391	-.0520
.0097	.0177	.2637	.0617	.0106	-.0181	.3768	-.0520
.0106	.0185	.2713	.0622	.0114	-.0186	.4144	-.0511
.0113	.0191	.2788	.0627	.0121	-.0190	.4521	-.0493
.0121	.0196	.2863	.0631	.0129	-.0195	.4898	-.0470
.0128	.0202	.2939	.0636	.0136	-.0199	.5275	-.0441
.0136	.0207	.3014	.0639	.0144	-.0203	.5652	-.0407
.0143	.0212	.3391	.0650	.0151	-.0207	.6029	-.0366
.0150	.0217	.3767	.0653	.0226	-.0239	.6405	-.0320
.0227	.0260	.4145	.0650	.0302	-.0264	.6782	-.0271
.0302	.0292	.4521	.0641	.0377	-.0284	.7158	-.0219
.0378	.0318	.4898	.0626	.0453	-.0302	.7535	-.0164
.0454	.0341	.5275	.0607	.0528	-.0316	.7912	-.0106
.0529	.0361	.5651	.0583	.0603	-.0330	.8289	-.0048
.0603	.0378	.6029	.0556	.0679	-.0343	.8665	.0014
.0679	.0394	.6405	.0525	.0754	-.0355	.9042	.0074
.0754	.0409	.6782	.0491	.0829	-.0365	.9419	.0135
.0829	.0424	.7159	.0456	.0904	-.0376	.9796	.0197
.0904	.0437	.7535	.0424	.0980	-.0386	1.0000	.0240
.0980	.0450	.7912	.0398	.1055	-.0395		
.1055	.0462	.8288	.0373	.1131	-.0404		
.1131	.0474	.8665	.0348	.1206	-.0412		
.1206	.0485	.9042	.0321	.1281	-.0420		
.1281	.0496	.9419	.0297	.1357	-.0428		
.1357	.0506	.9795	.0273	.1432	-.0434		
.1432	.0515	1.0000	.0259	.1507	-.0440		
.1507	.0524			.1582	-.0446		
.1582	.0532			.1658	-.0452		

TABLE II.- Continued

(b) $\eta = 0.515$; $c = 30.5112$ cm (12.0123 in.)

Upper surface				Lower surface			
x/c	z/c	x/c	z/c	x/c	z/c	x/c	z/c
0.0000	0.0000	.1832	.0509	0.0000	0.0000	.2498	-.0478
.0009	.0055	.1915	.0517	.0009	-.0055	.2914	-.0488
.0017	.0073	.1998	.0526	.0017	-.0077	.3330	-.0518
.0025	.0086	.2081	.0533	.0025	-.0093	.3748	-.0517
.0034	.0100	.2165	.0541	.0033	-.0106	.4163	-.0515
.0042	.0109	.2248	.0548	.0042	-.0117	.4579	-.0502
.0050	.0118	.2331	.0555	.0050	-.0126	.4996	-.0483
.0058	.0127	.2414	.0562	.0058	-.0136	.5412	-.0449
.0067	.0135	.2498	.0569	.0067	-.0144	.5828	-.0413
.0075	.0142	.2581	.0576	.0075	-.0151	.6244	-.0366
.0084	.0149	.2665	.0582	.0084	-.0157	.6661	-.0317
.0092	.0155	.2748	.0589	.0092	-.0166	.7077	-.0260
.0100	.0161	.2832	.0595	.0100	-.0172	.7493	-.0207
.0108	.0166	.2915	.0601	.0109	-.0176	.7909	-.0152
.0117	.0171	.2997	.0607	.0117	-.0182	.8326	-.0094
.0125	.0176	.3080	.0612	.0125	-.0187	.8742	-.0016
.0134	.0181	.3164	.0617	.0134	-.0192	.9158	.0054
.0142	.0186	.3239	.0618	.0142	-.0197	.9574	.0120
.0150	.0190	.3331	.0618	.0150	-.0201	1.0000	.0182
.0159	.0195	.3748	.0625	.0159	-.0205		
.0167	.0200	.4162	.0623	.0167	-.0209		
.0250	.0235	.4579	.0616	.0250	-.0241		
.0333	.0262	.4995	.0603	.0333	-.0265		
.0417	.0285	.5411	.0581	.0417	-.0289		
.0500	.0308	.5828	.0553	.0499	-.0307		
.0583	.0323	.6244	.0520	.0583	-.0322		
.0667	.0340	.6660	.0486	.0666	-.0337		
.0749	.0356	.7077	.0452	.0750	-.0350		
.0833	.0372	.7493	.0417	.0833	-.0361		
.0916	.0386	.7909	.0388	.0916	-.0372		
.0999	.0400	.8325	.0361	.0999	-.0382		
.1083	.0413	.8741	.0330	.1083	-.0390		
.1166	.0425	.9156	.0292	.1166	-.0400		
.1249	.0437	.9574	.0250	.1249	-.0409		
.1332	.0449	1.0000	.0201	.1333	-.0417		
.1416	.0459			.1415	-.0426		
.1499	.0470			.1499	-.0433		
.1582	.0481			.1582	-.0437		
.1665	.0491			.1666	-.0442		
.1748	.0500			.2081	-.0461		

TABLE II.- Concluded

(c) $\eta = 0.640$; $c = 27.2945$ cm (10.7459 in.)

Upper surface				Lower surface			
x/c	z/c	x/c	z/c	x/c	z/c	x/c	z/c
0.0000	0.0000	.2048	.0500	0.0000	0.0000	.2327	-.0457
.0010	.0053	.2327	.0513	.0009	-.0054	.2792	-.0473
.0019	.0066	.2792	.0532	.0019	-.0070	.3258	-.0486
.0028	.0080	.3257	.0547	.0028	-.0086	.3723	-.0493
.0038	.0094	.3722	.0552	.0038	-.0099	.4188	-.0493
.0047	.0103	.4188	.0552	.0047	-.0108	.4654	-.0486
.0056	.0111	.4653	.0546	.0056	-.0118	.5119	-.0469
.0065	.0119	.5118	.0531	.0065	-.0127	.5584	-.0437
.0075	.0125	.5584	.0506	.0075	-.0135	.6049	-.0395
.0084	.0131	.6049	.0473	.0084	-.0143	.6515	-.0351
.0094	.0136	.6514	.0435	.0093	-.0150	.6980	-.0300
.0103	.0141	.6979	.0393	.0103	-.0156	.7446	-.0245
.0112	.0147	.7445	.0355	.0112	-.0162	.7911	-.0190
.0122	.0152	.7910	.0320	.0121	-.0168	.8376	-.0134
.0131	.0158	.8375	.0281	.0130	-.0173	.8842	-.0071
.0140	.0162	.8840	.0232	.0140	-.0178	.9307	-.0011
.0149	.0167	.9306	.0188	.0149	-.0183	.9772	.0049
.0159	.0172	.9771	.0136	.0158	-.0187	1.0000	.0088
.0168	.0177	1.0000	.0107	.0168	-.0192		
.0177	.0180			.0177	-.0197		
.0186	.0184			.0186	-.0200		
.0280	.0218			.0279	-.0235		
.0372	.0243			.0373	-.0261		
.0466	.0263			.0465	-.0282		
.0559	.0279			.0558	-.0301		
.0652	.0292			.0652	-.0317		
.0745	.0307			.0745	-.0330		
.0838	.0320			.0838	-.0343		
.0931	.0334			.0931	-.0354		
.1024	.0347			.1024	-.0365		
.1117	.0360			.1118	-.0375		
.1210	.0372			.1210	-.0384		
.1303	.0384			.1304	-.0392		
.1396	.0397			.1397	-.0400		
.1489	.0411			.1490	-.0408		
.1582	.0426			.1582	-.0416		
.1675	.0444			.1676	-.0422		
.1768	.0464			.1769	-.0429		
.1862	.0484			.1862	-.0434		
.1955	.0496			.1955	-.0440		

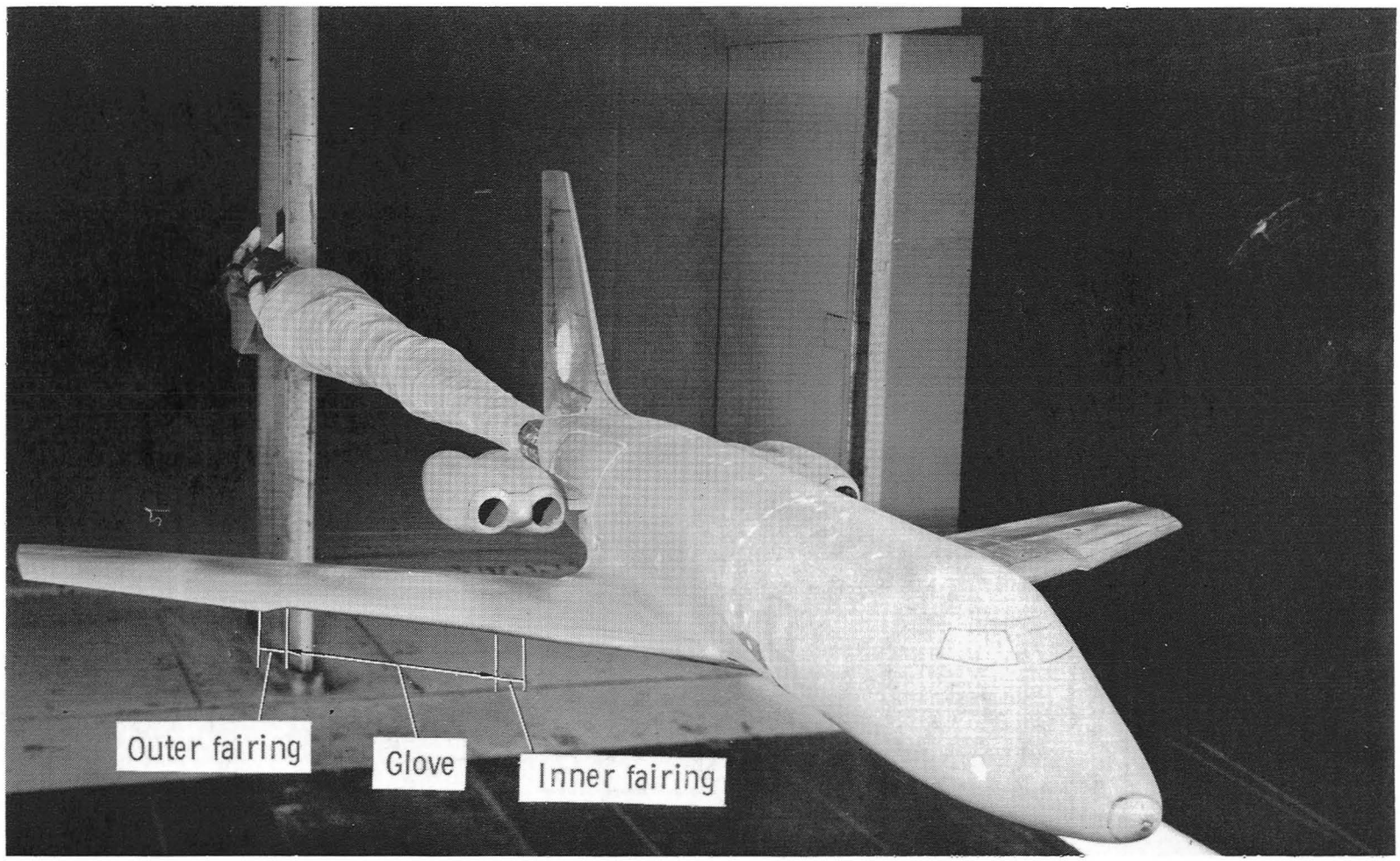

L-79-8763

Figure 1.- Executive-jet model installed in tunnel.

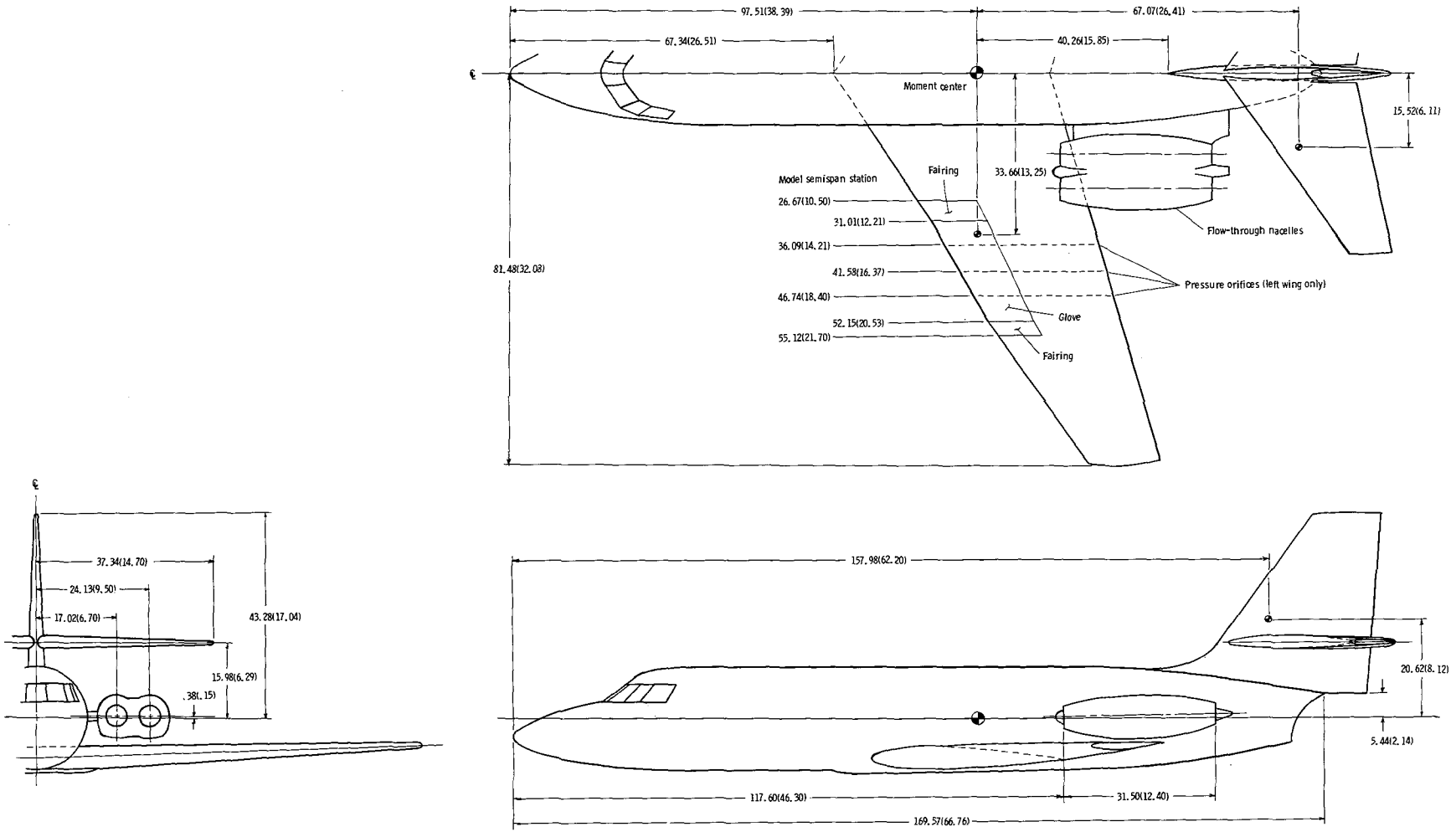

Figure 2.- Model geometry. Dimensions are in centimeters (inches).

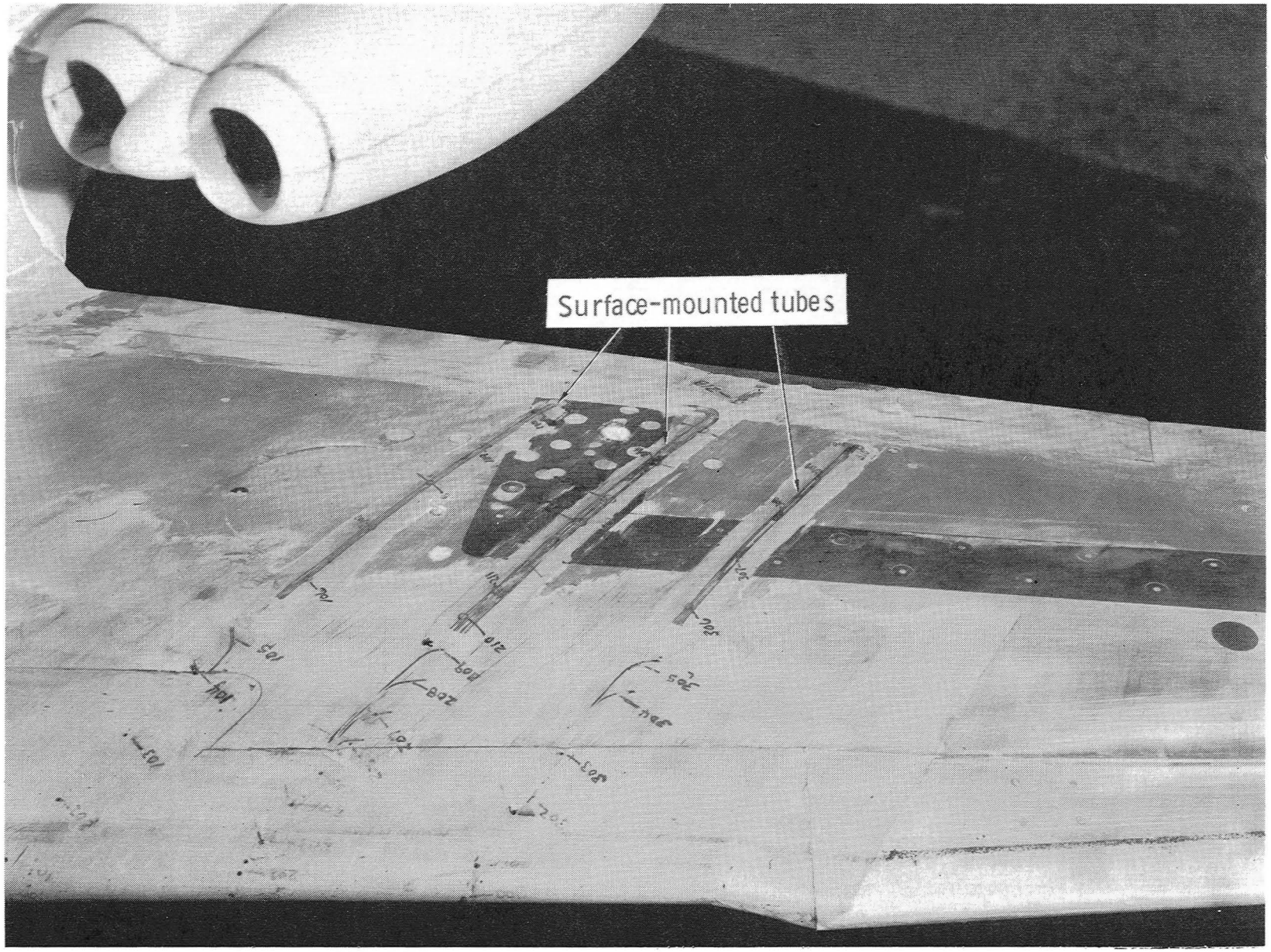

L-79-8764.1

Figure 3.- Wing pressure orifices.

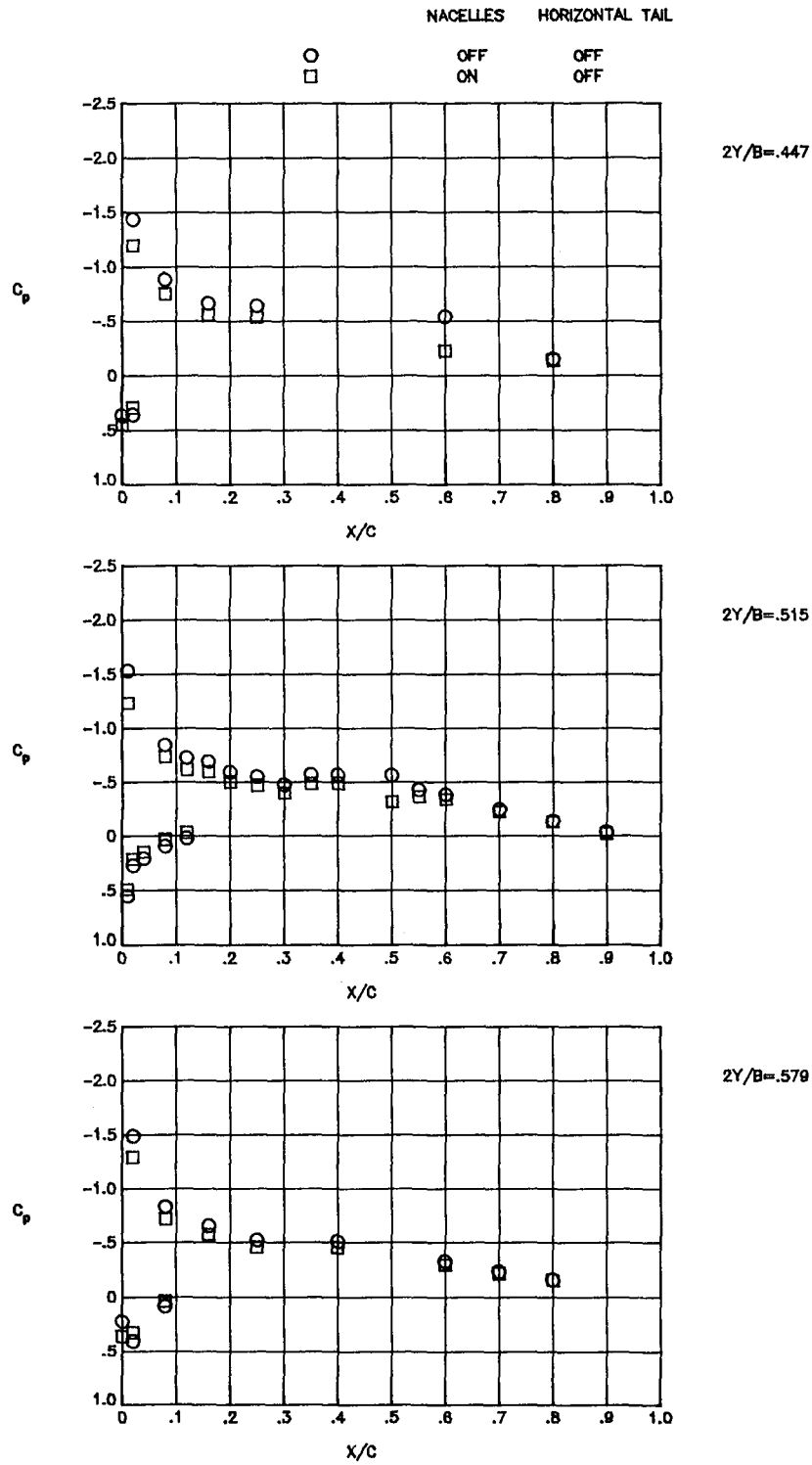

(a) α = 3.29.

Figure 4.- Effect of nacelles on wing pressure distributions at M = 0.40.

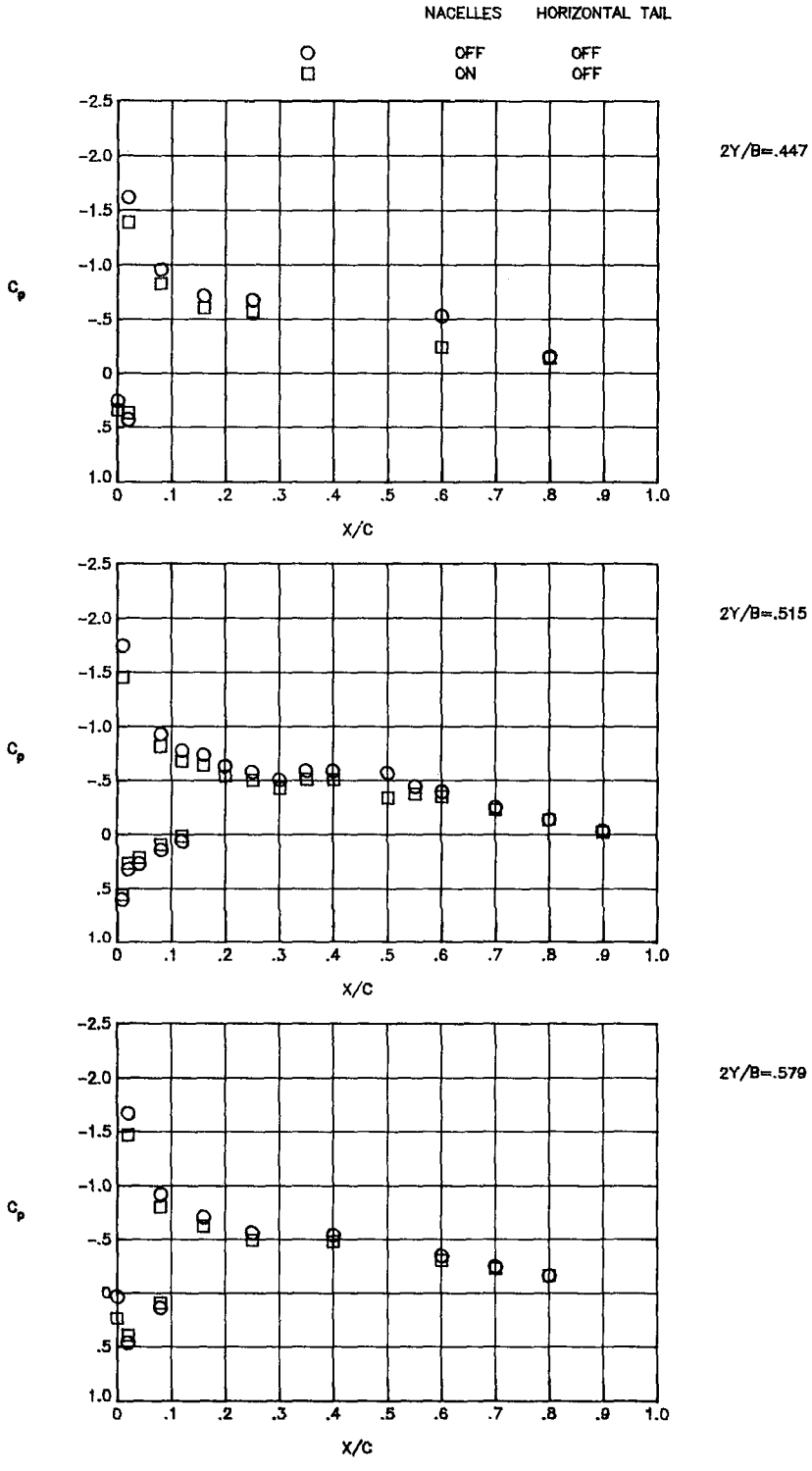

(b) α = 3.90.

Figure 4.- Continued.

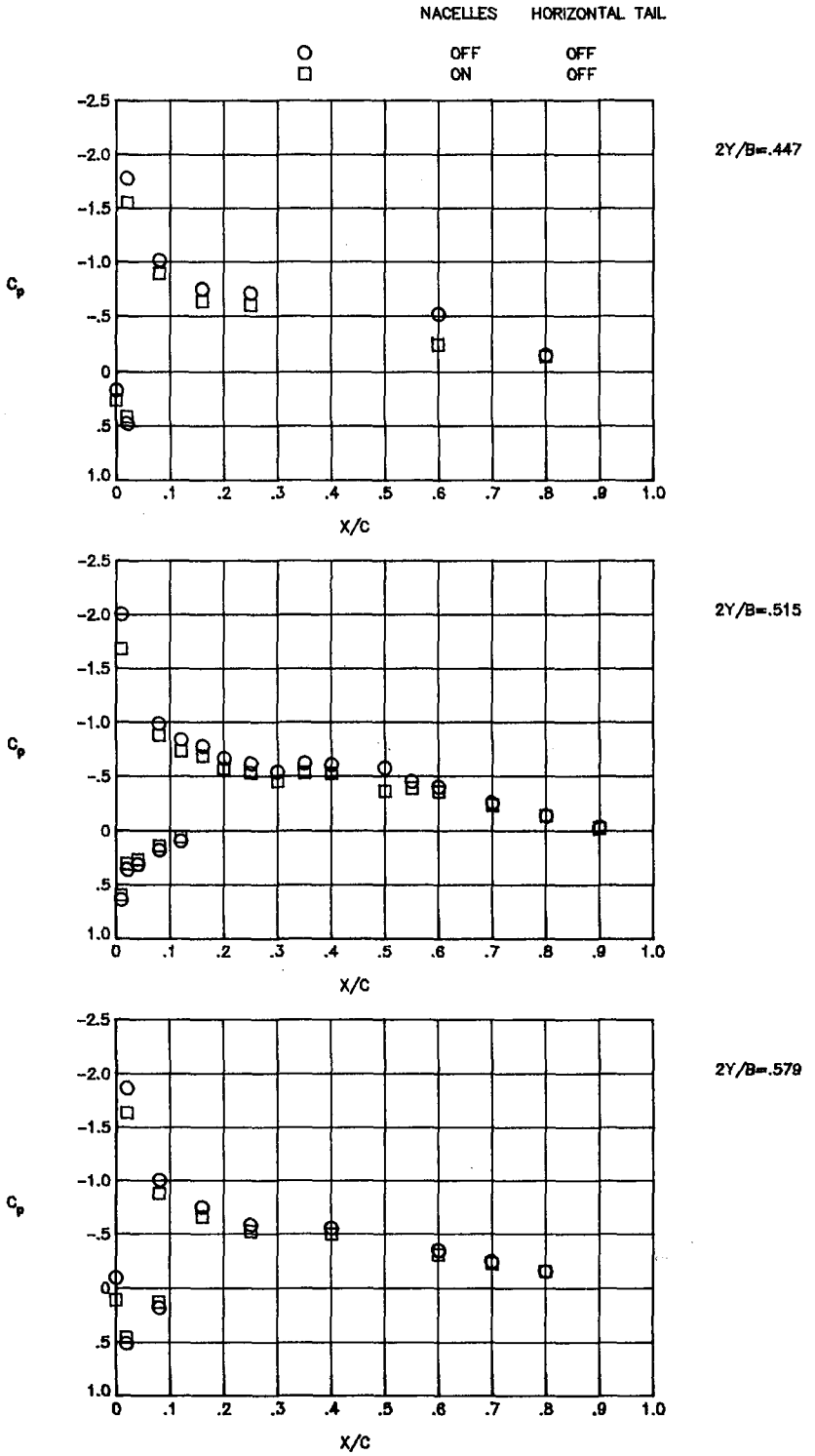

(c) α = 4.43.

Figure 4.- Continued.

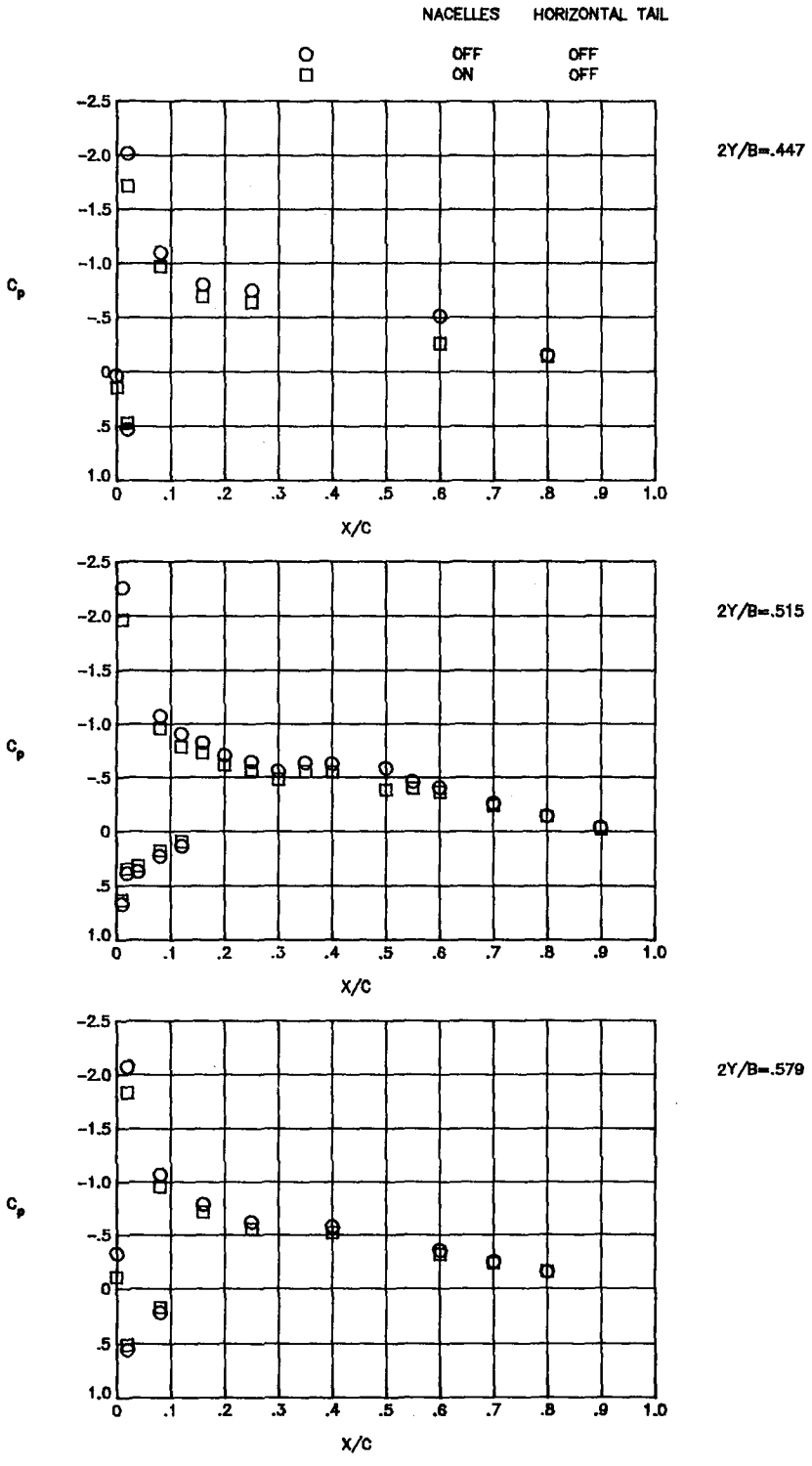

(d) $\alpha = 5.00$.

Figure 4.- Continued.

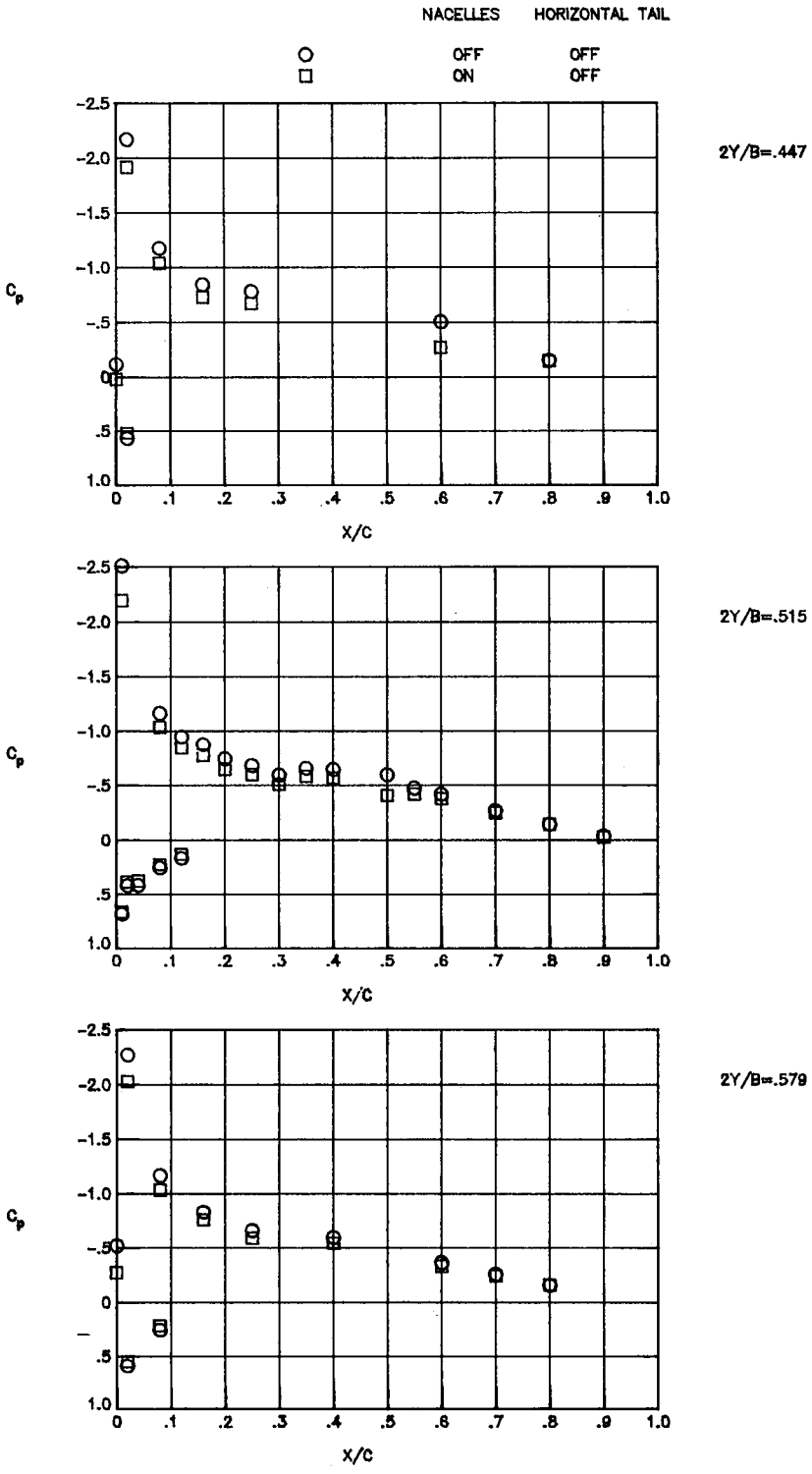

(e) α = 5.57.

Figure 4.- Concluded.

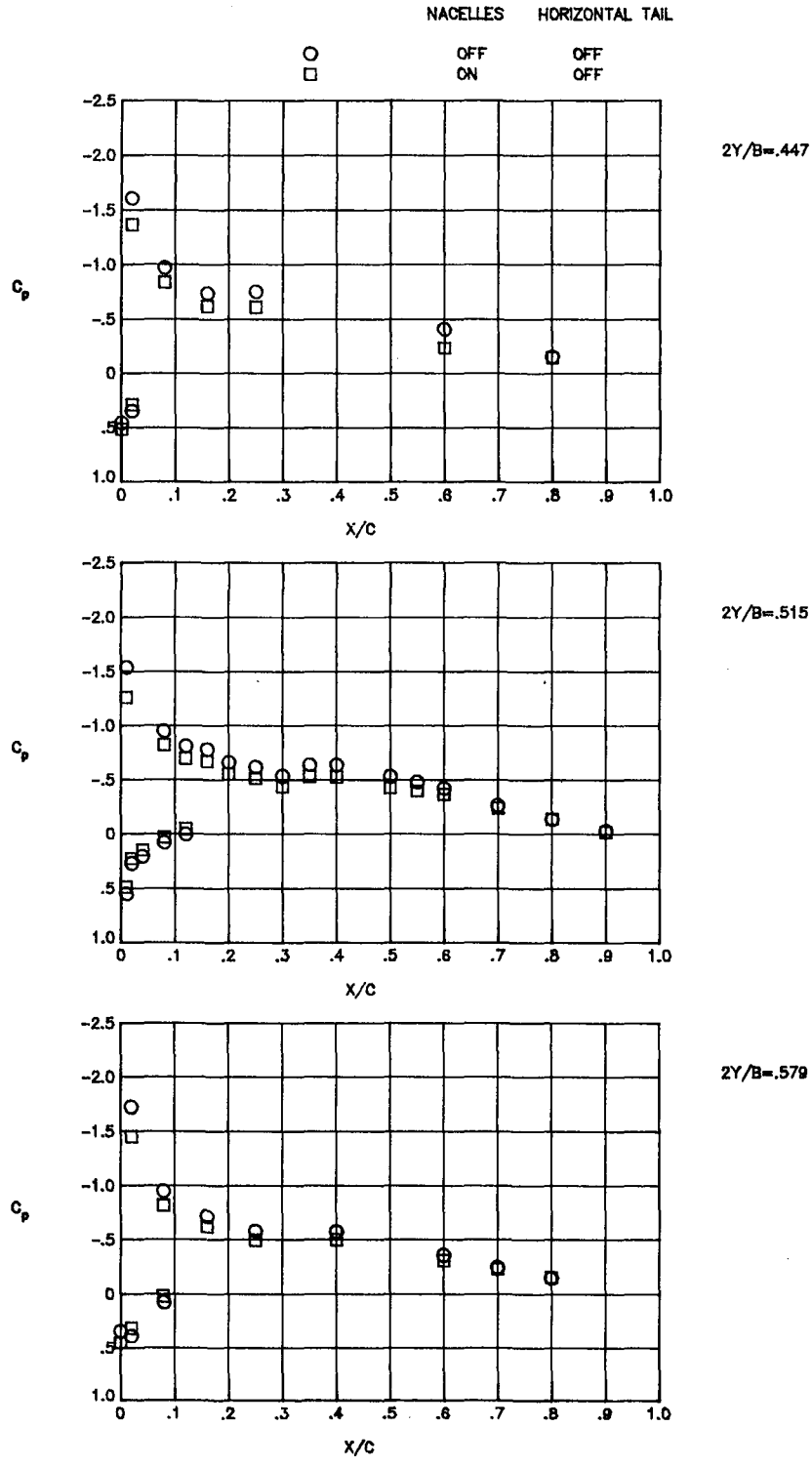

(a) α = 3.30.

Figure 5.- Effect of nacelles on wing pressure distributions at M = 0.60.

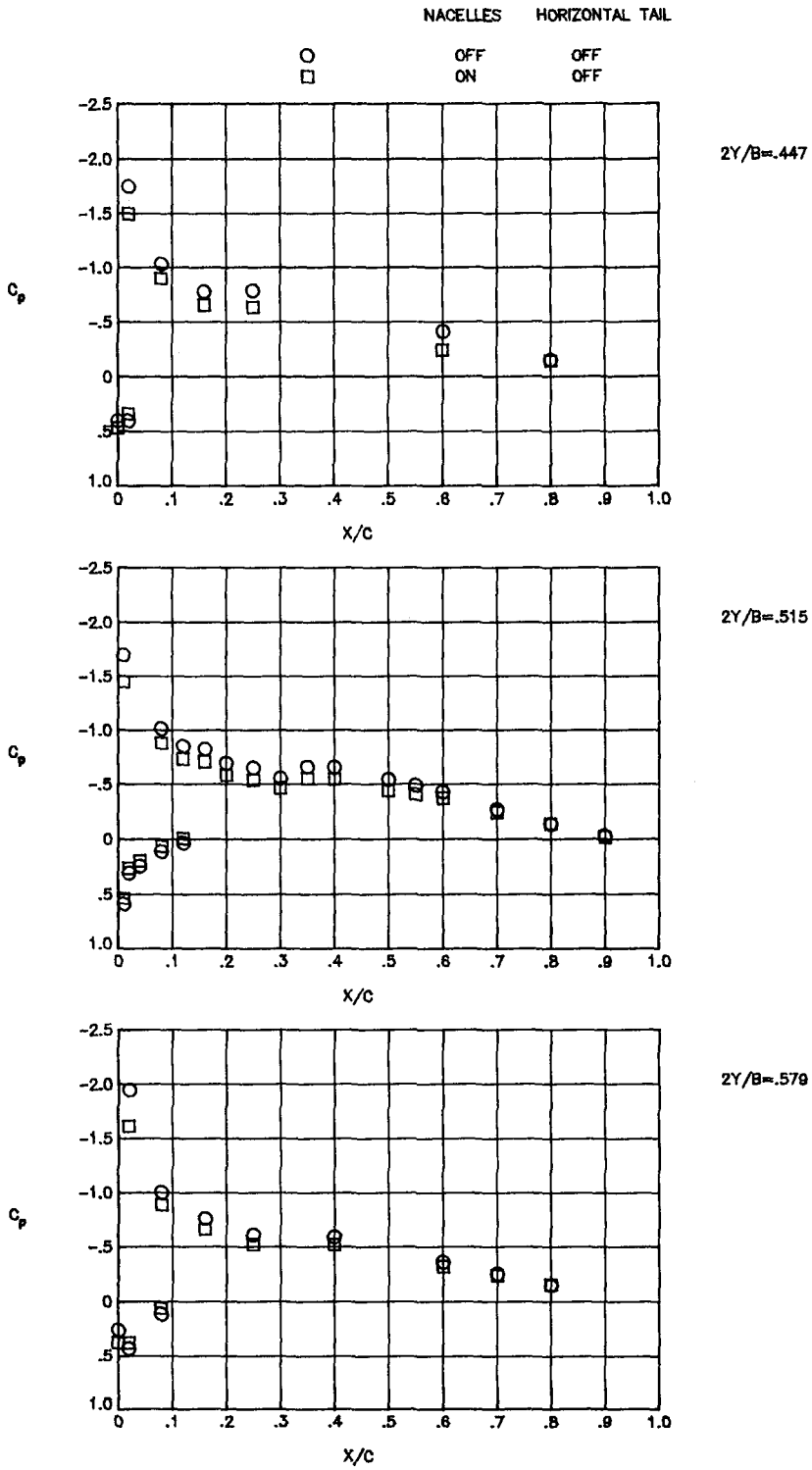

(b) $\alpha = 3.75$.

Figure 5.- Continued.

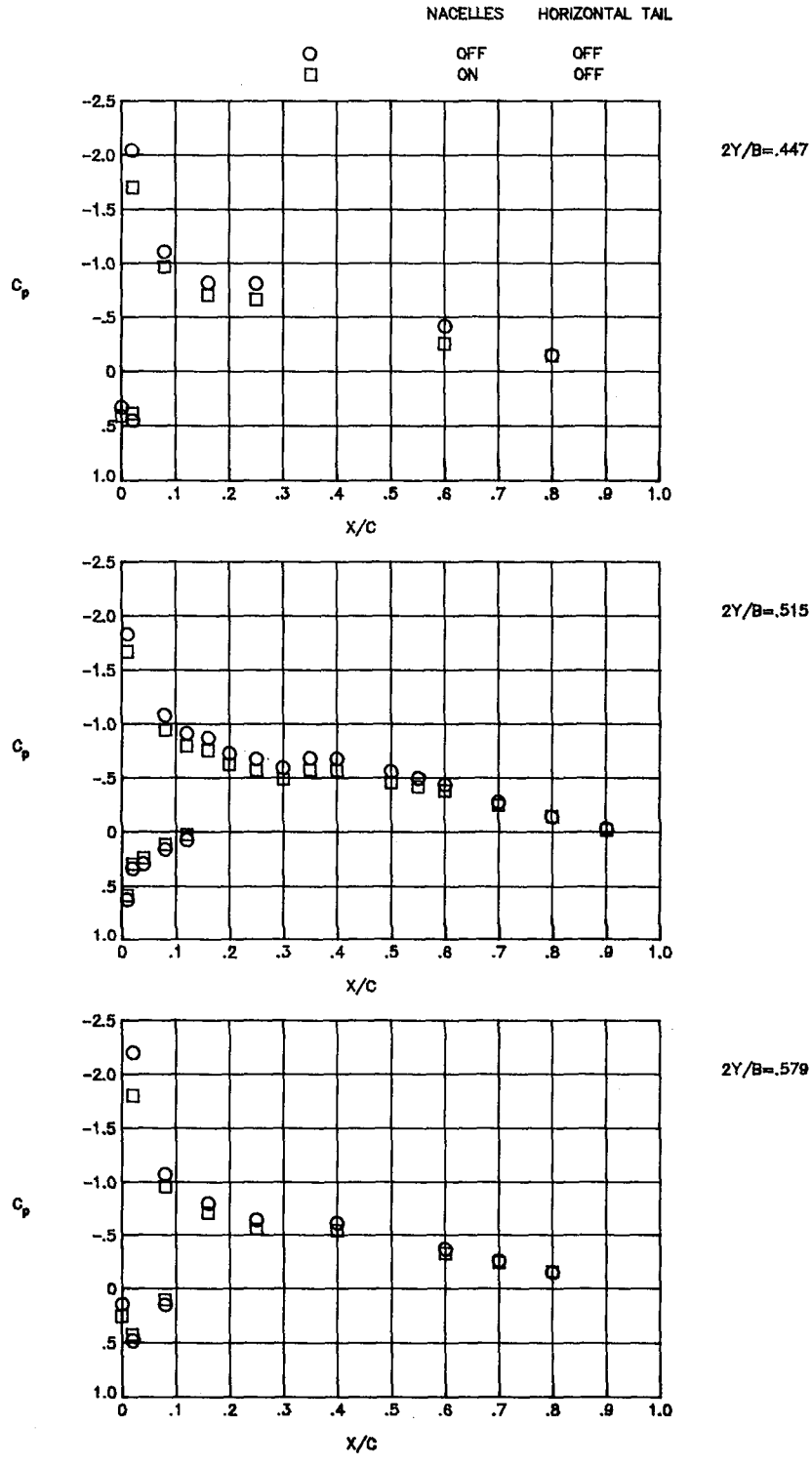

(c) α = 4.28.

Figure 5.- Continued.

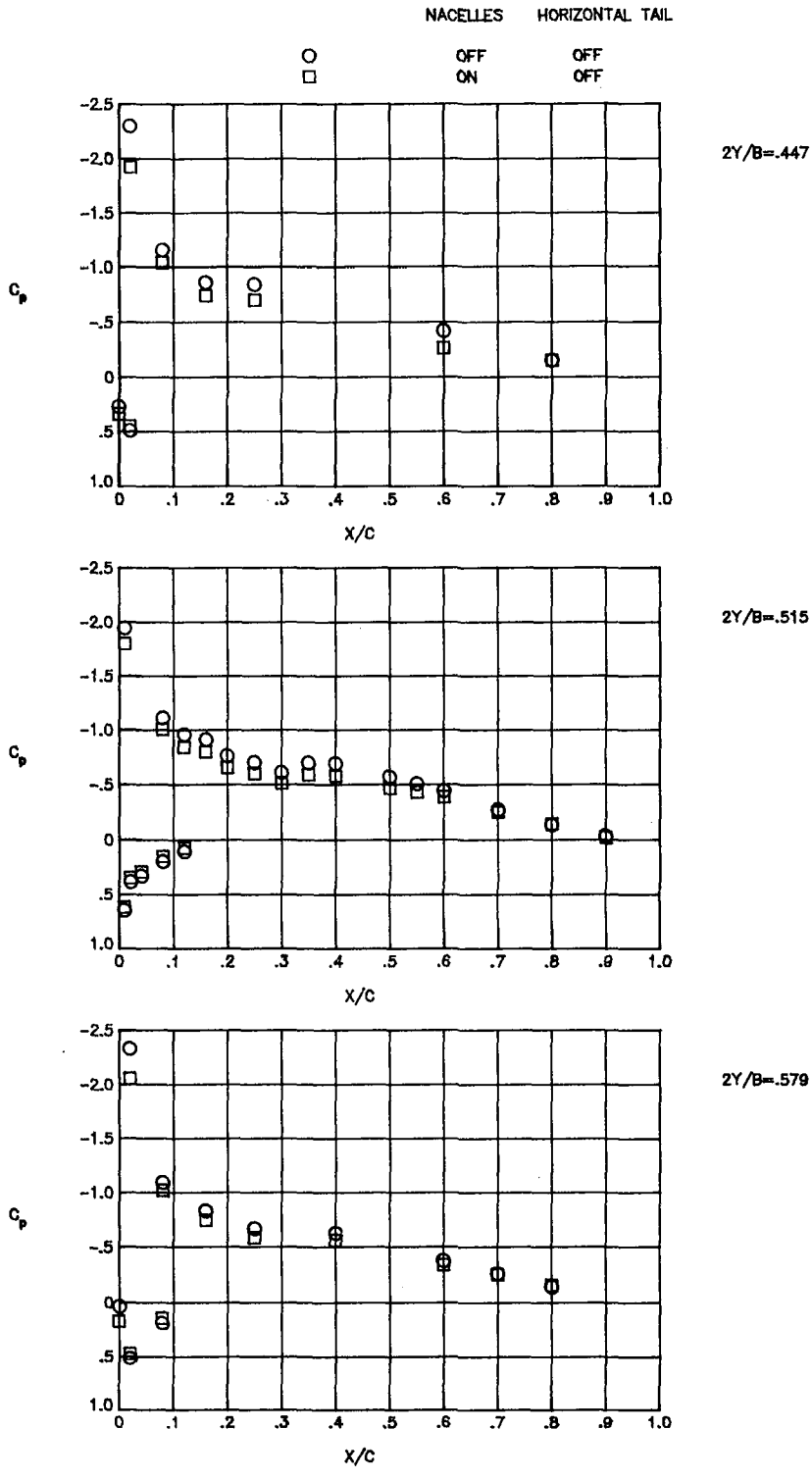

(d) α = 4.79.

Figure 5.- Continued.

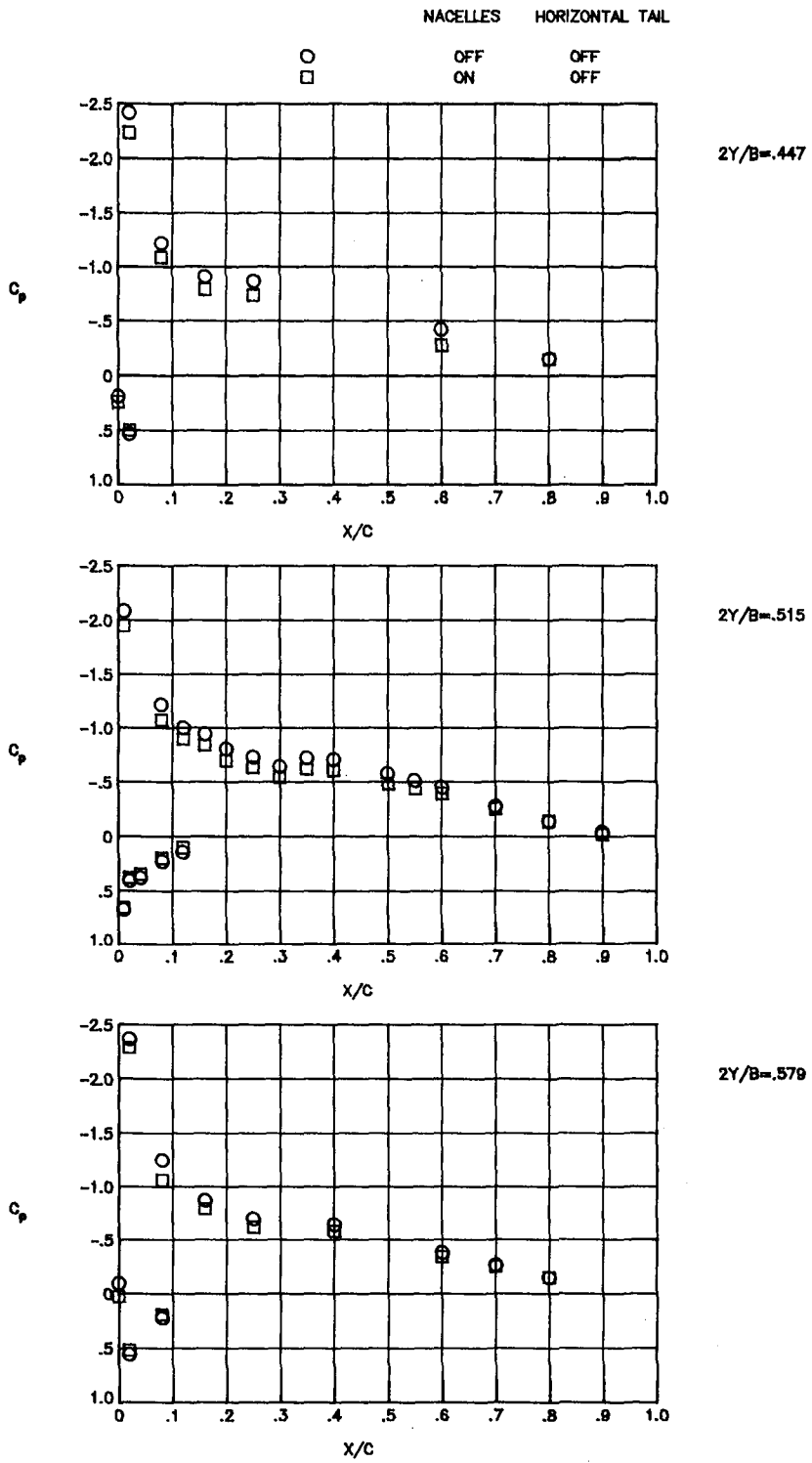

(e) α = 5.36.

Figure 5.- Concluded.

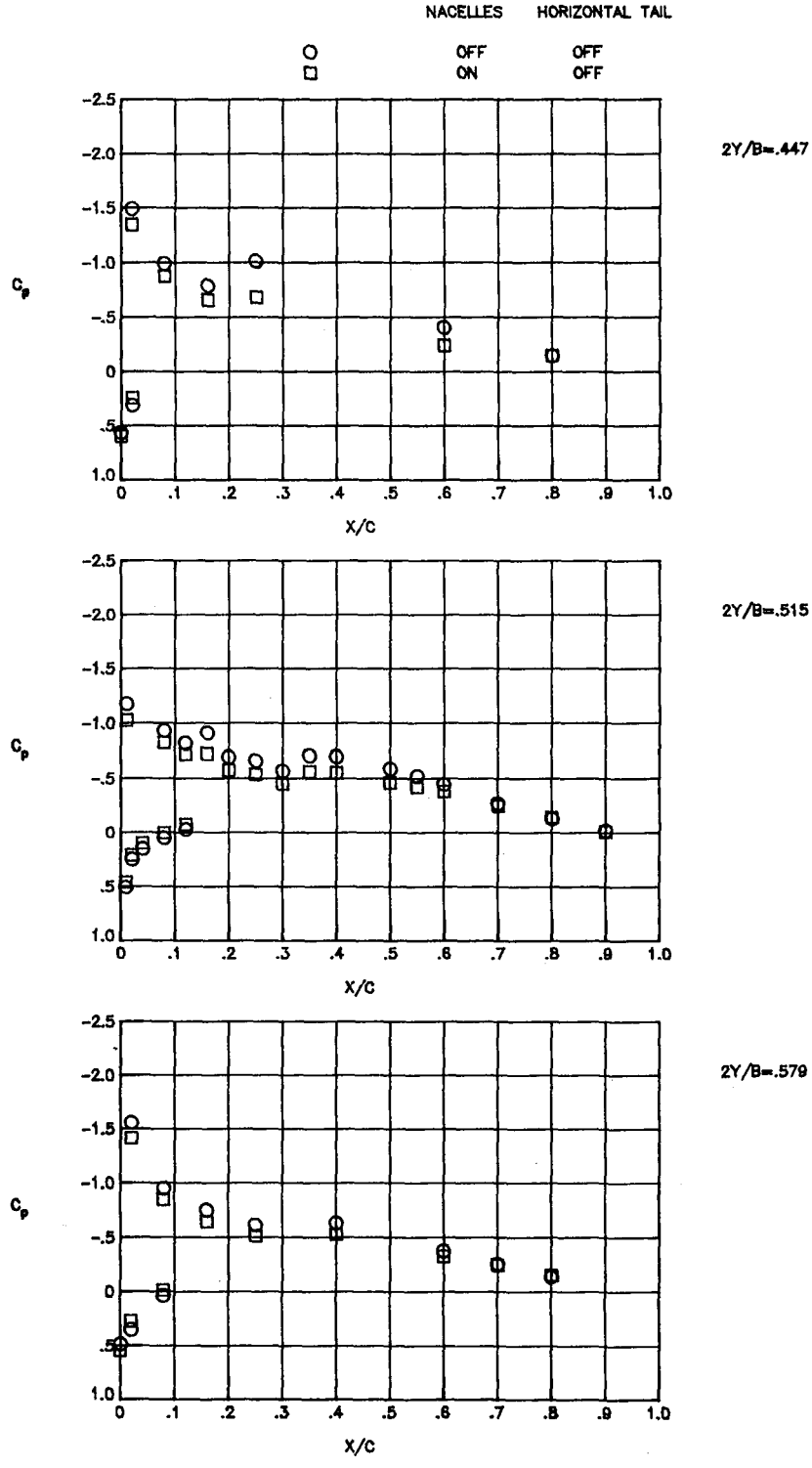

(a) α = 3.10.

Figure 6.- Effect of nacelles on wing pressure distributions at M = 0.70.

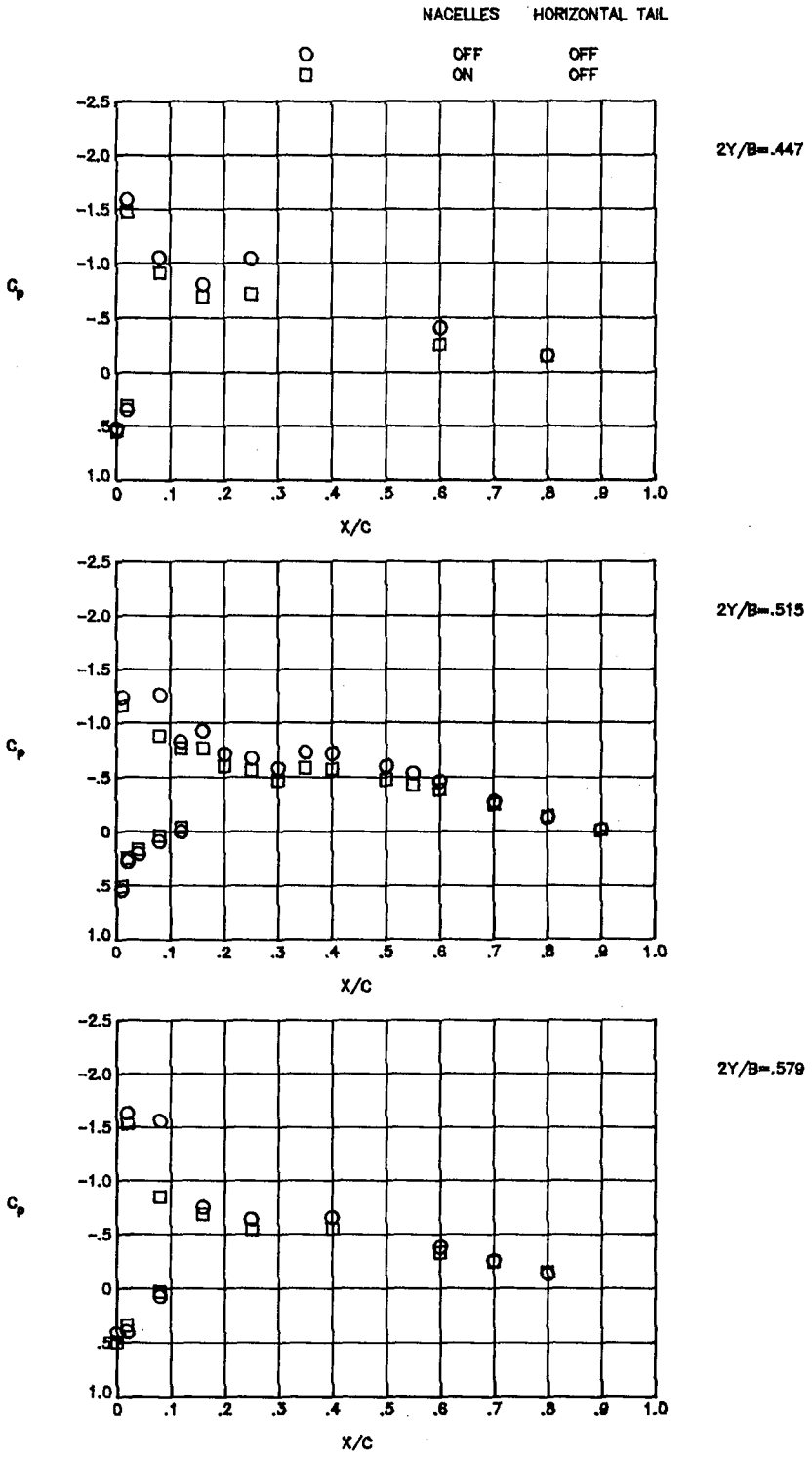

(b) α = 3.59.

Figure 6.- Continued.

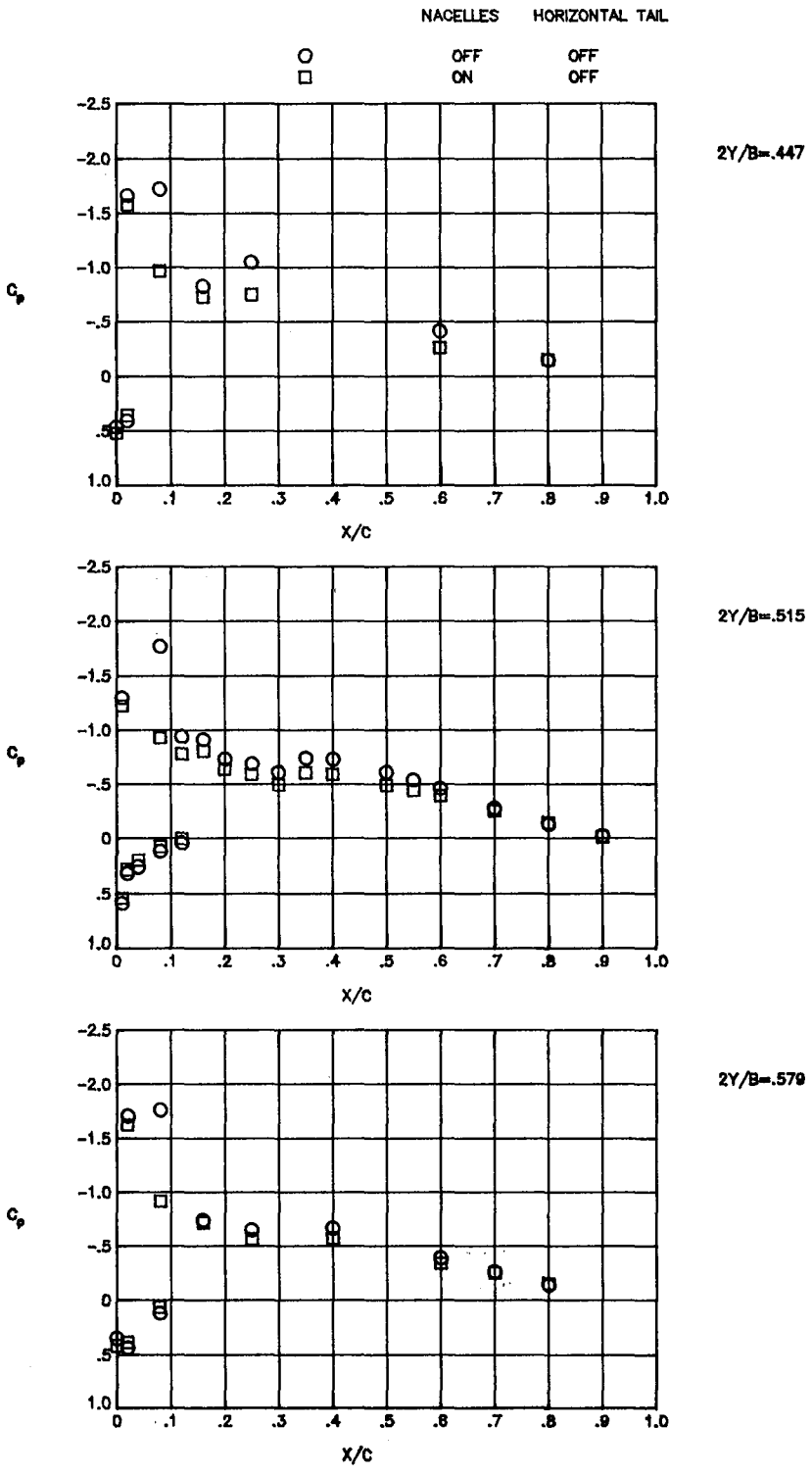

(c) α = 4.09.

Figure 6.- Continued.

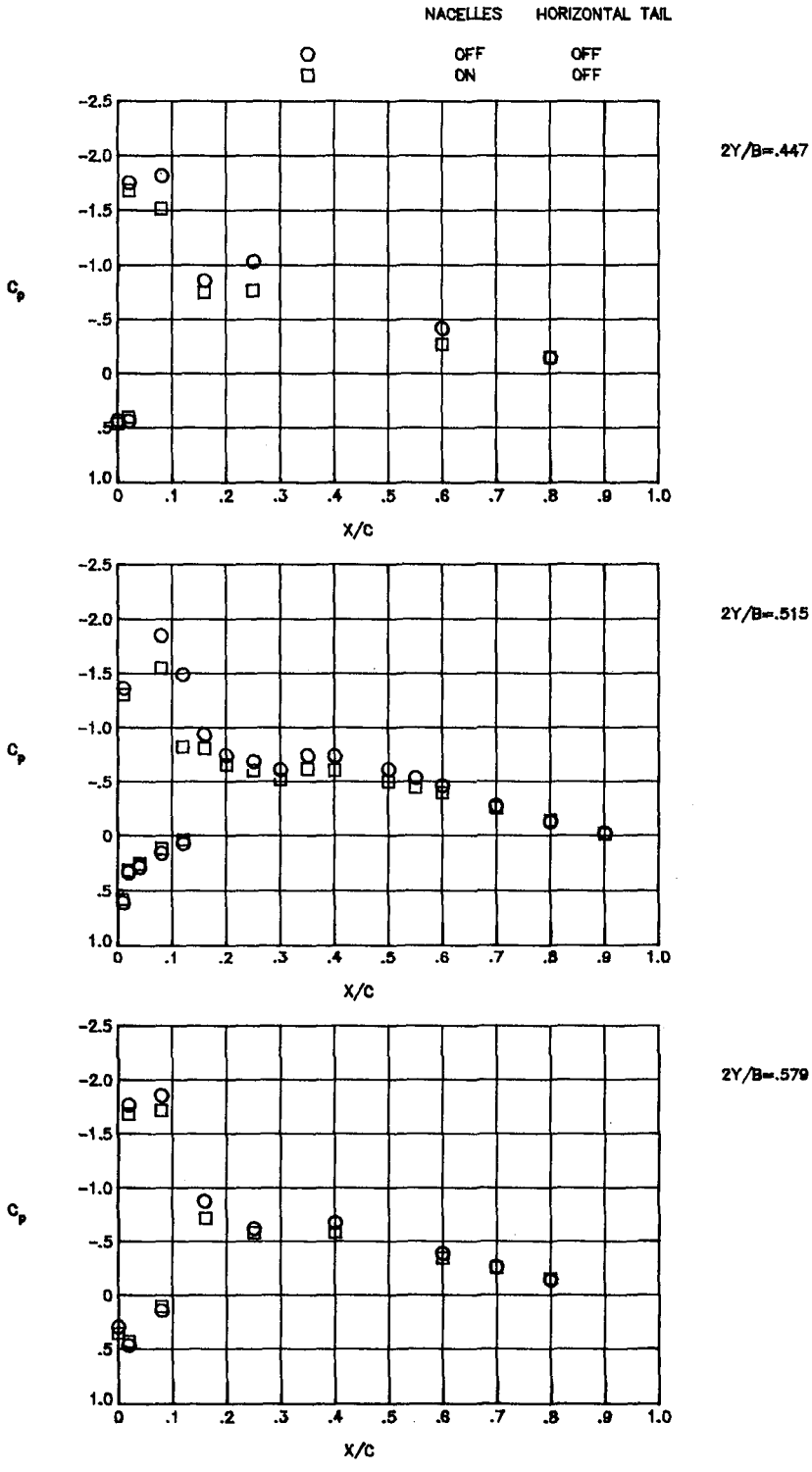

(d) α = 4.56.

Figure 6.- Continued.

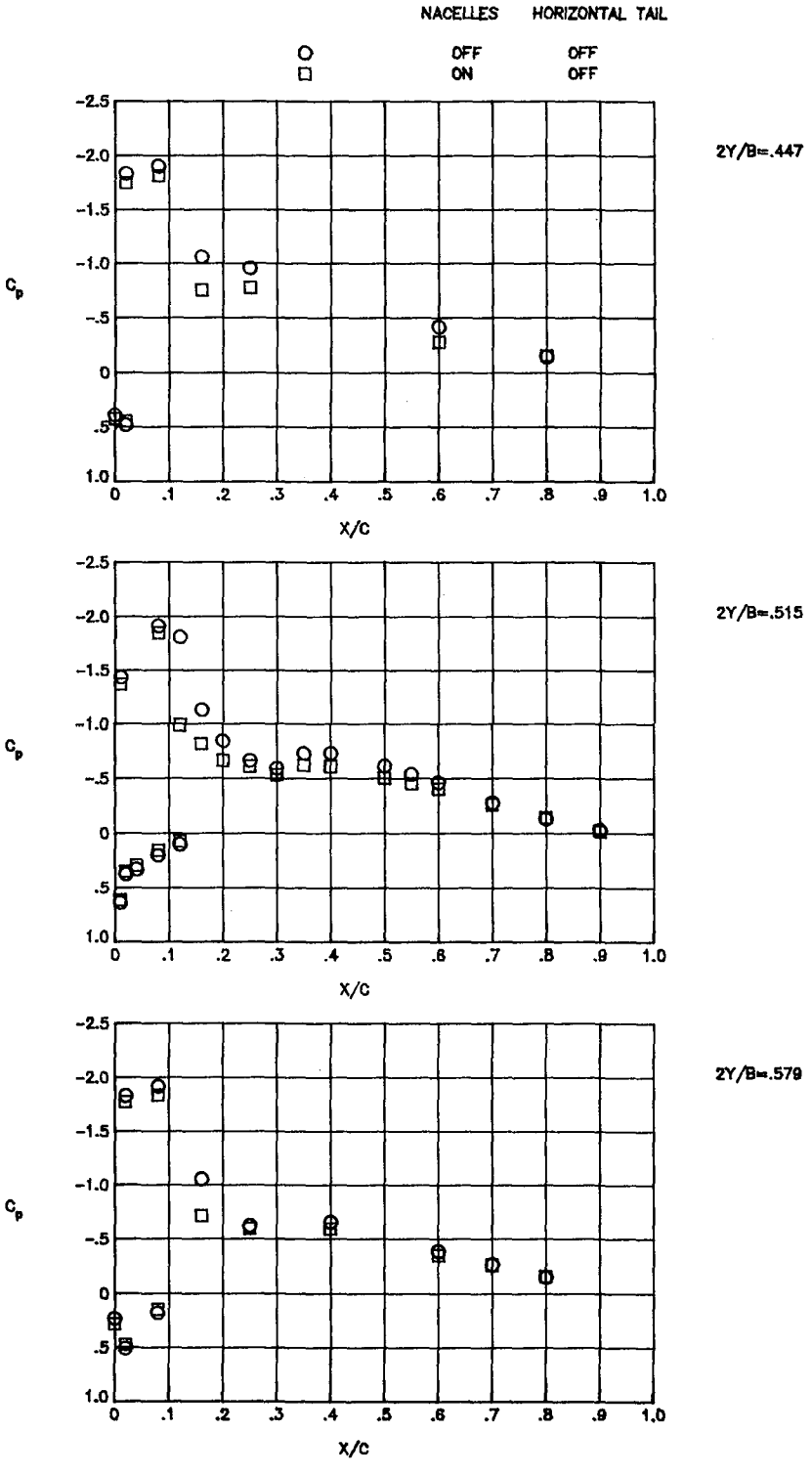

(e) α = 5.07.

Figure 6.- Concluded.

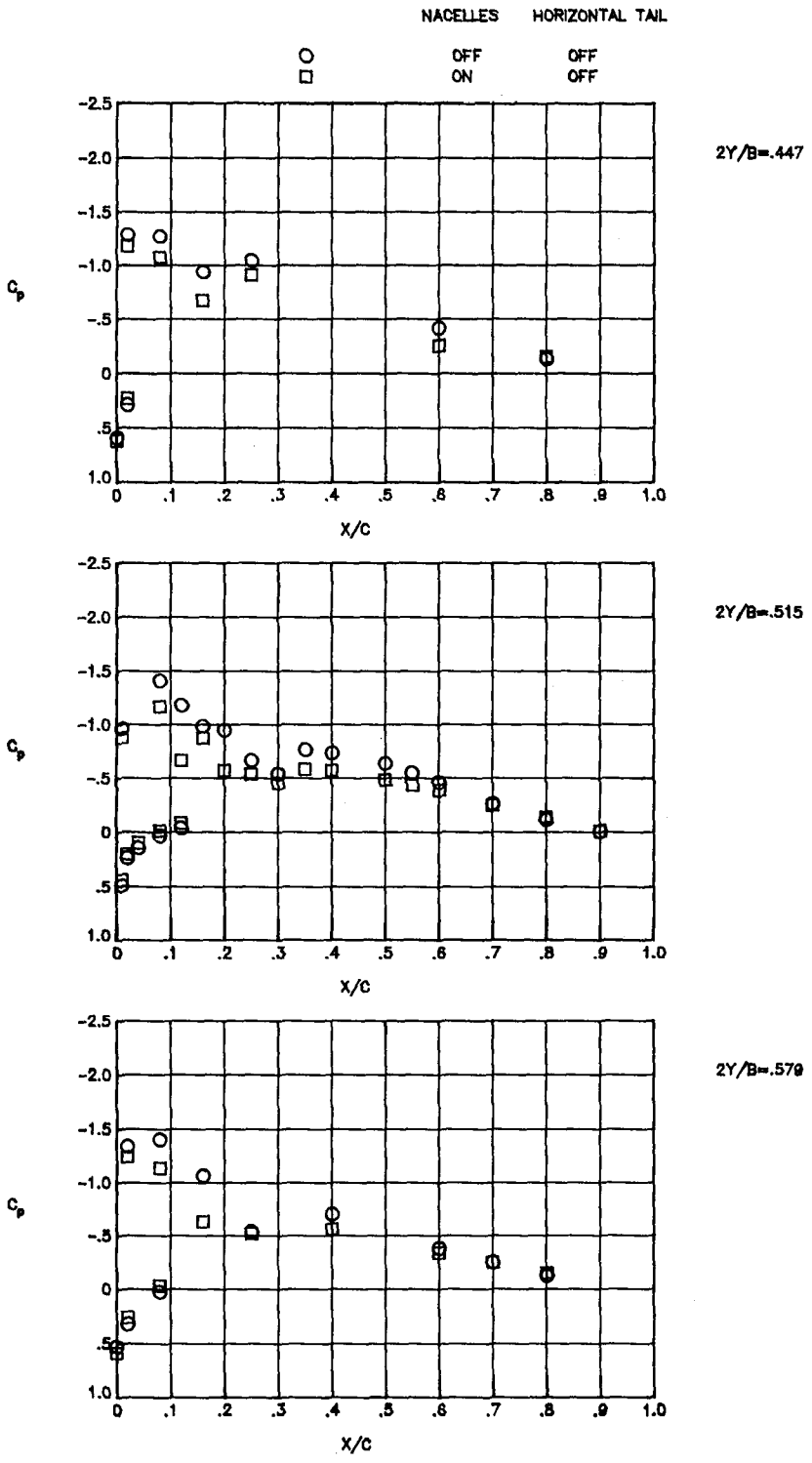

(a) α = 3.07.

Figure 7.- Effect of nacelles on wing pressure distributions at M = 0.75.

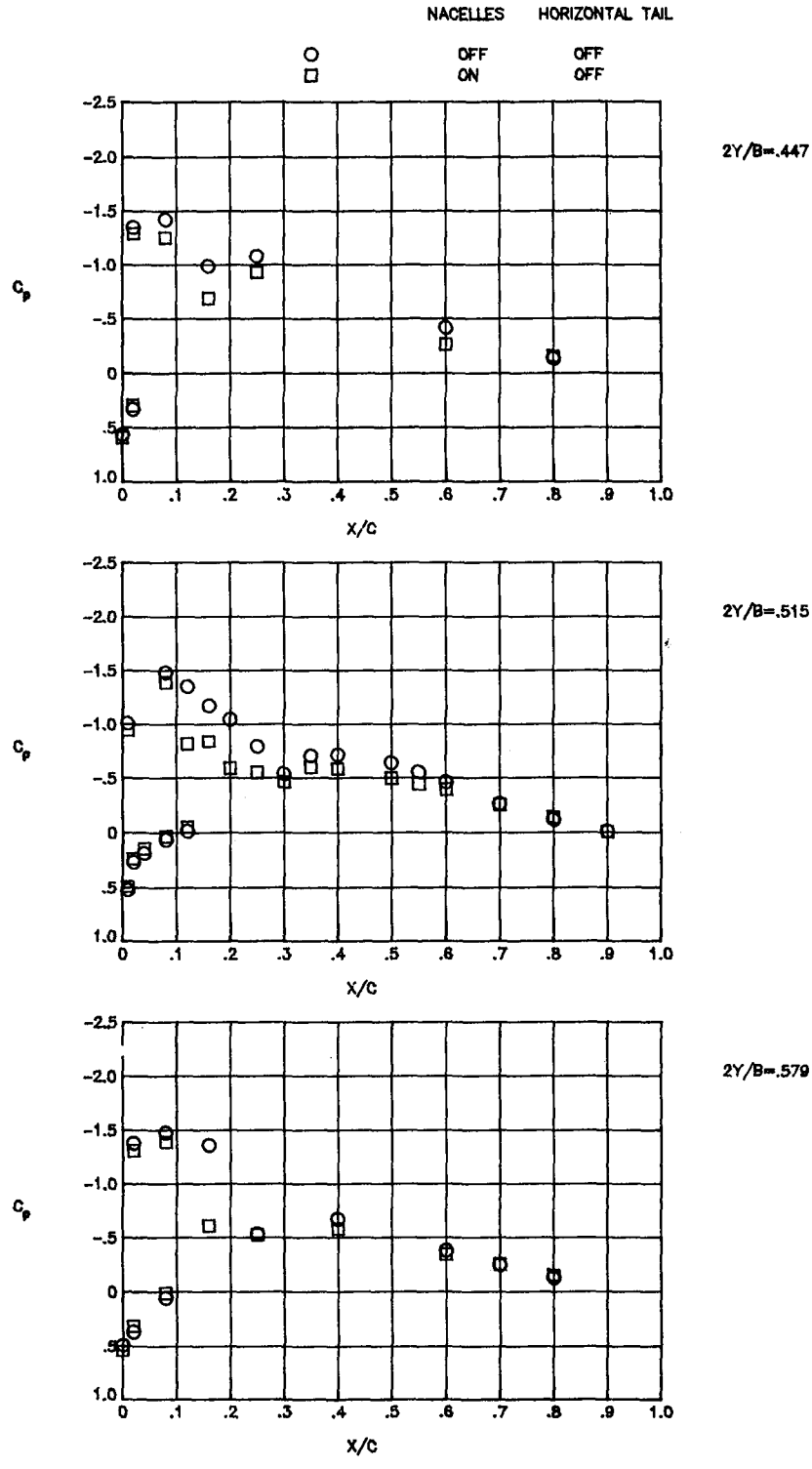

(b) α = 3.51.

Figure 7.- Continued.

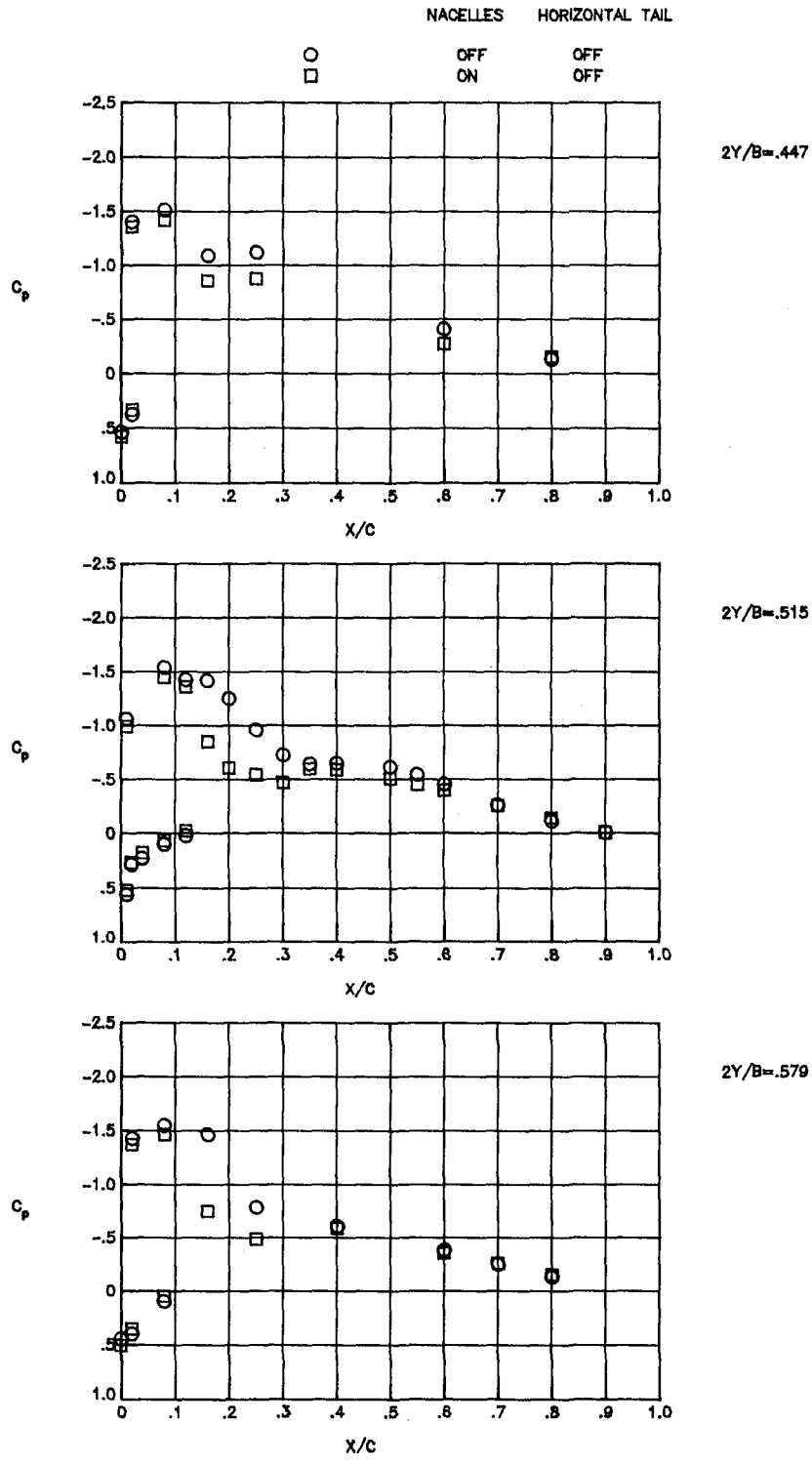

(c) α = 3.98.

Figure 7.- Continued.

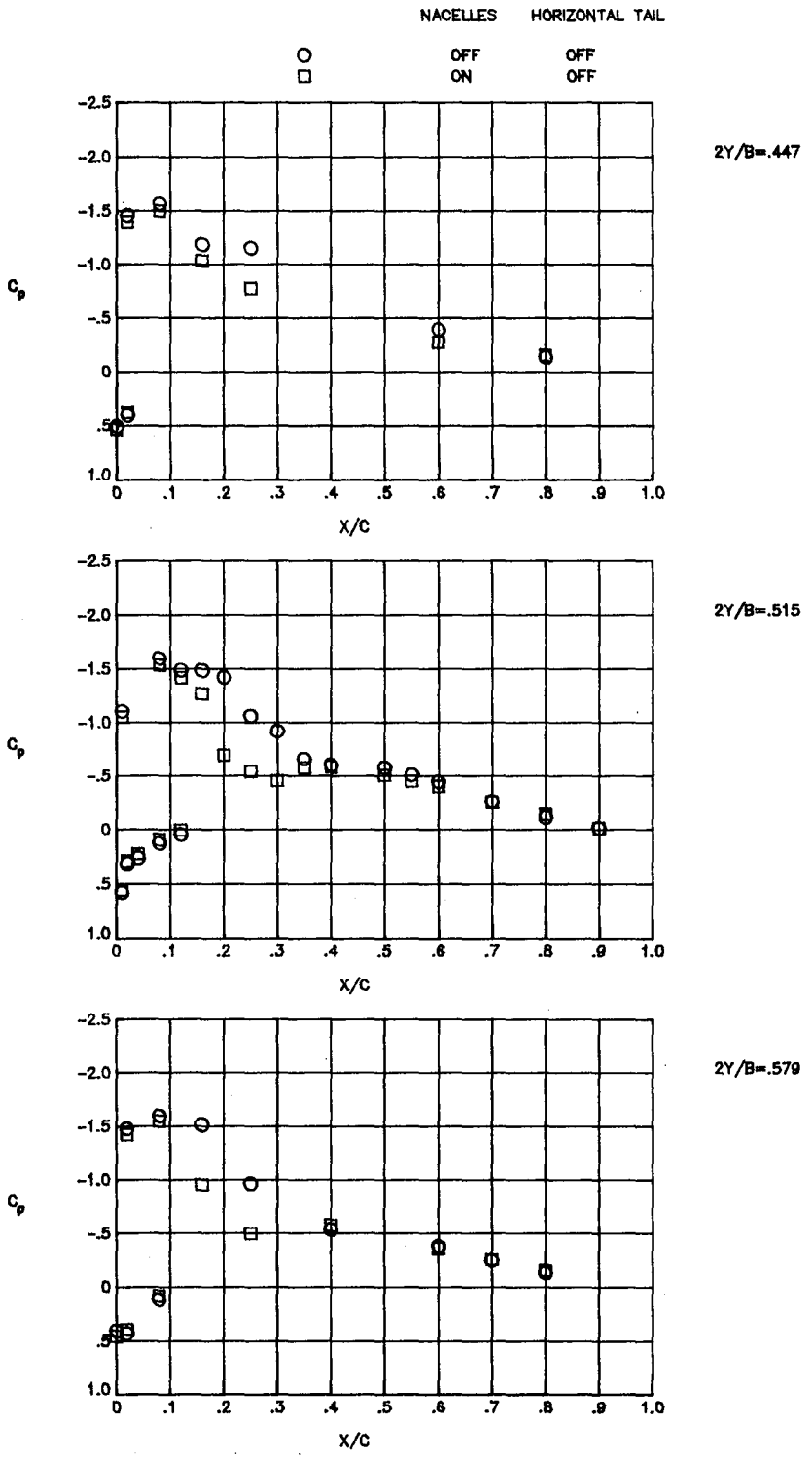

(d) α = 4.42.

Figure 7.- Continued.

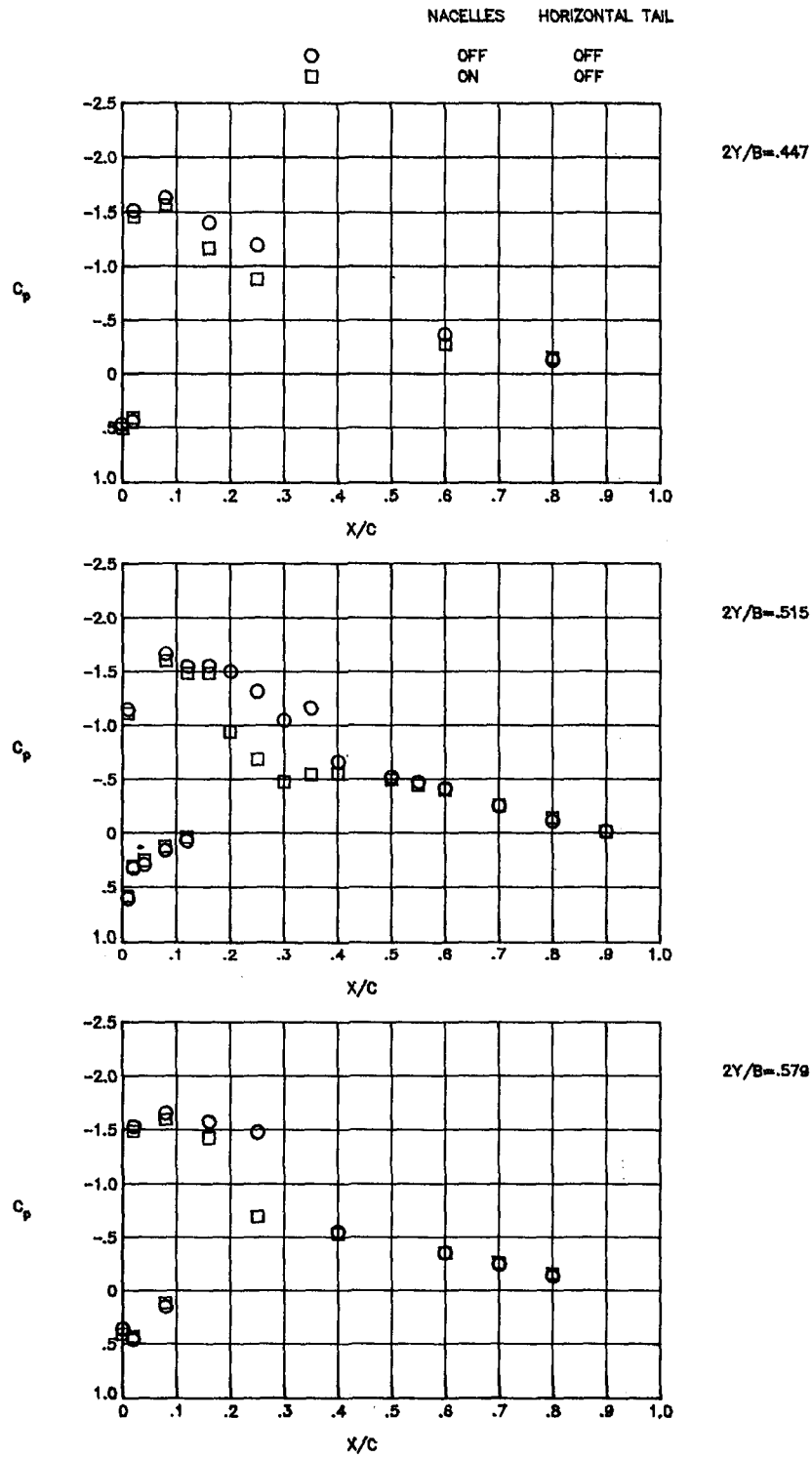

(e) α = 4.90.

Figure 7.- Concluded.

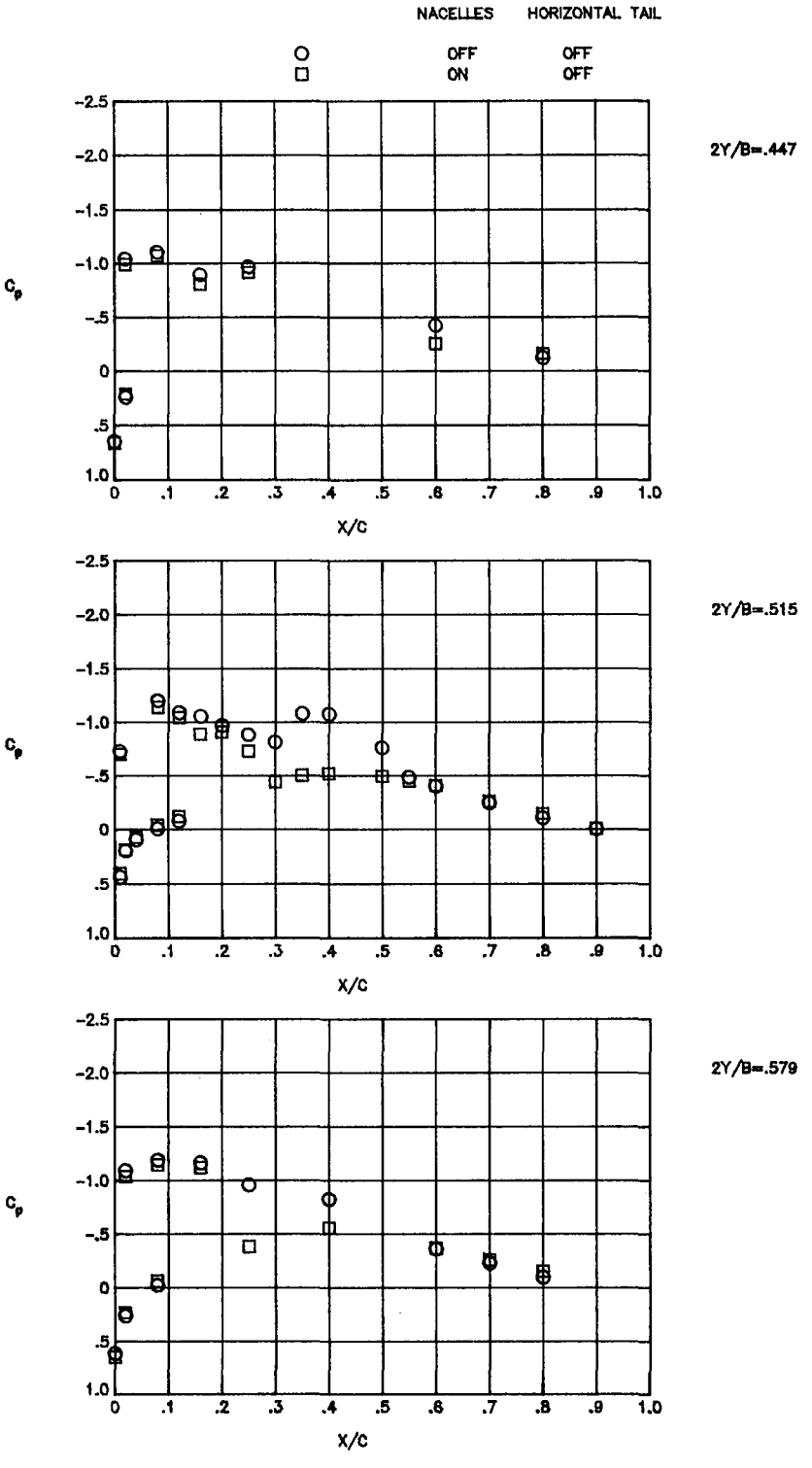

(a) α = 2.93.

Figure 8.- Effect of nacelles on wing pressure distributions at M = 0.80.

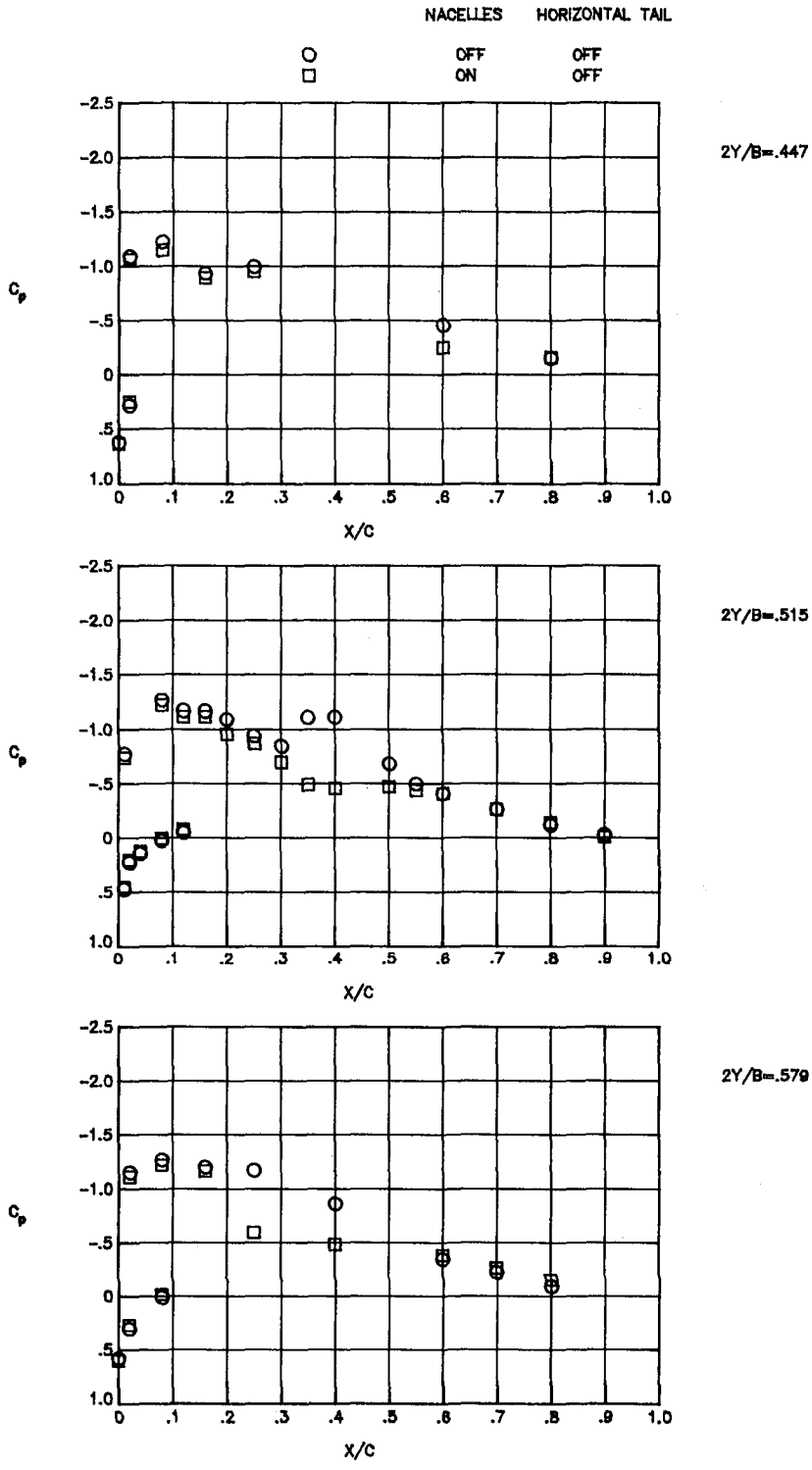

(b) α = 3.43.

Figure 8.- Continued.

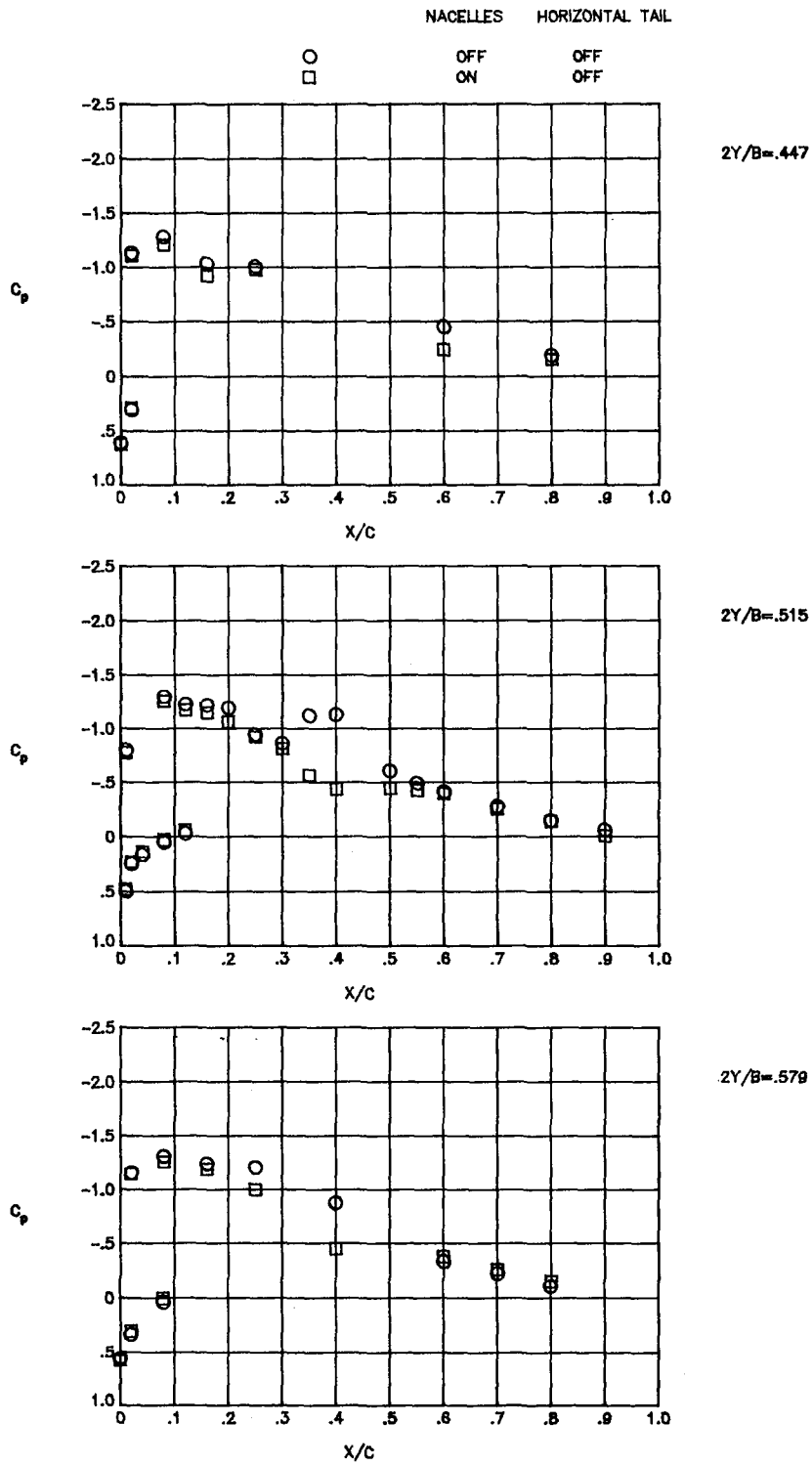

(c) α = 3.73.

Figure 8.- Continued.

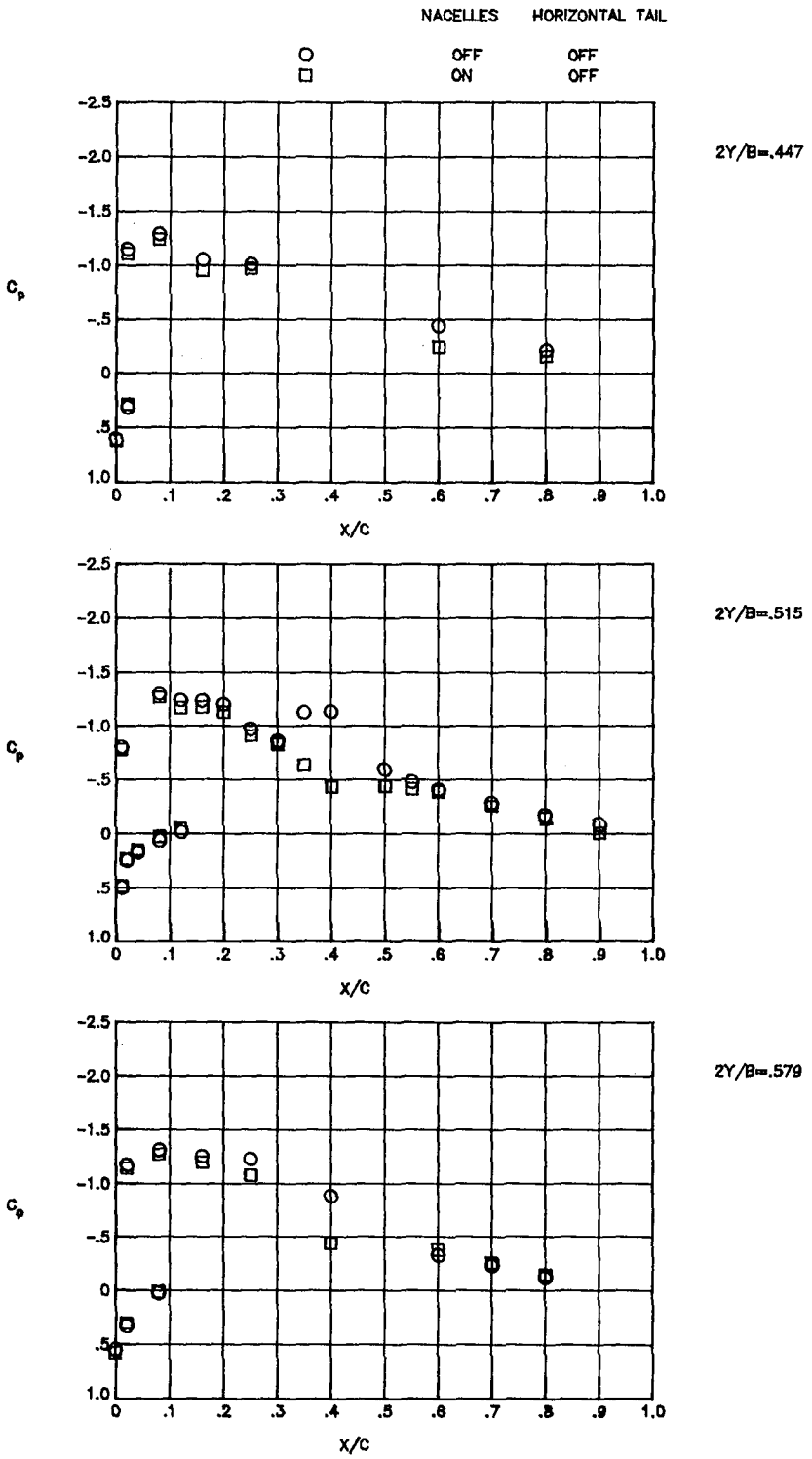

(d) α = 3.83.

Figure 8.- Continued.

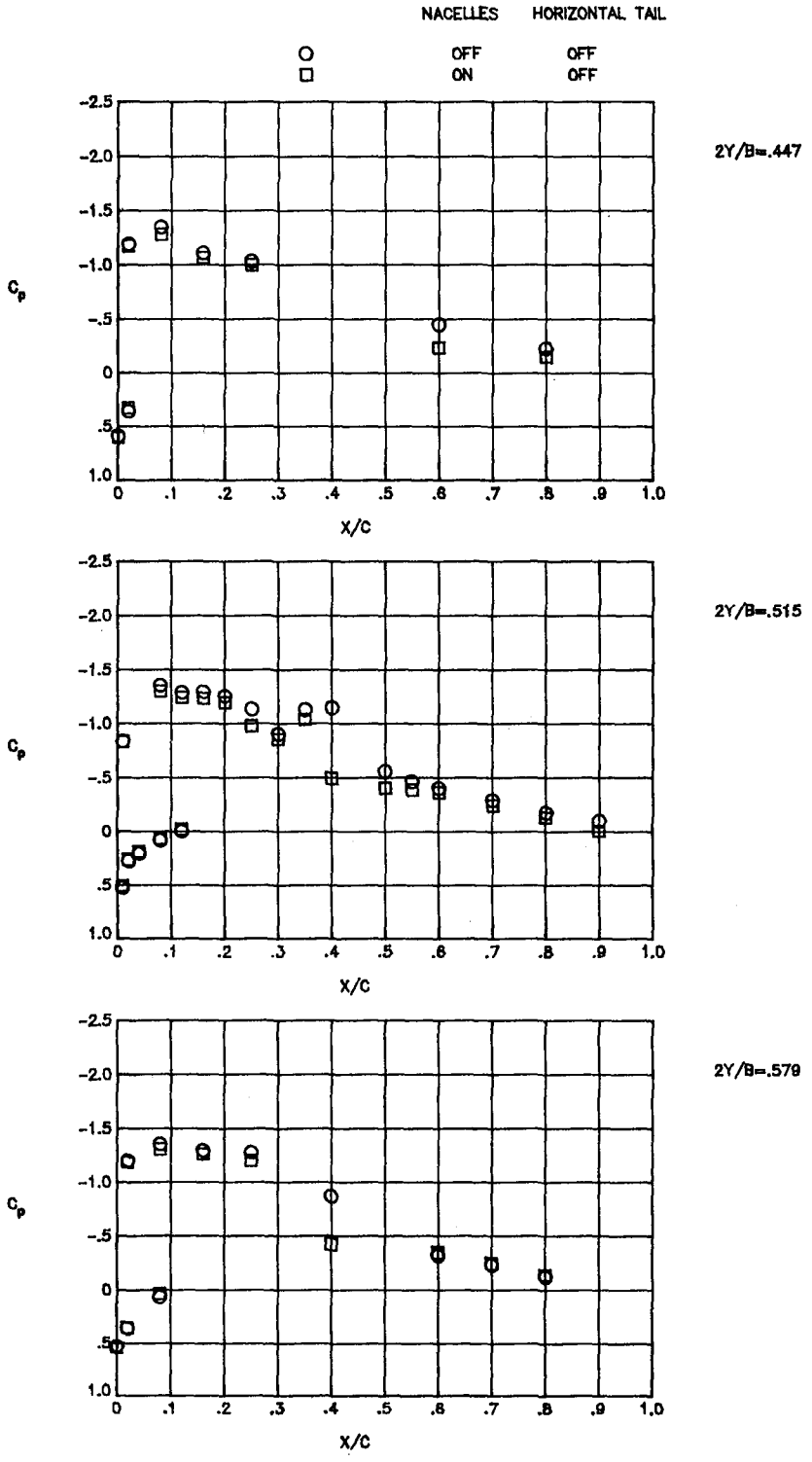

(e) $\alpha = 4.22$.

Figure 8.- Continued.

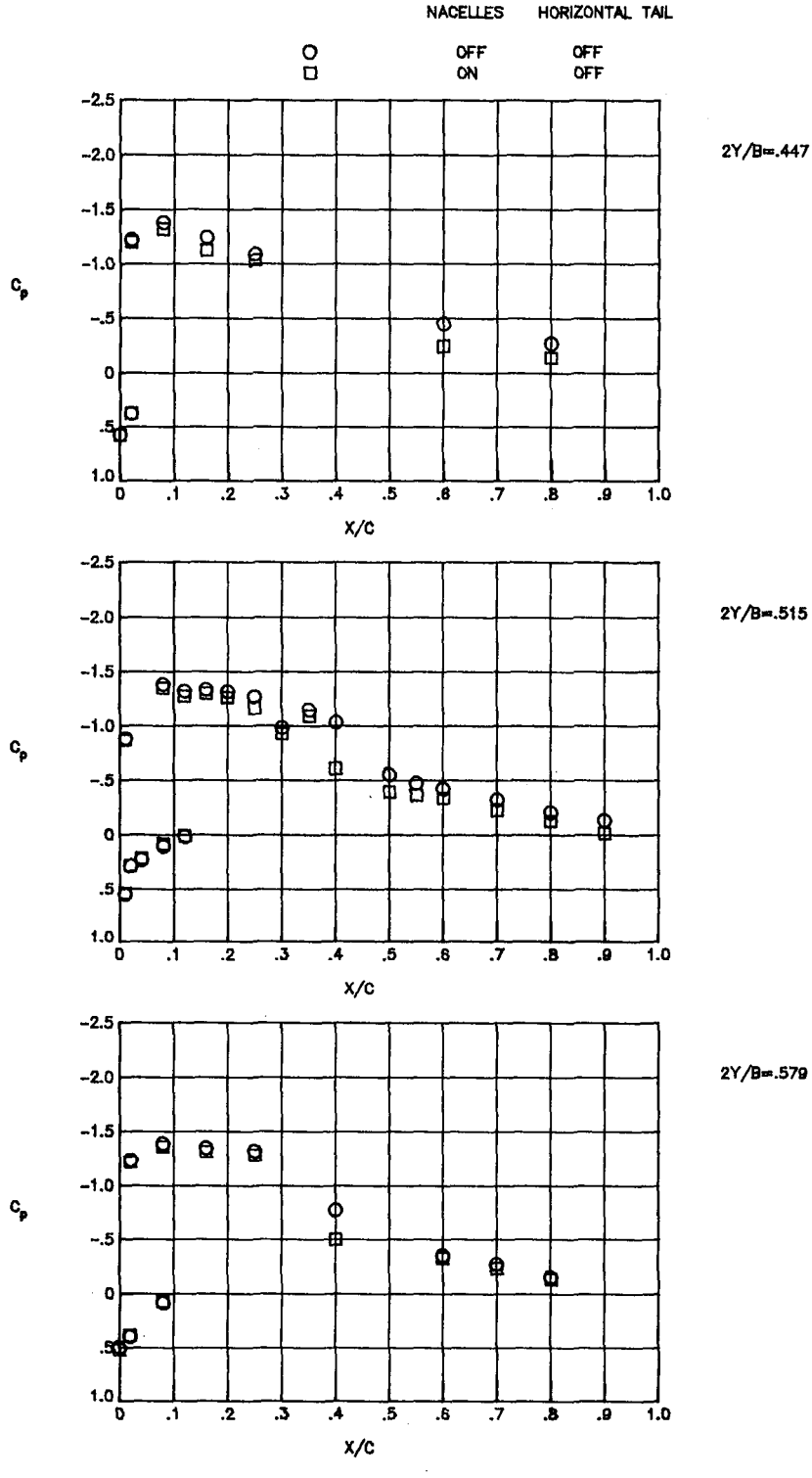

(f) α = 4.65.

Figure 8.- Concluded.

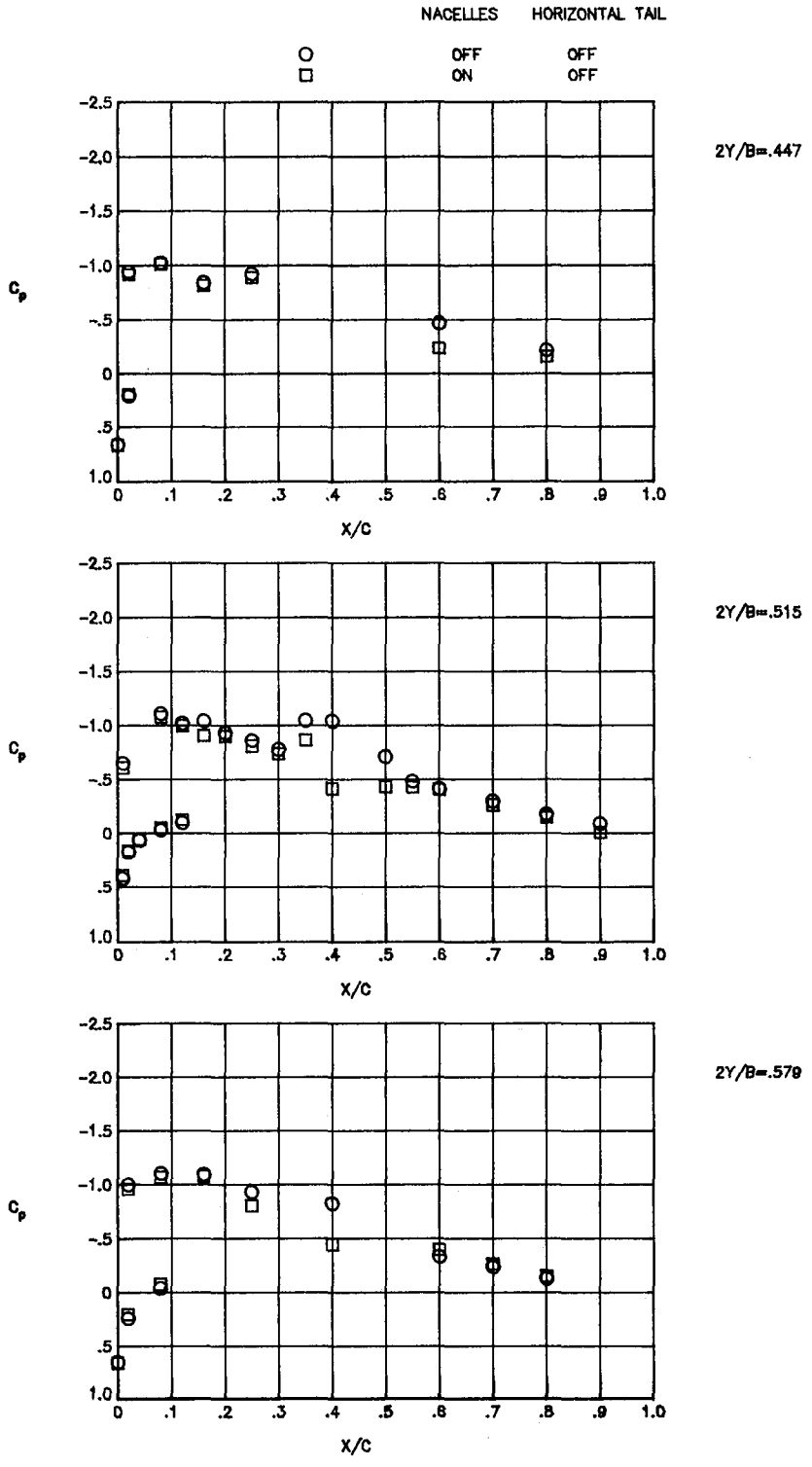

(a) α = 2.89.

Figure 9.- Effect of nacelles on wing pressure distributions at M = 0.82.

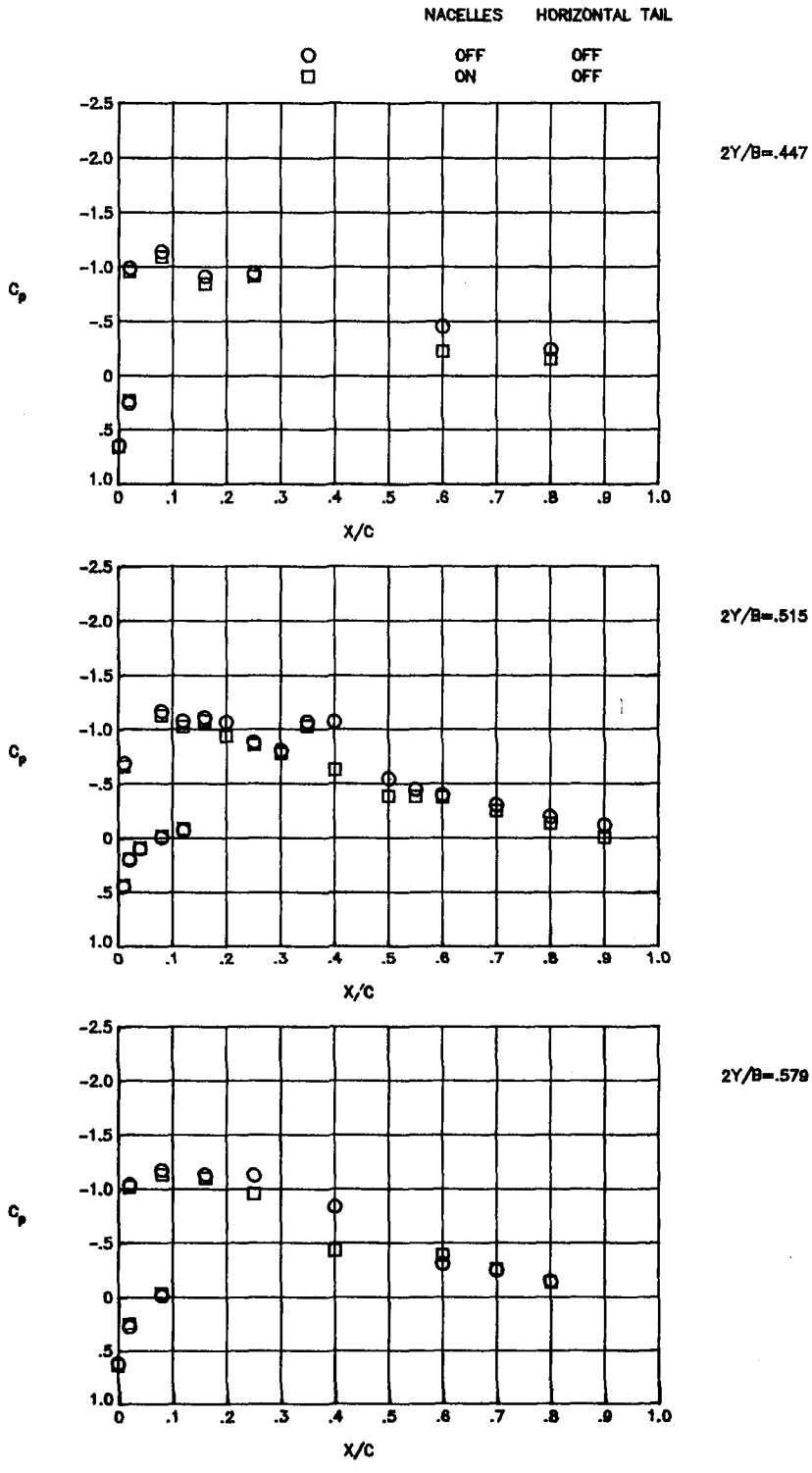

(b) α = 3.32.

Figure 9.- Continued.

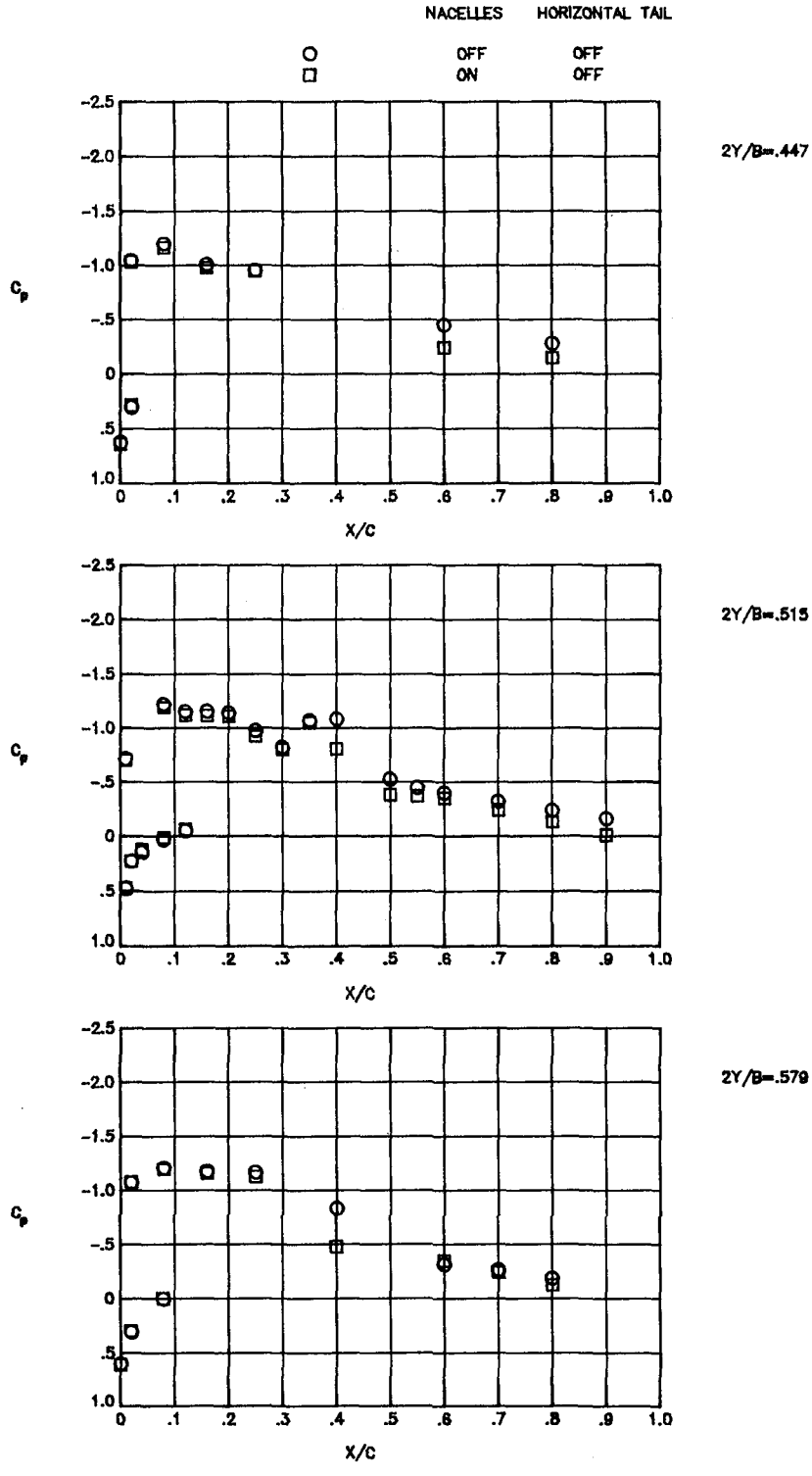

(c) α = 3.78.

Figure 9.- Continued.

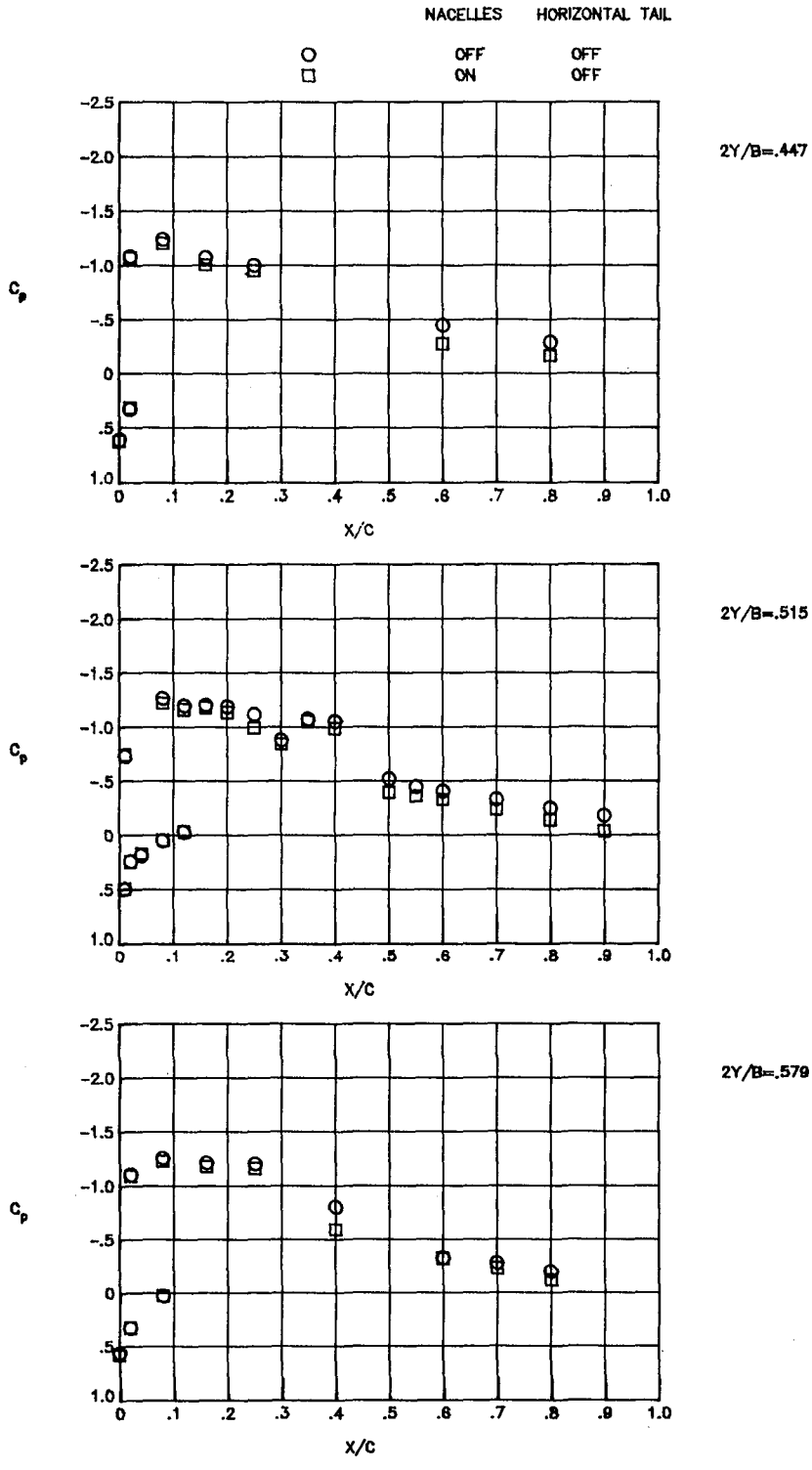

(d) α = 4.14.

Figure 9.- Continued.

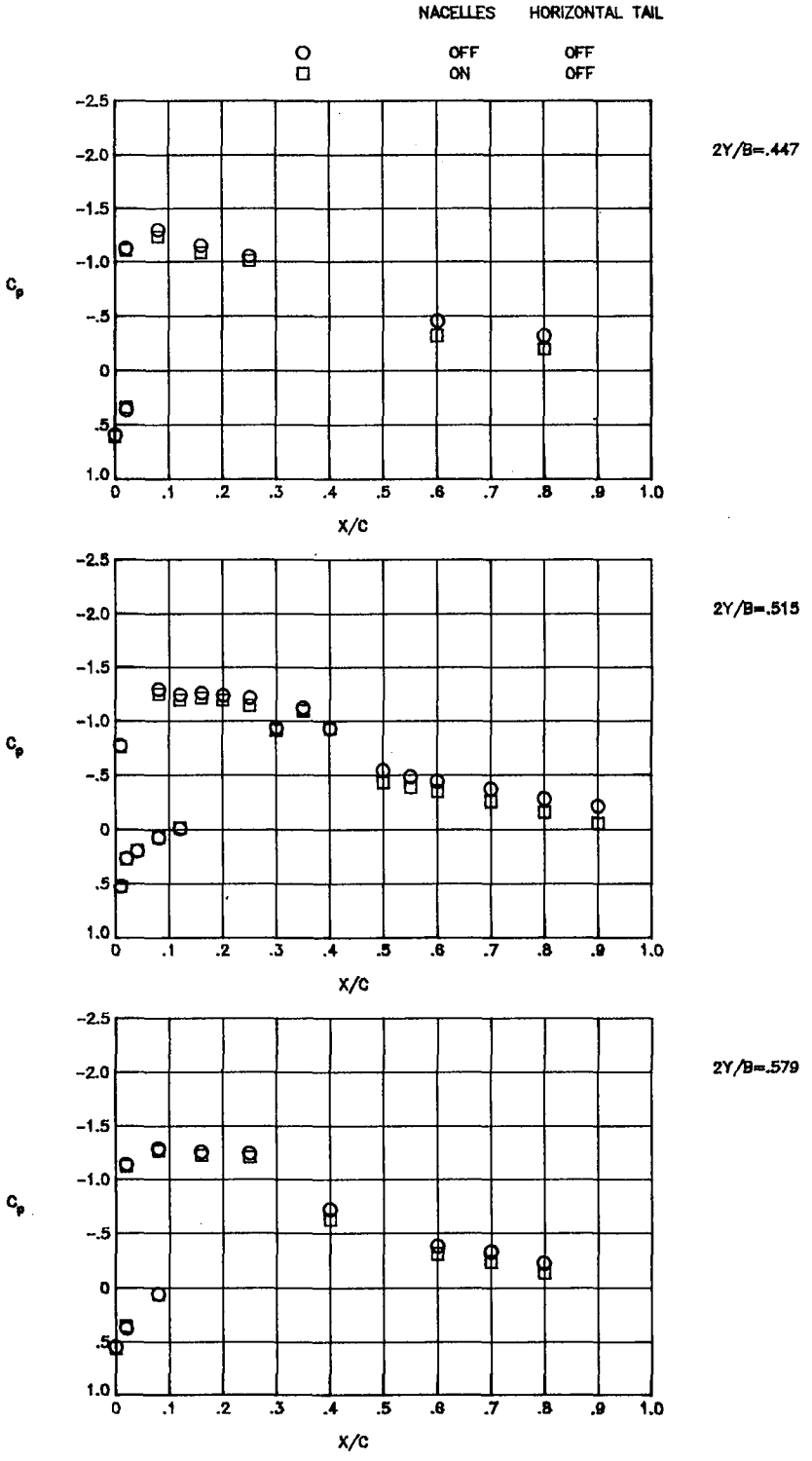

(e) α = 4.58.

Figure 9.- Concluded.

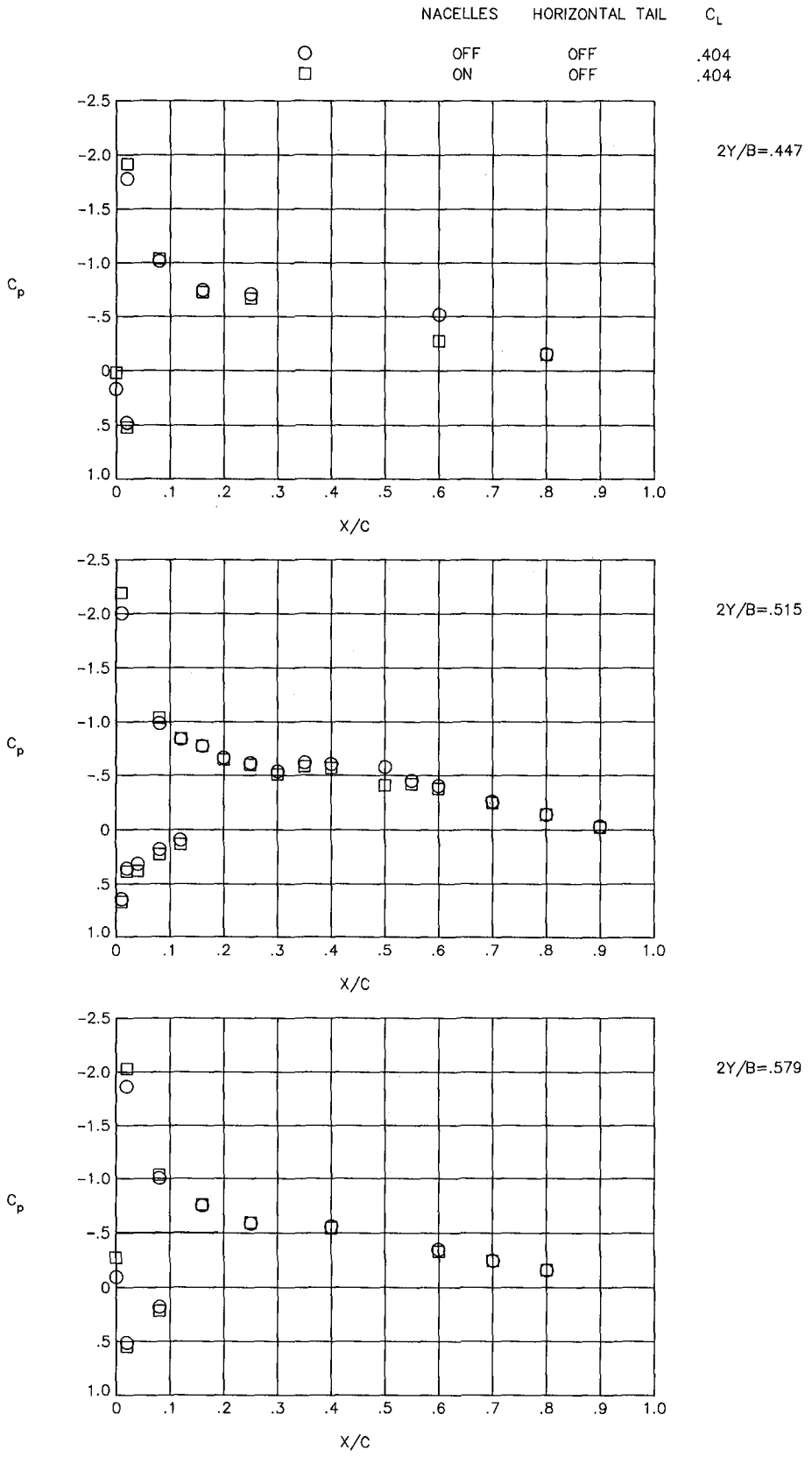

Figure 10.- Effect of nacelles on wing pressure distributions at M = 0.40.

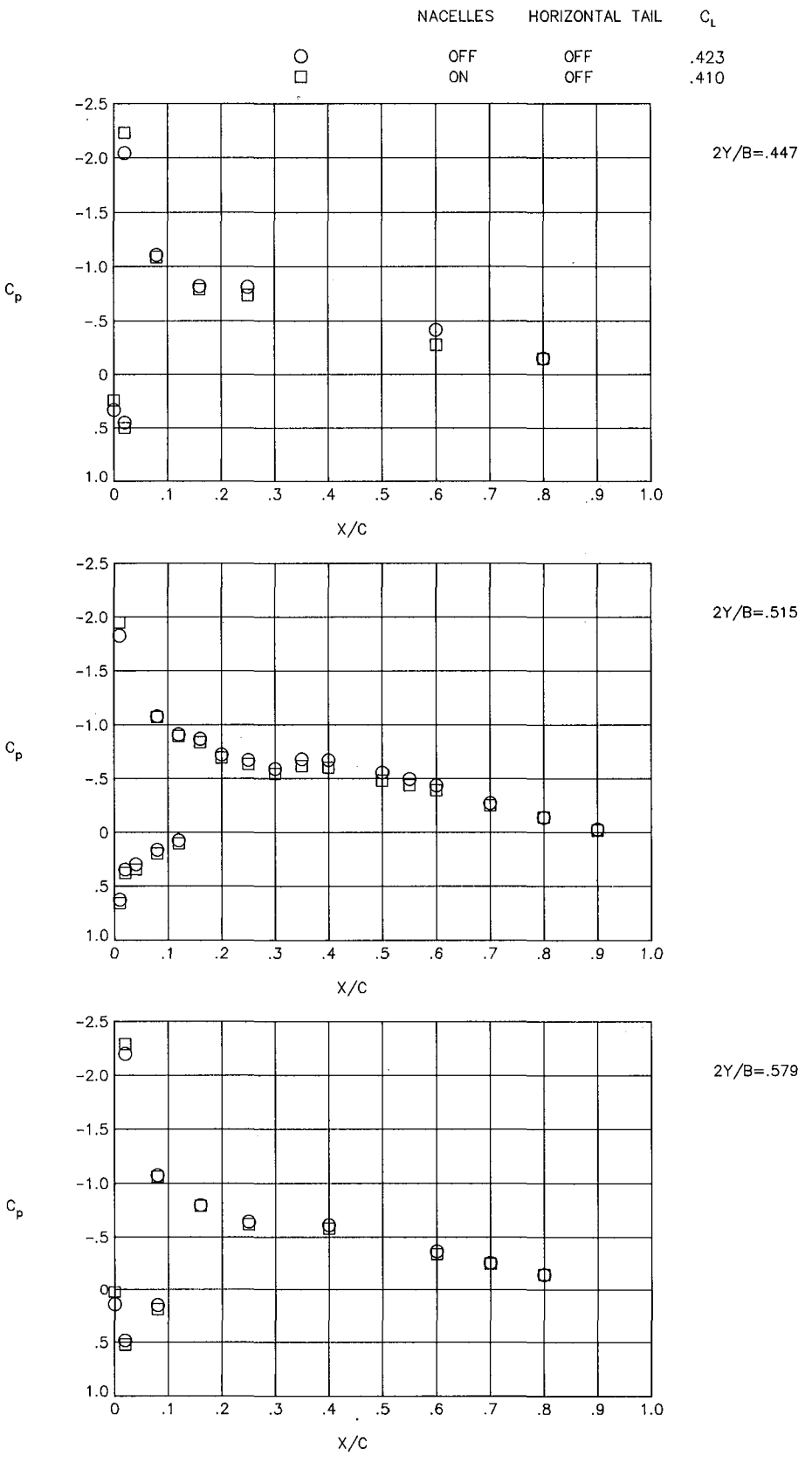

Figure 11.- Effect of nacelles on wing pressure distributions at M = 0.60.

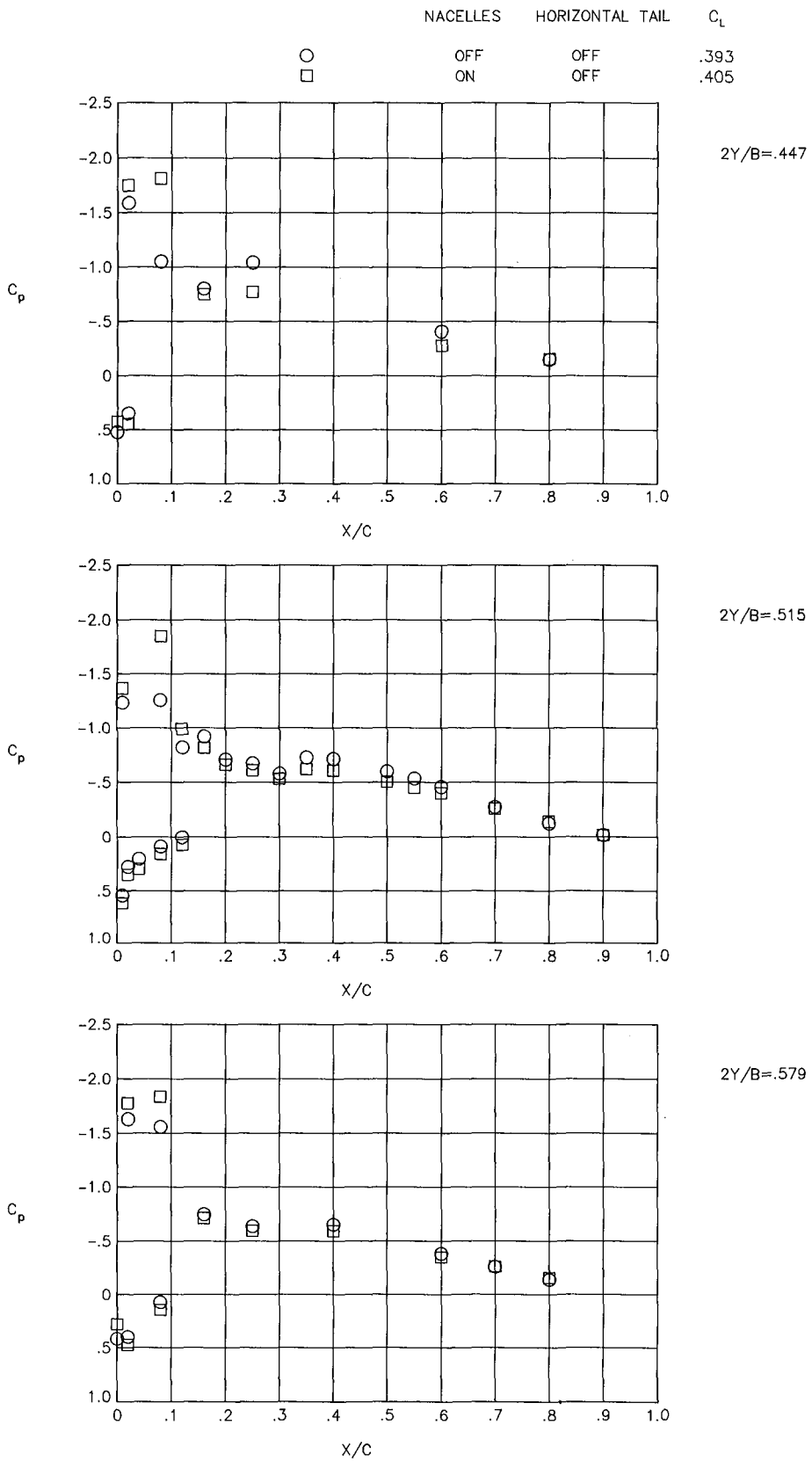

Figure 12.- Effect of nacelles on wing pressure distributions at M = 0.70.

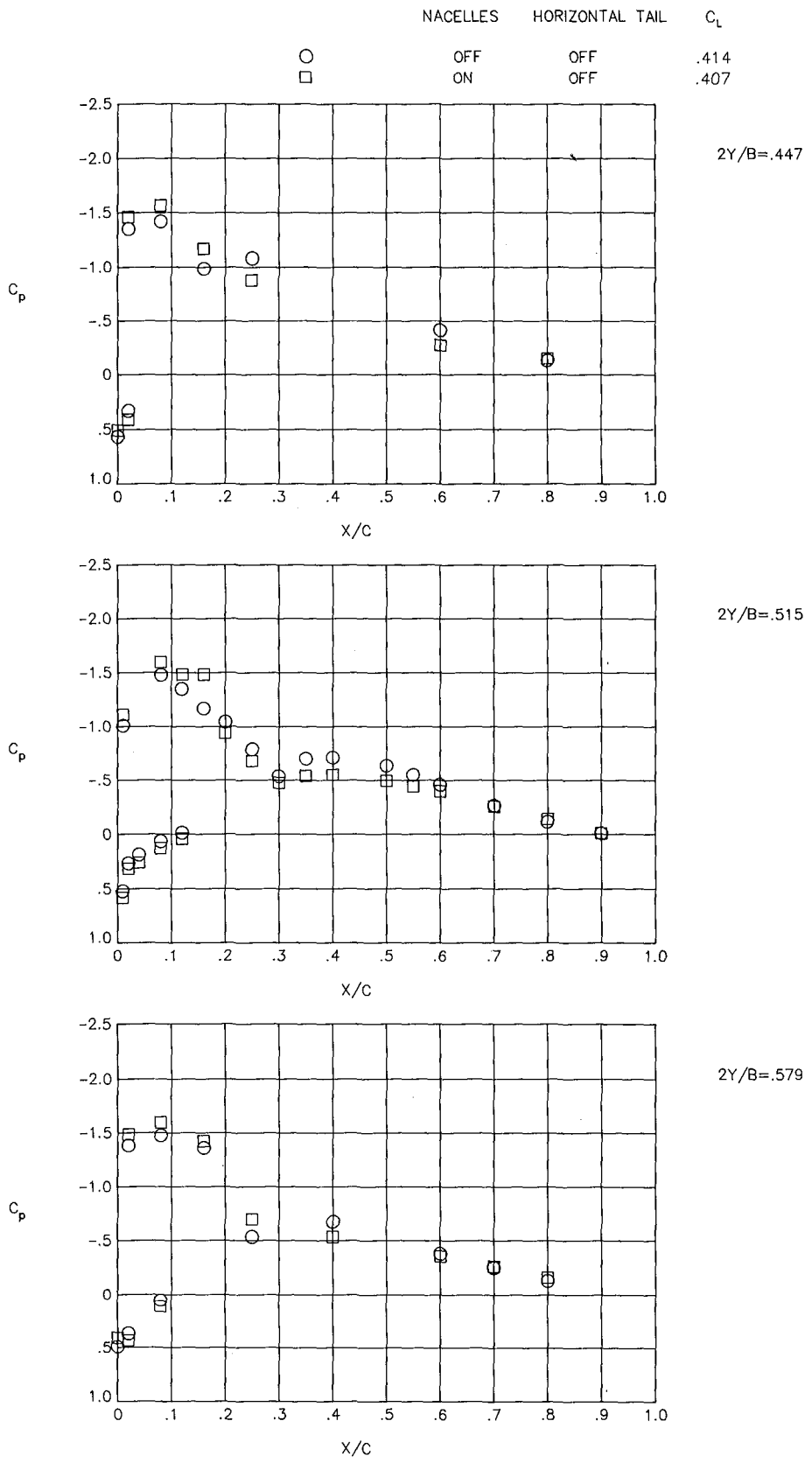

Figure 13.- Effect of nacelles on wing pressure distributions at M = 0.75.

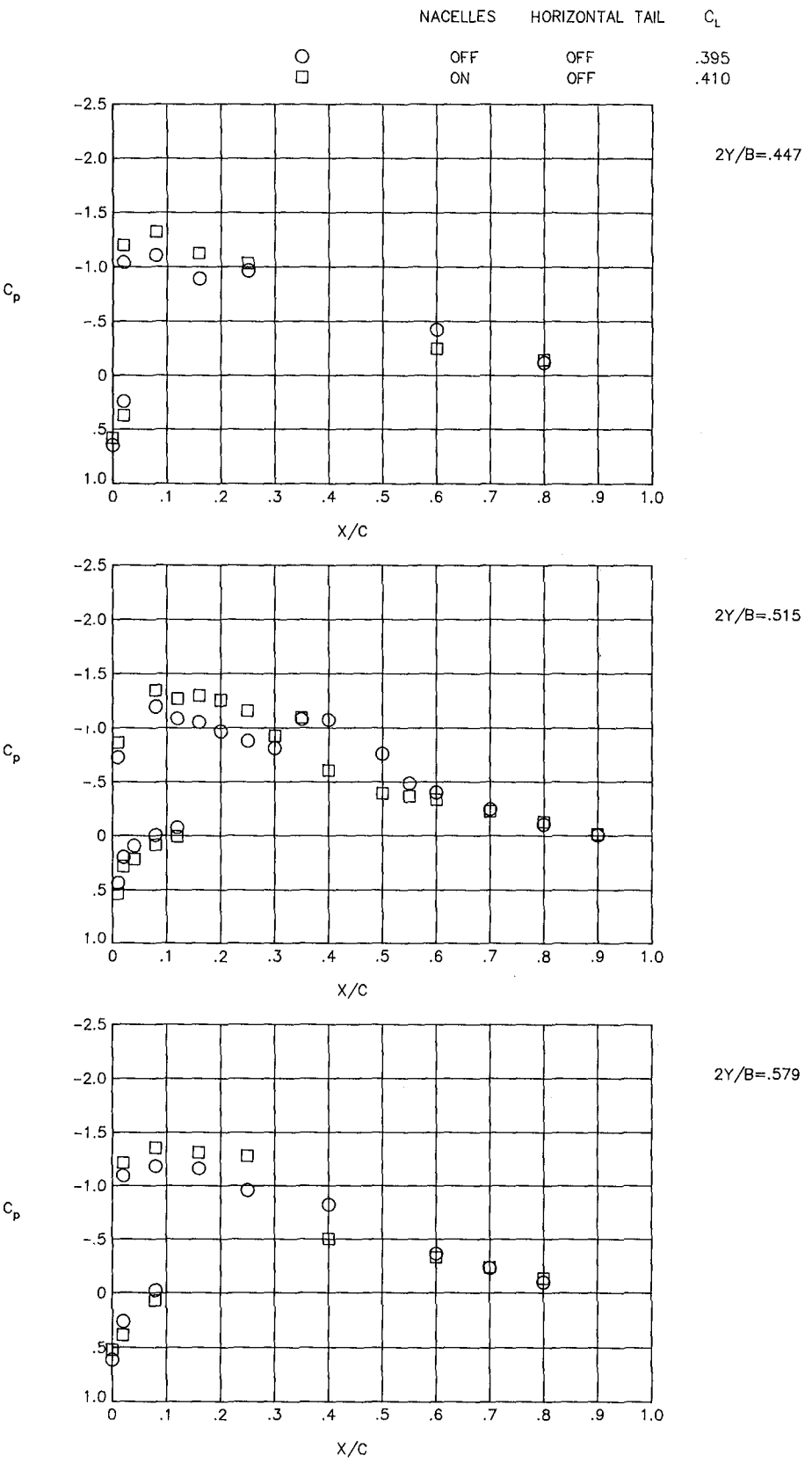

Figure 14.- Effect of nacelles on wing pressure distributions at M = 0.80.

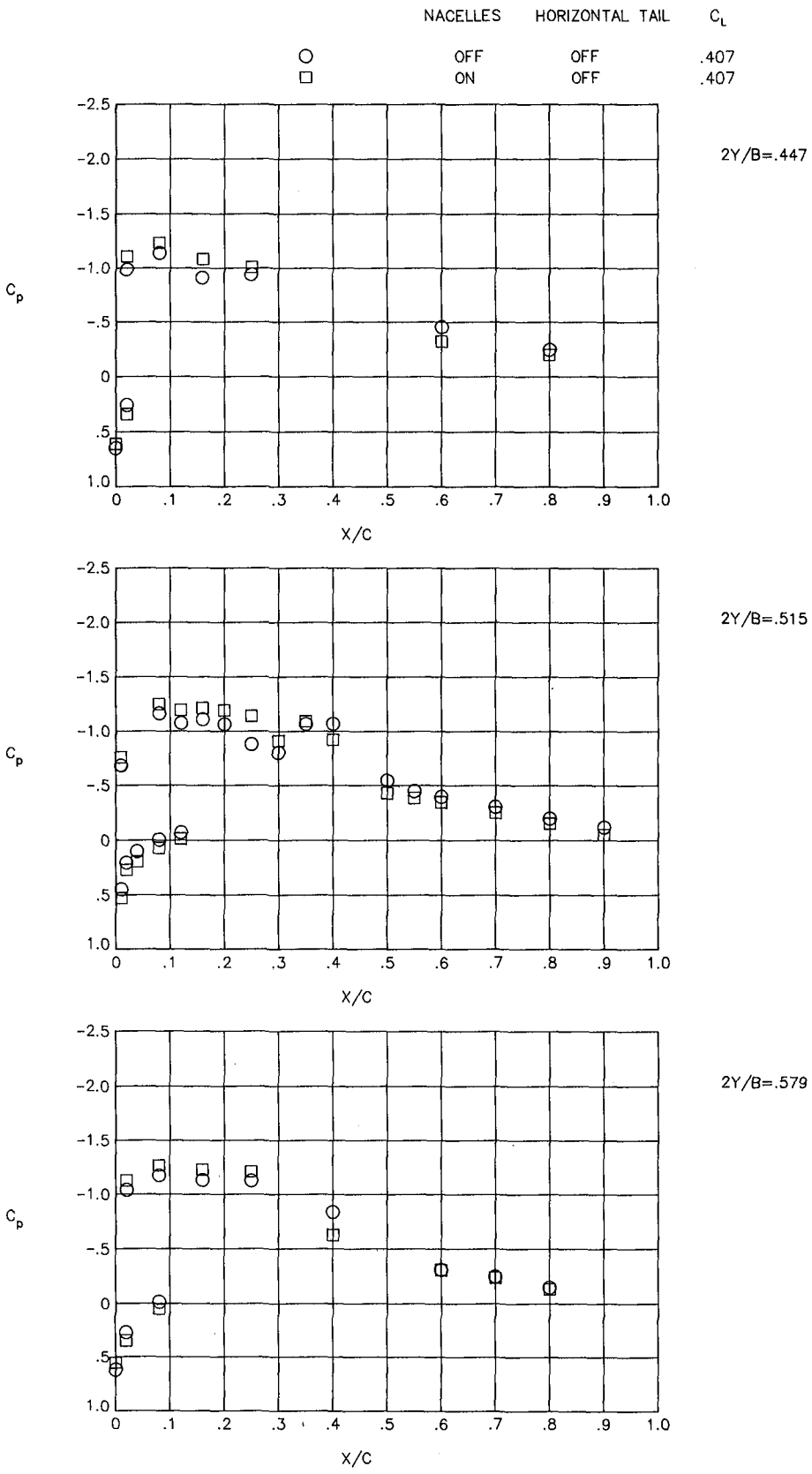

Figure 15.- Effect of nacelles on wing pressure distributions at M = 0.82.

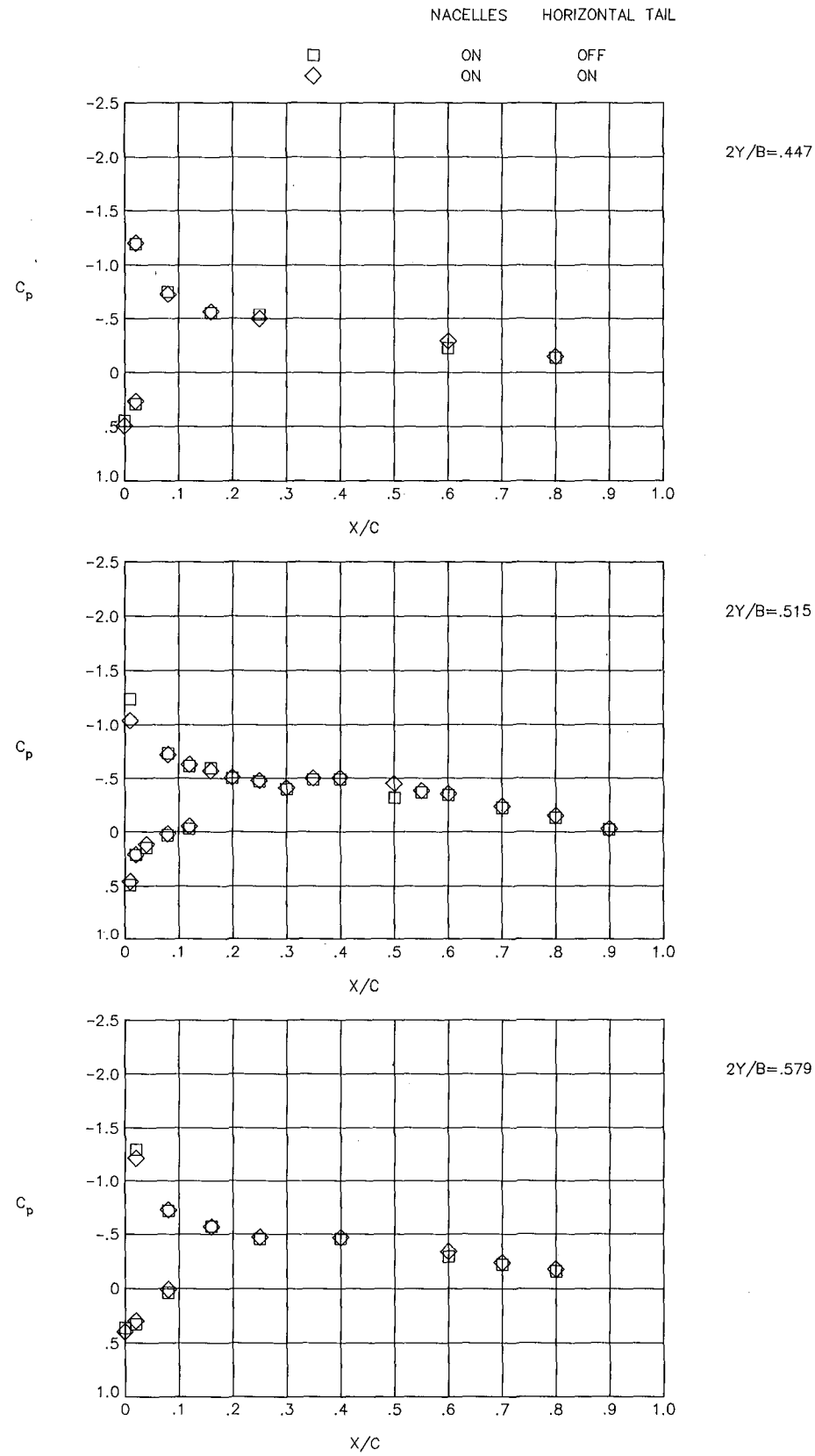

(a) α = 3.29.

Figure 16.- Effect of horizontal tail on wing pressure distributions at M = 0.40.

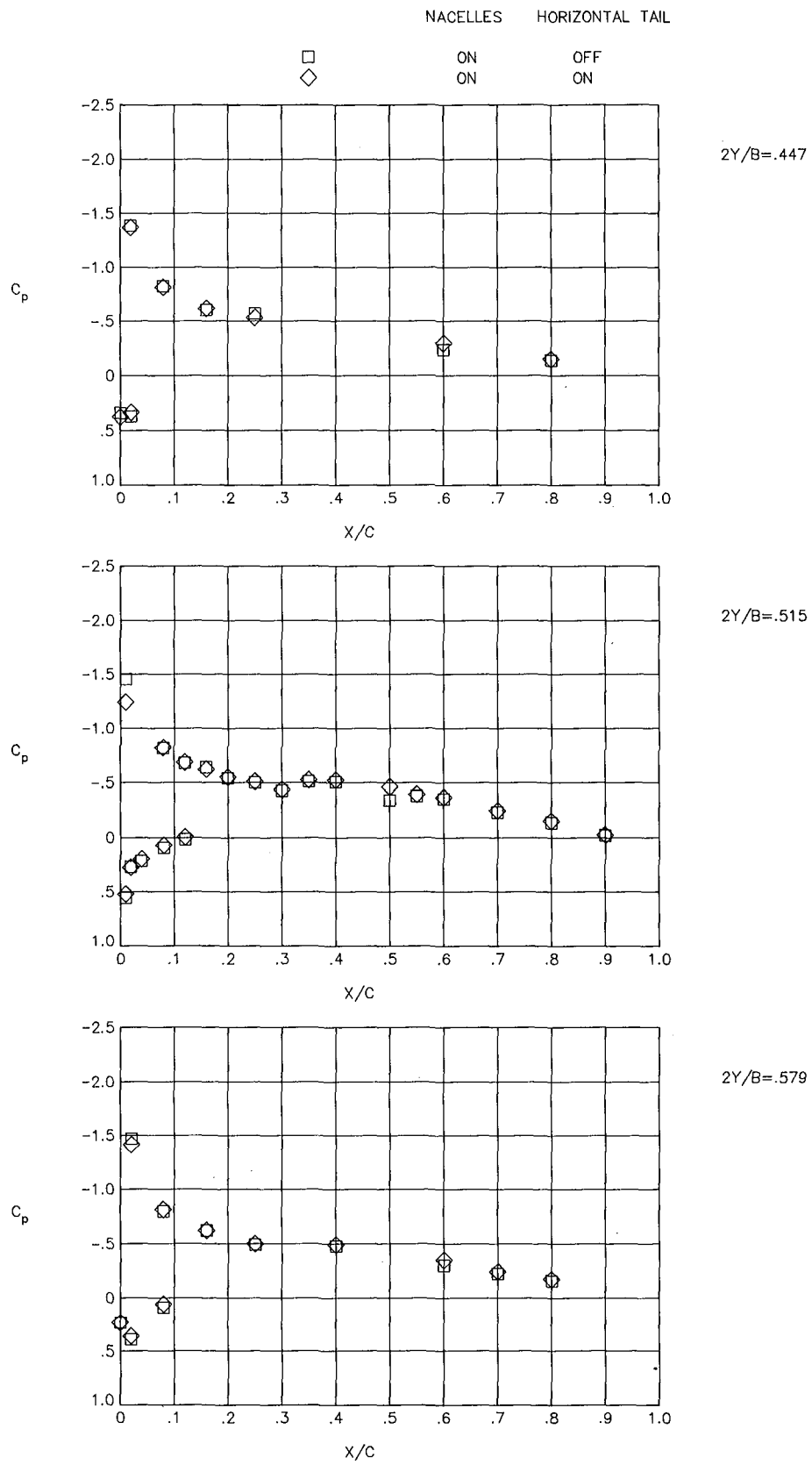

(b) α = 3.90.

Figure 16.- Continued.

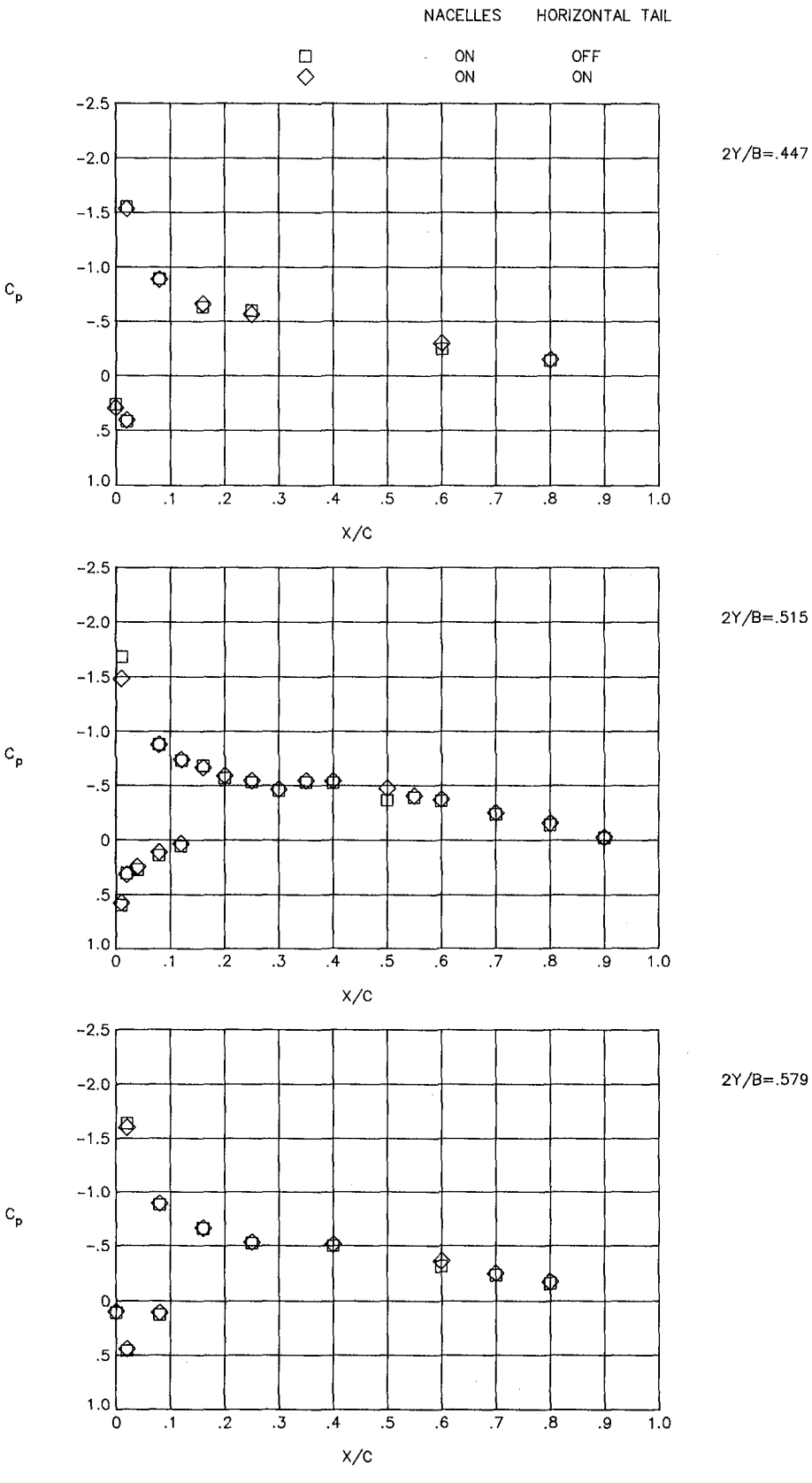

(c) α = 4.44.

Figure 16.- Continued.

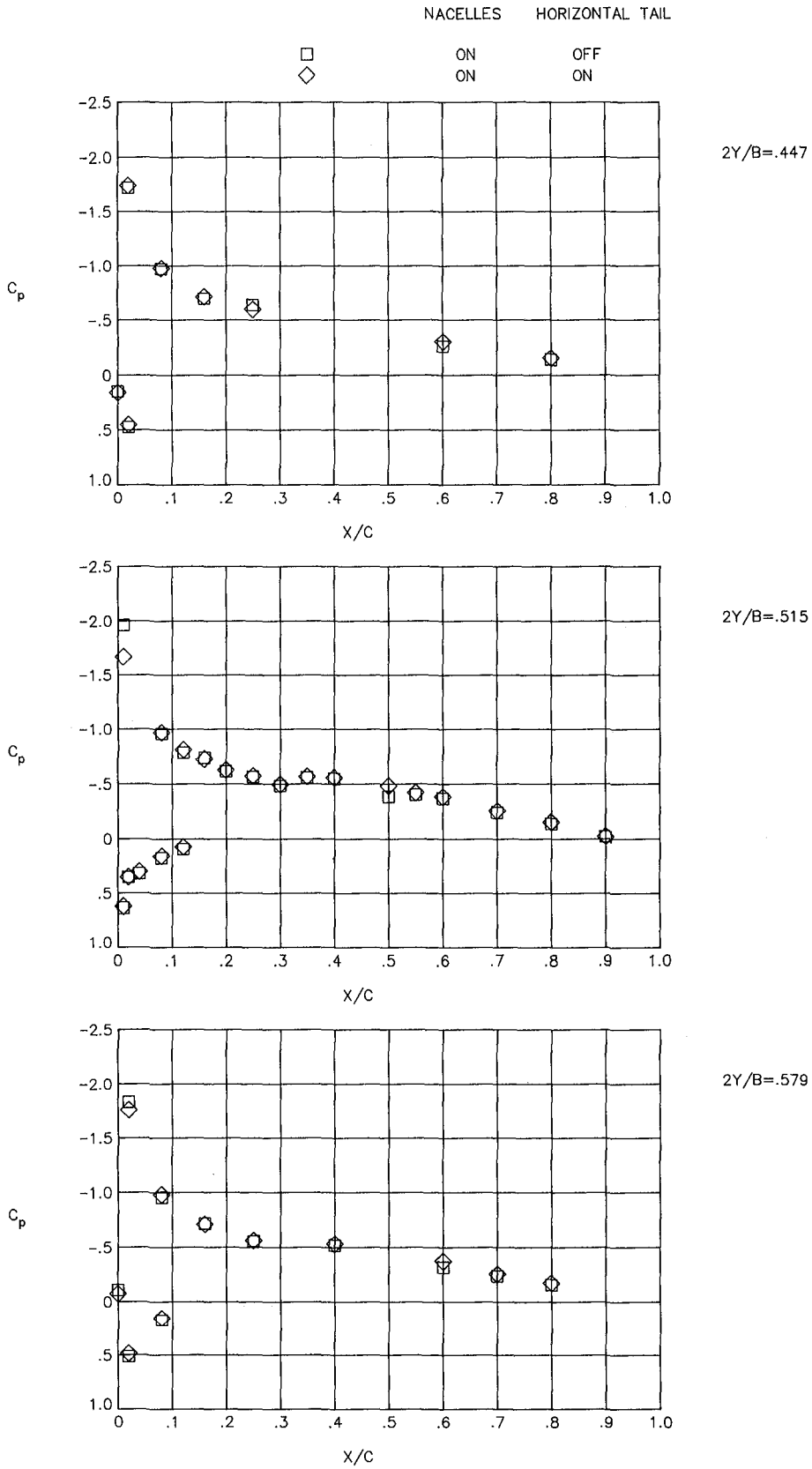

(d) α = 5.01.

Figure 16.- Continued.

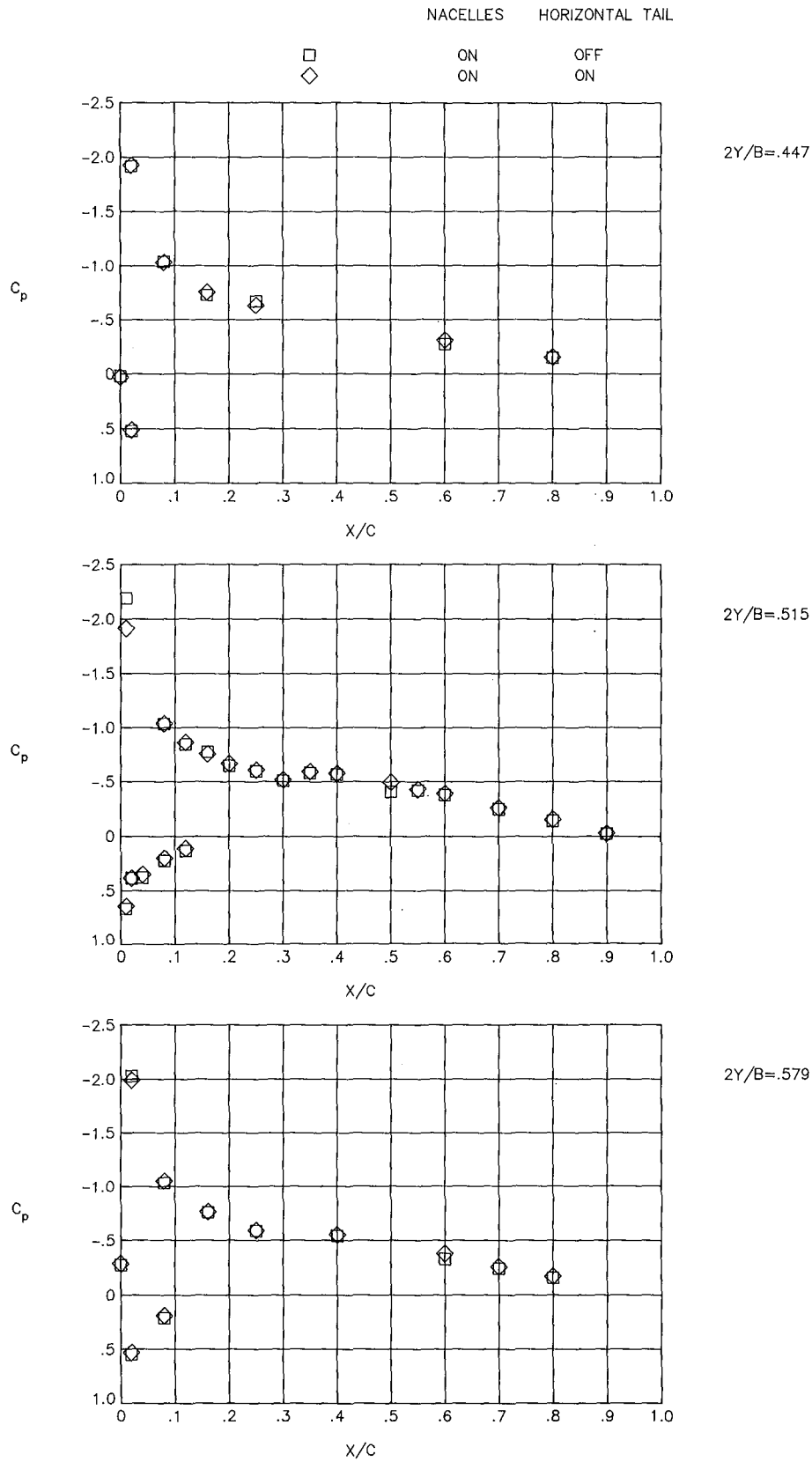

(e) α = 5.58.

Figure 16.- Concluded.

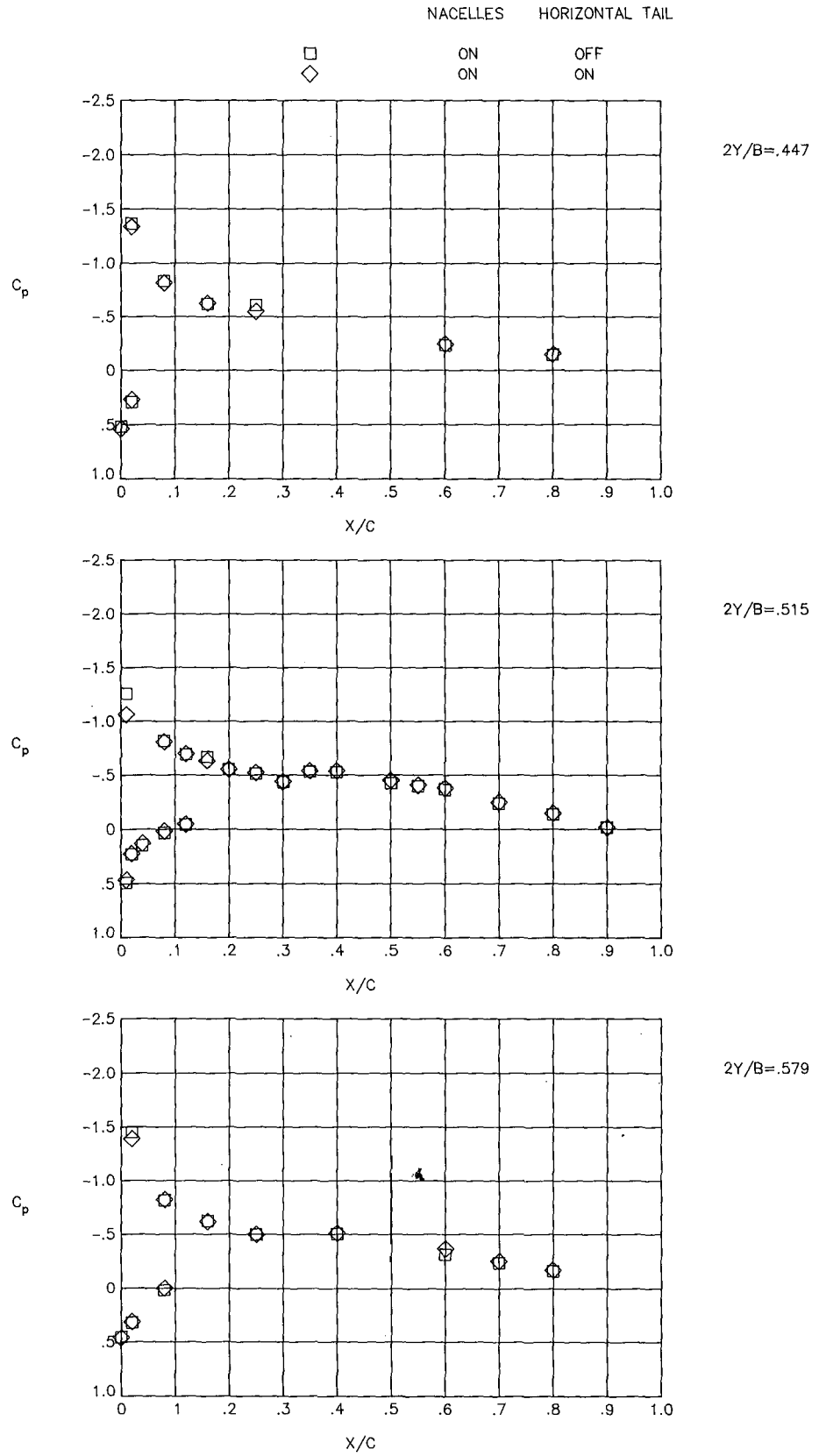

(a) α = 3.30.

Figure 17.- Effect of horizontal tail on wing pressure distributions at M = 0.60.

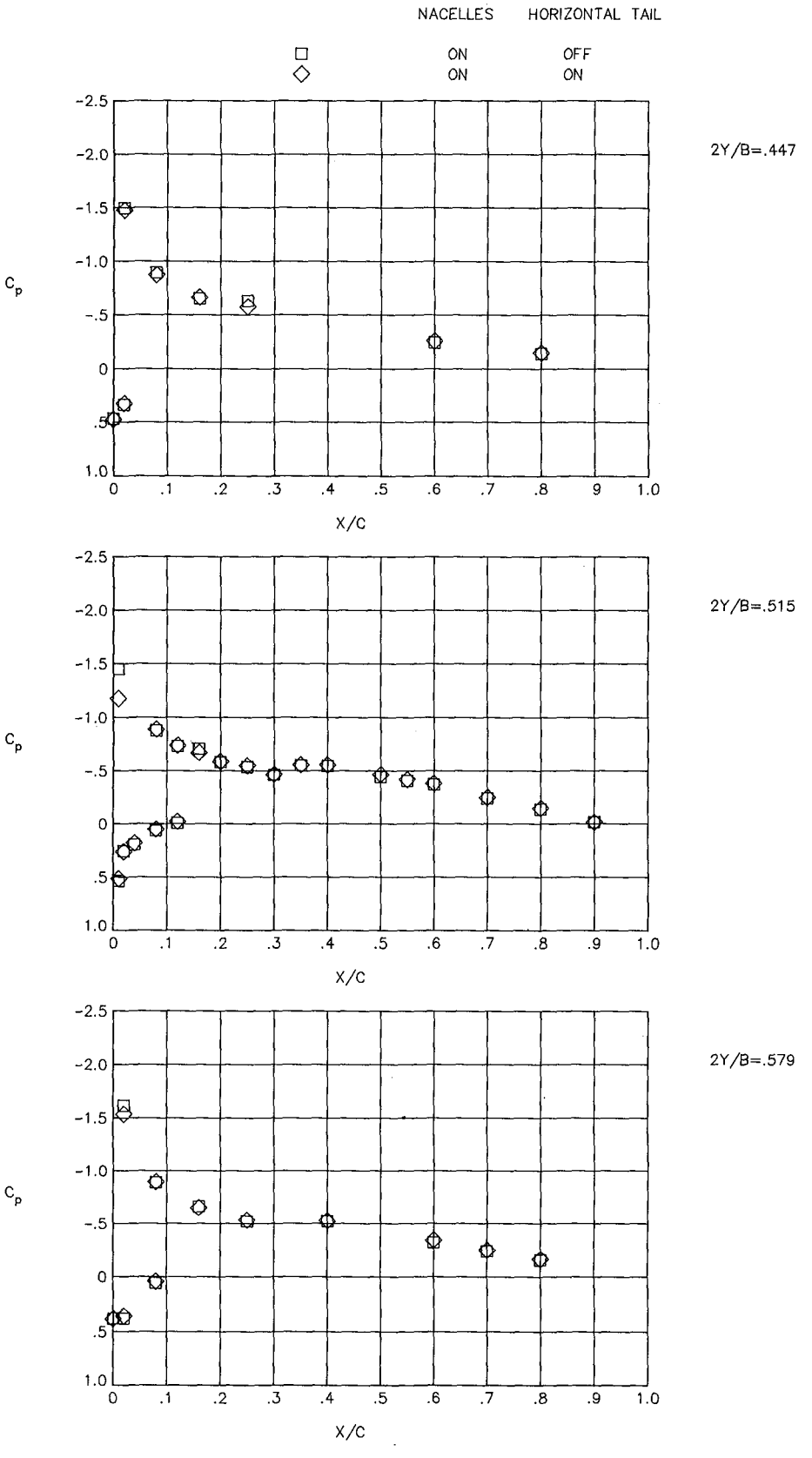

(b) α = 3.75.

Figure 17.- Continued.

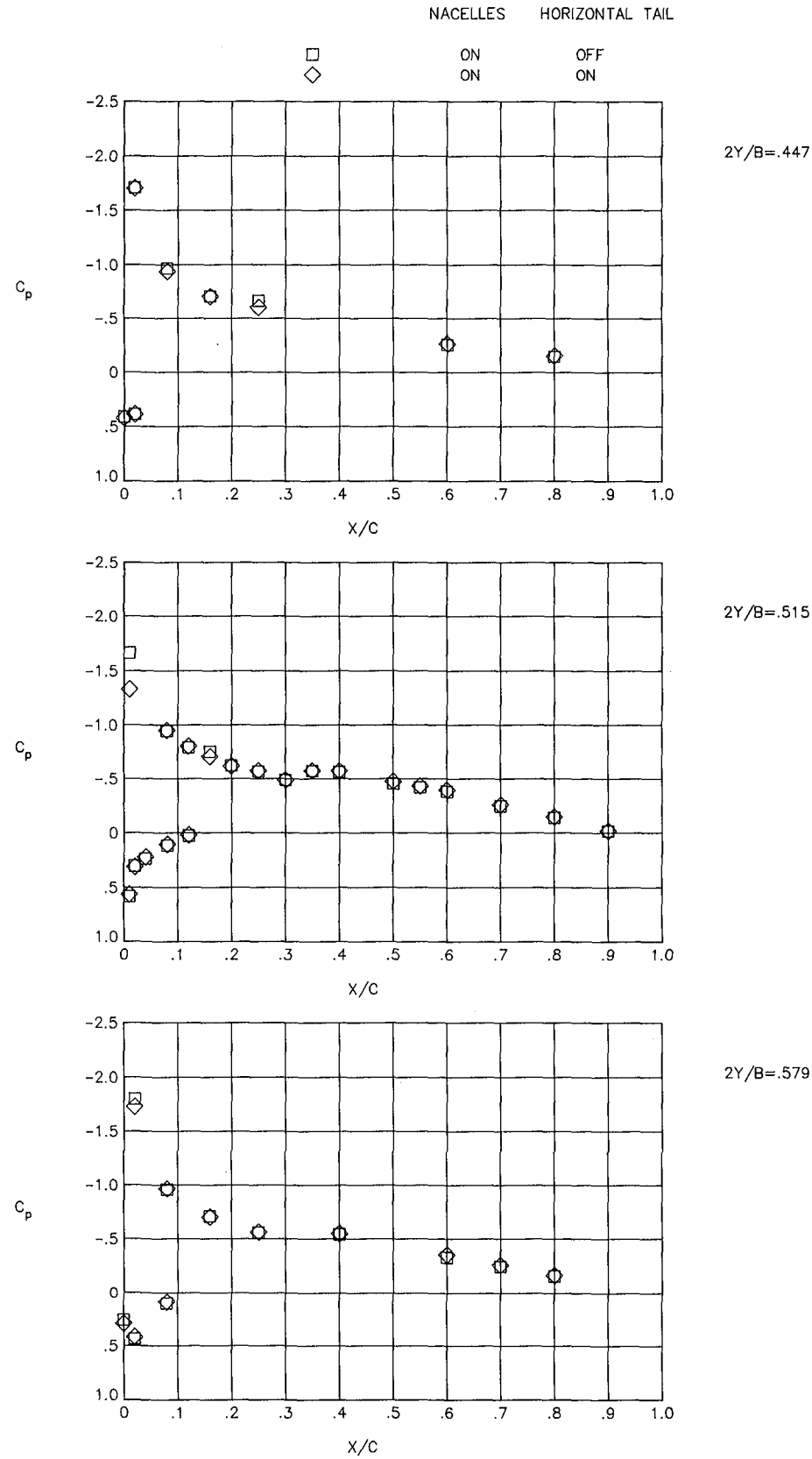

(c) α = 4.28.

Figure 17.- Continued.

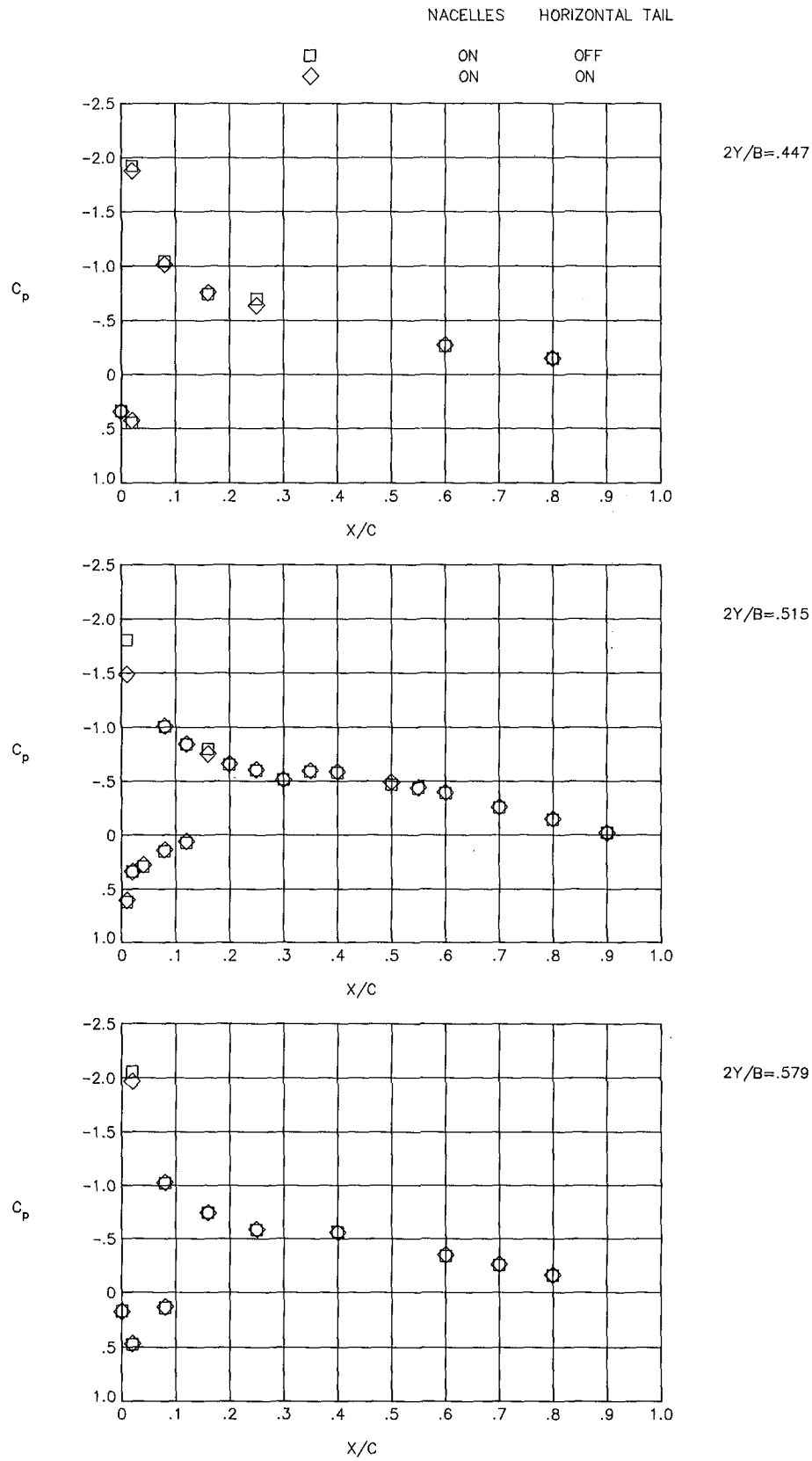

(d) α = 4.79.

Figure 17.- Continued.

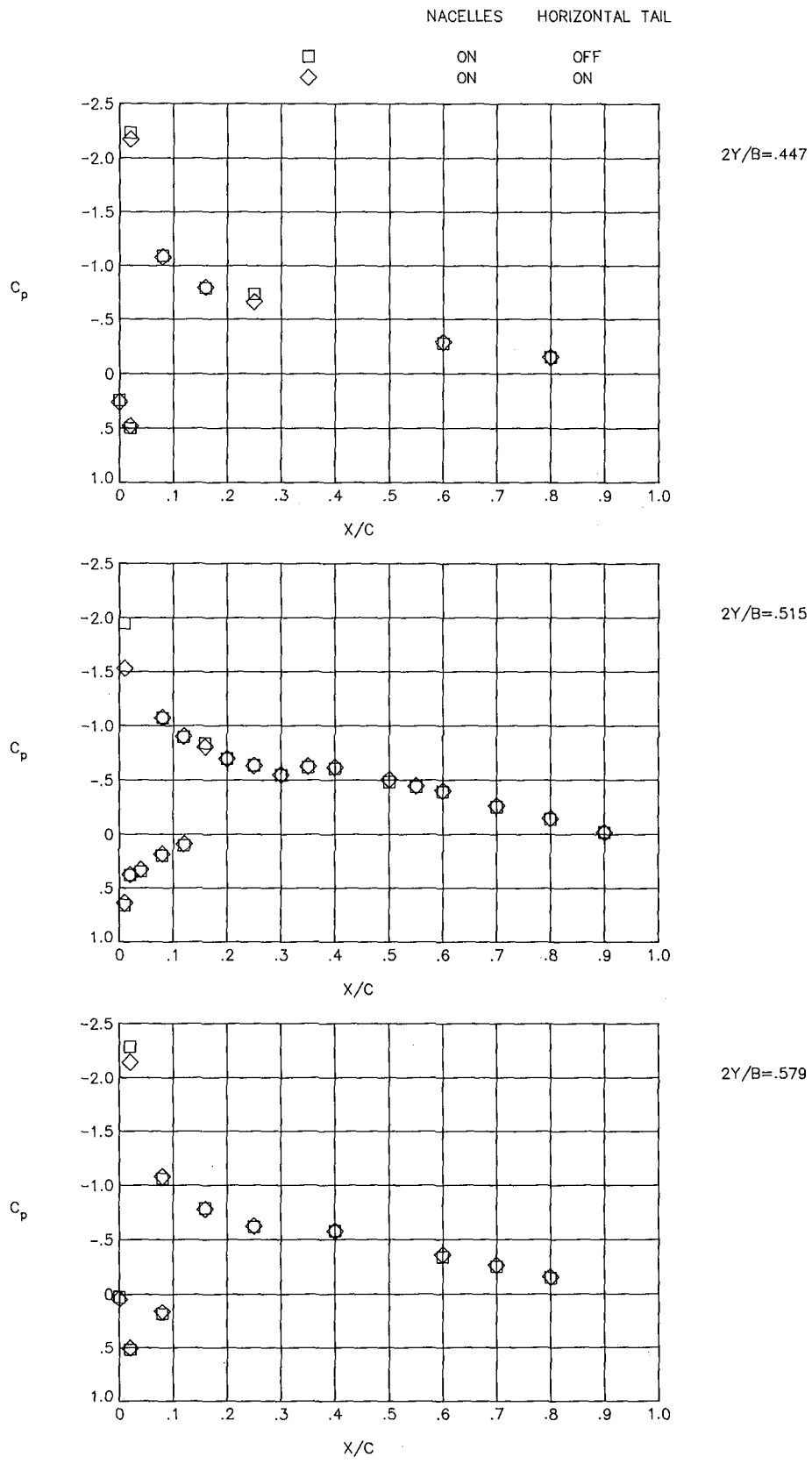

(e) α = 5.36.

Figure 17.- Concluded.

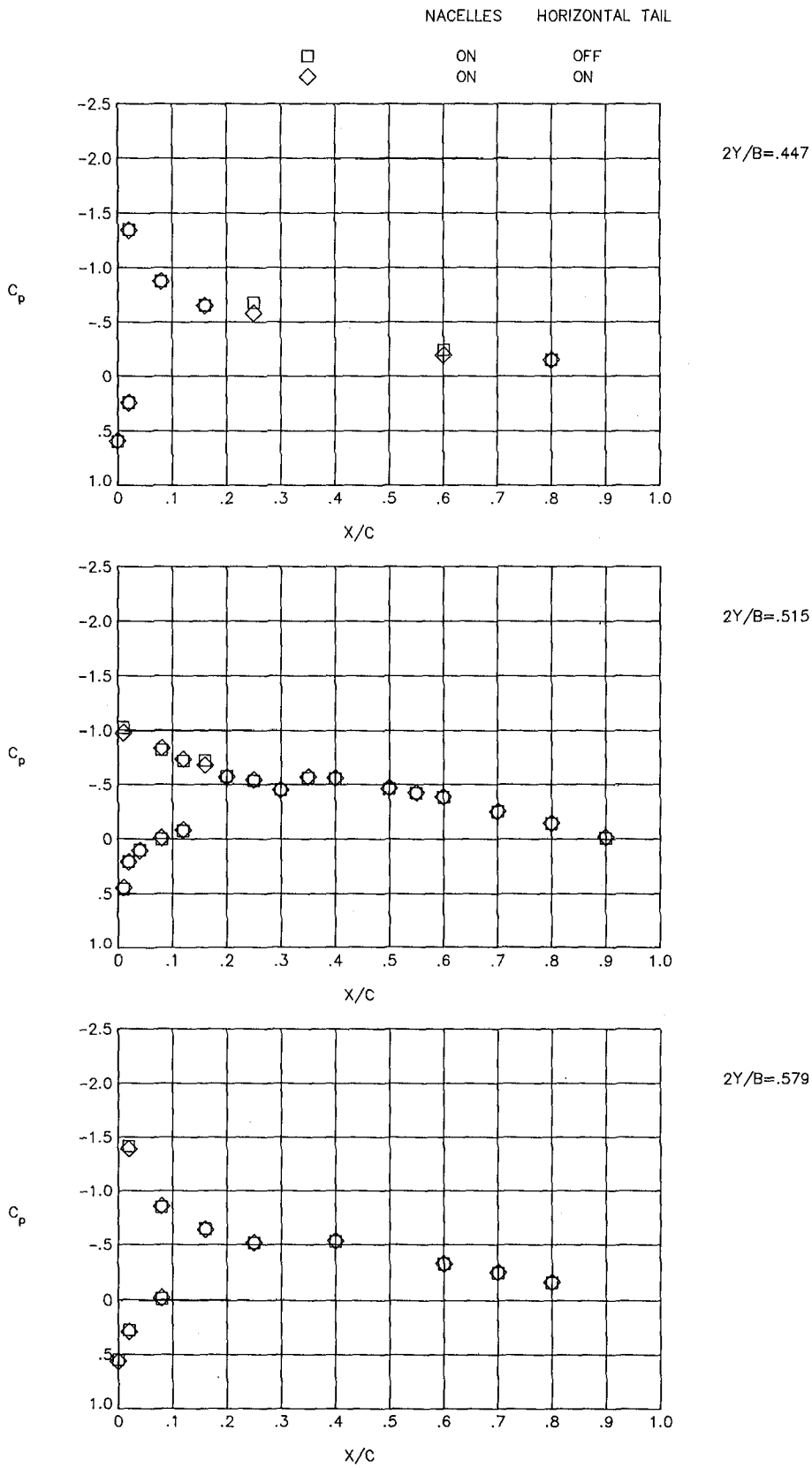

(a) α = 3.09.

Figure 18.- Effect of horizontal tail on wing pressure distributions at M = 0.70.

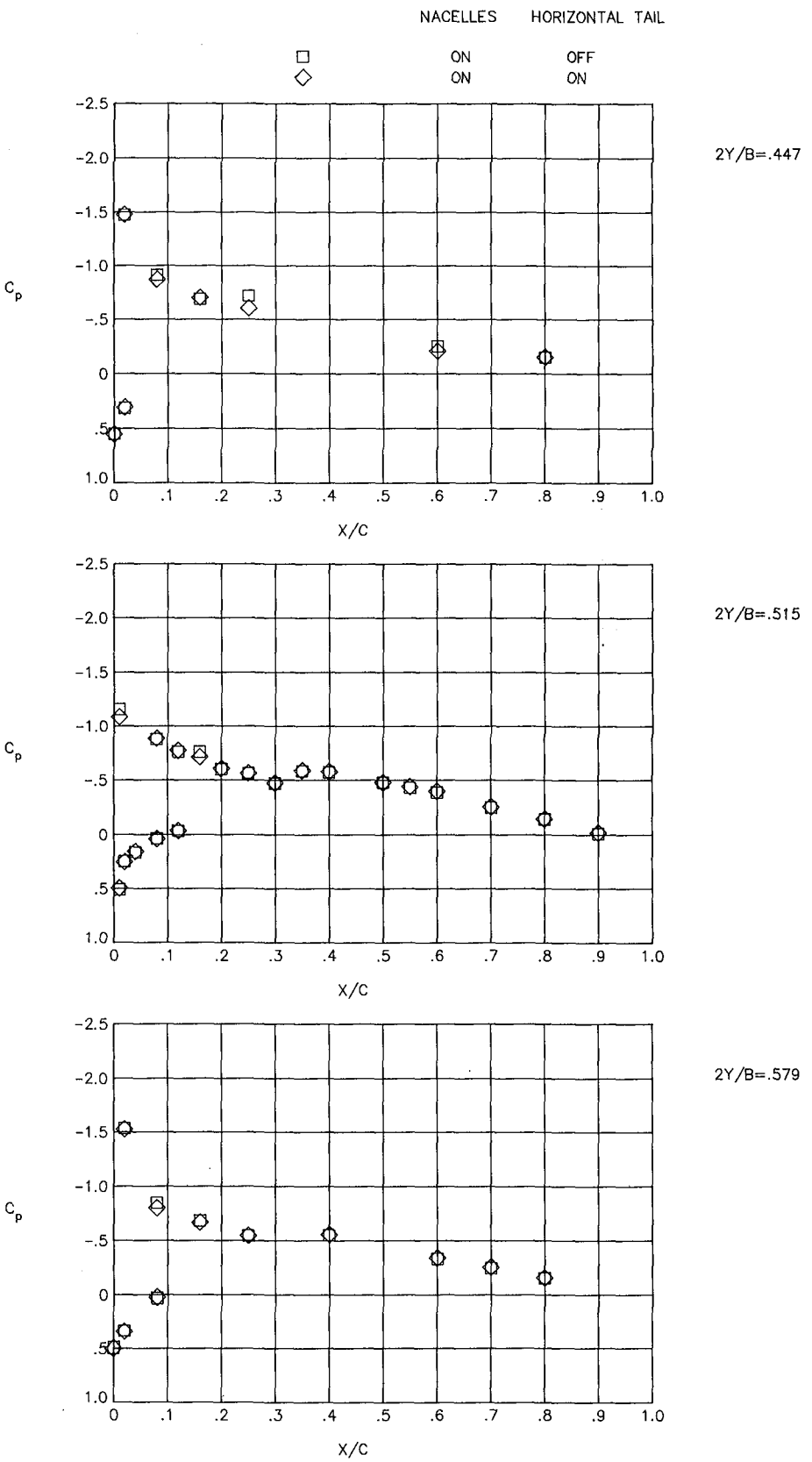

(b) α = 3.59.

Figure 18.- Continued.

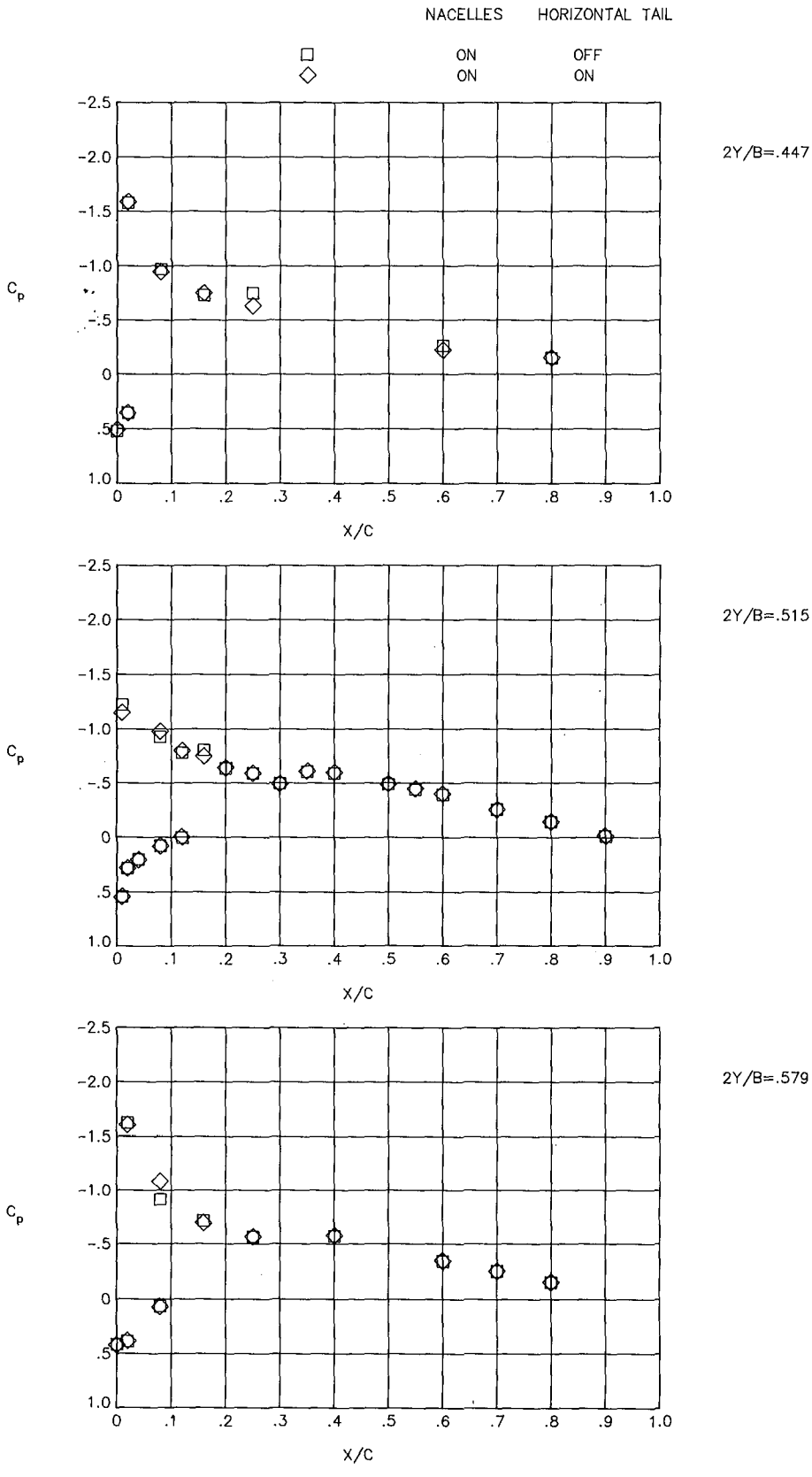

(c) α = 4.08.

Figure 18.- Continued.

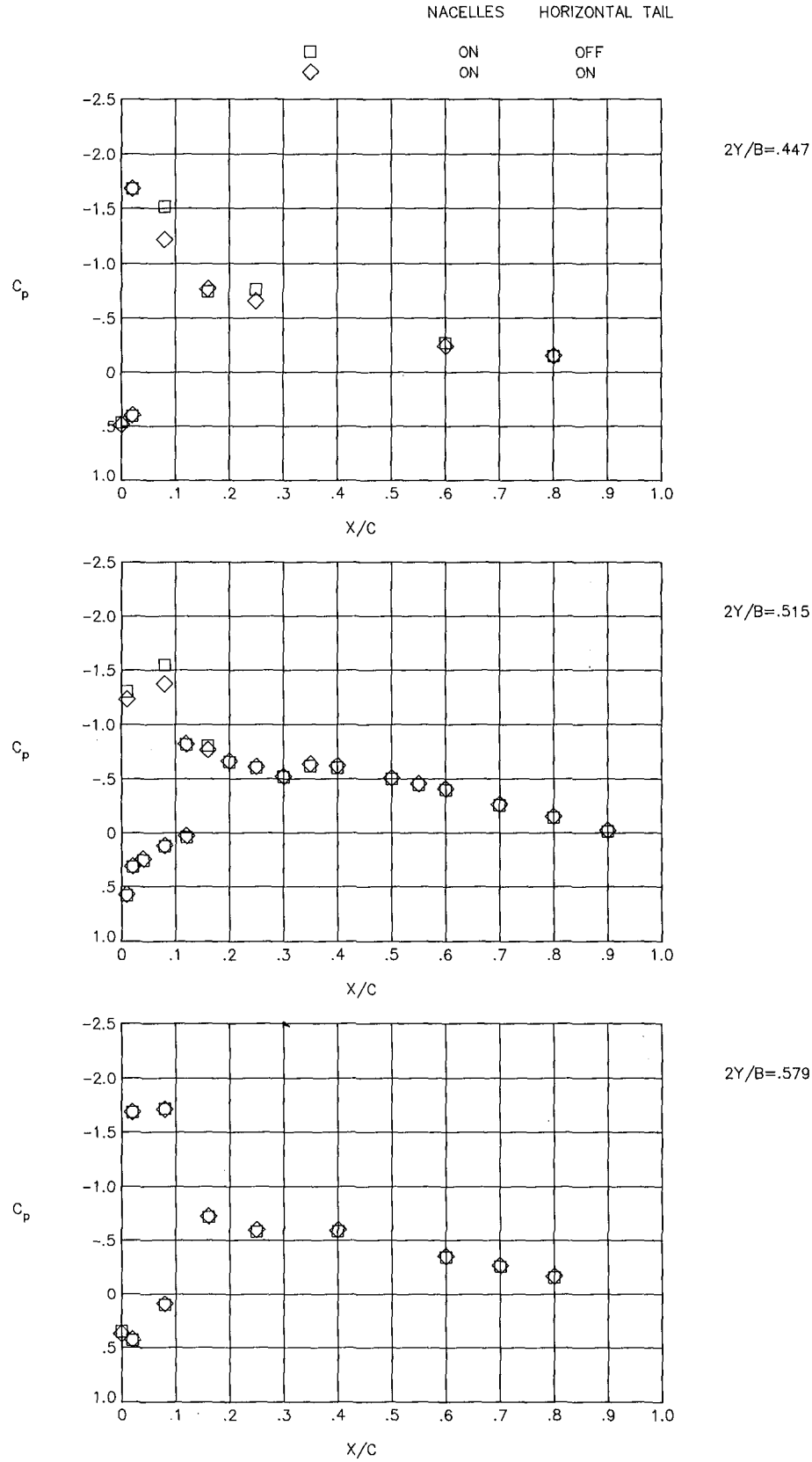

(d) α = 4.58.

Figure 18.- Continued.

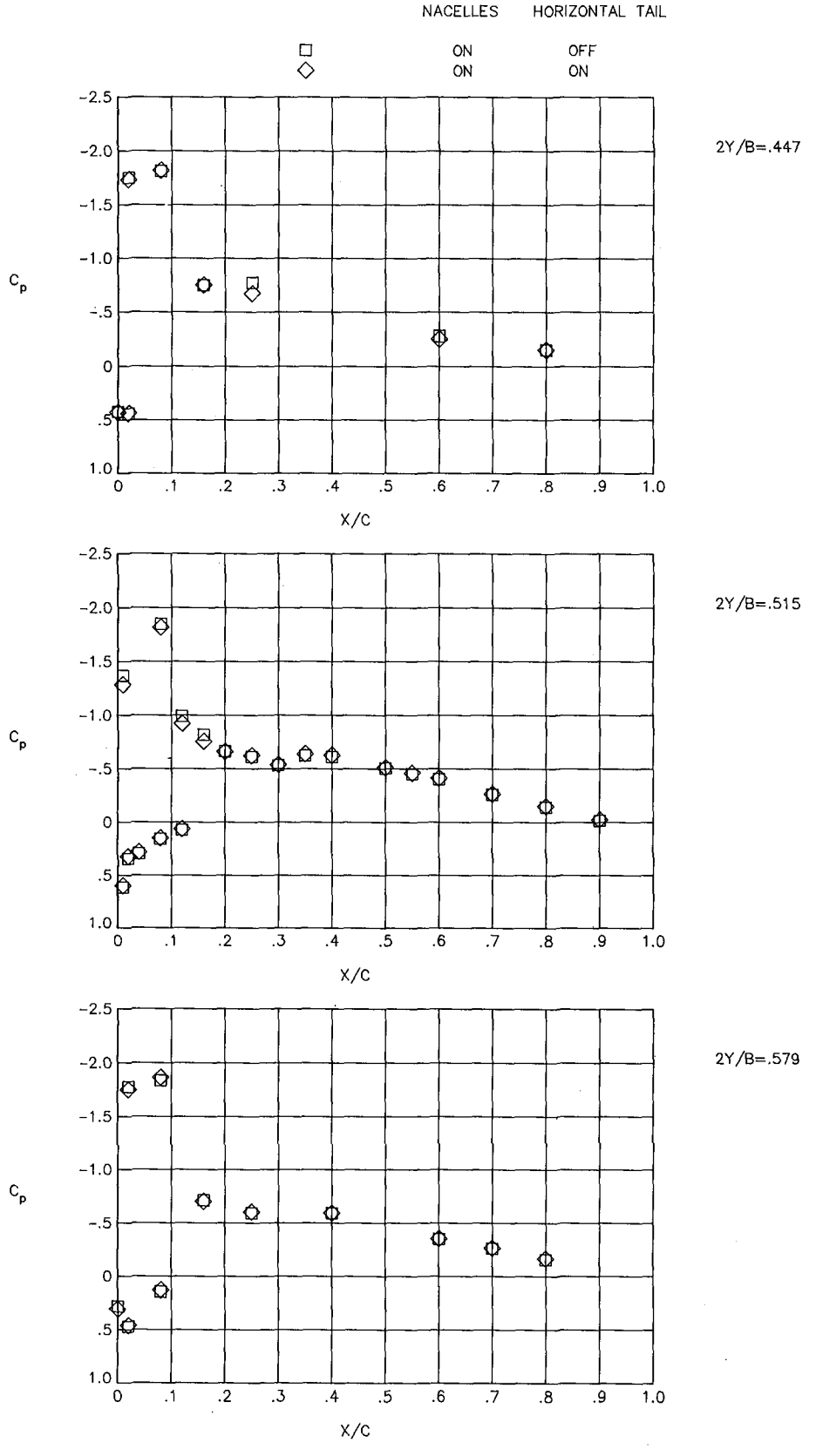

(e) α = 5.06.

Figure 18.- Concluded.

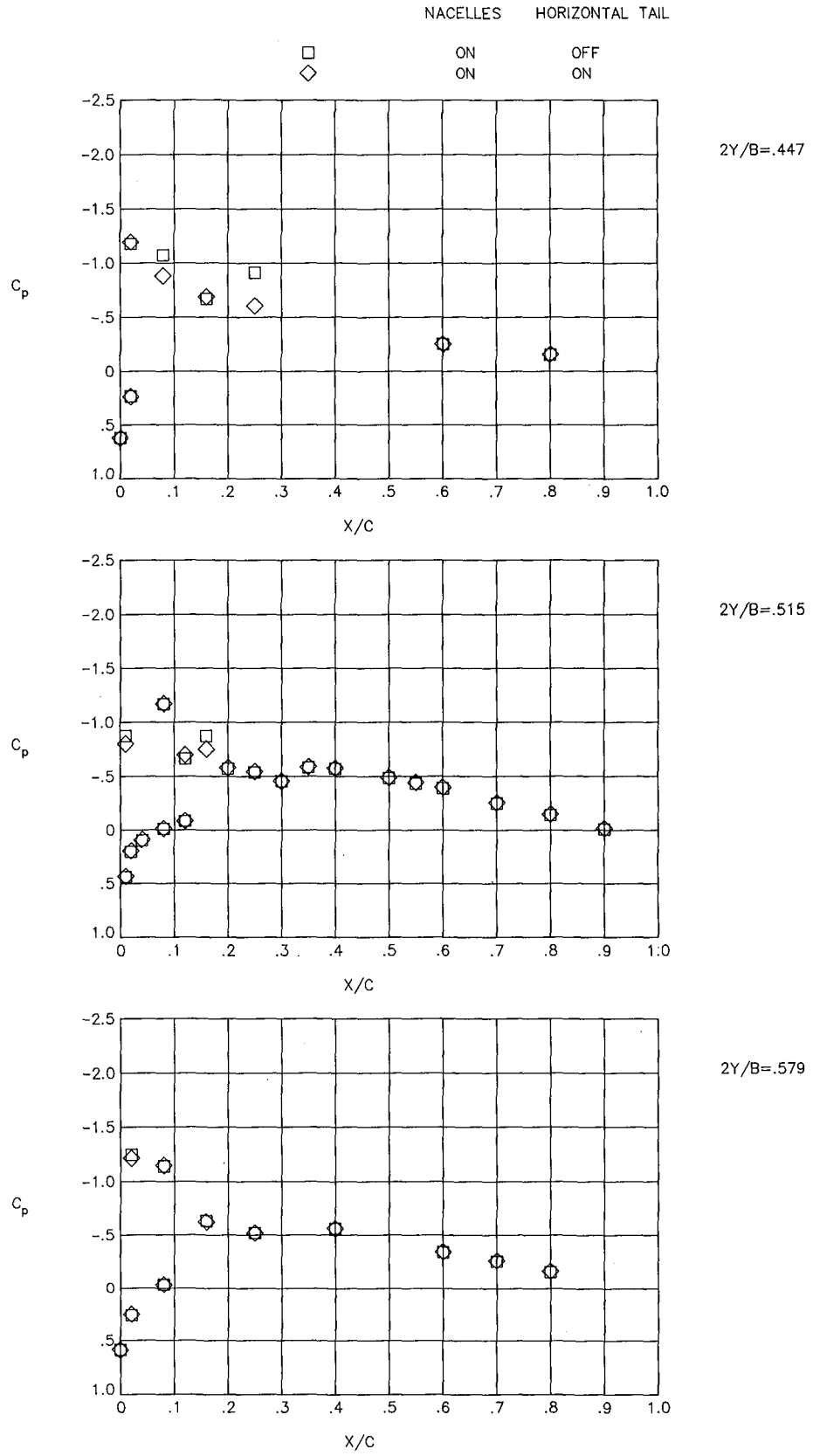

(a) α = 3.07.

Figure 19.- Effect of horizontal tail on wing pressure distributions at M = 0.75.

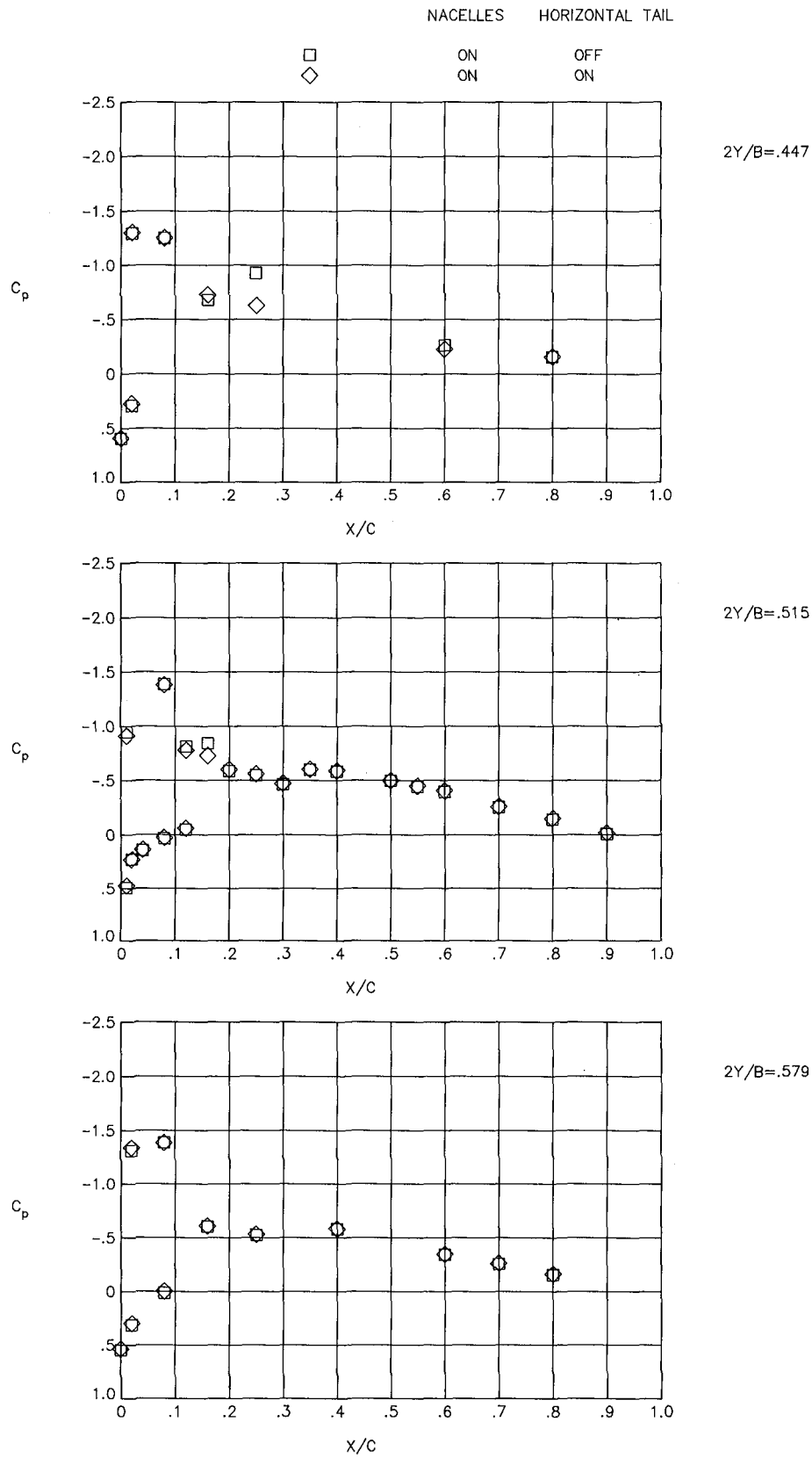

(b) α = 3.52.

Figure 19.- Continued.

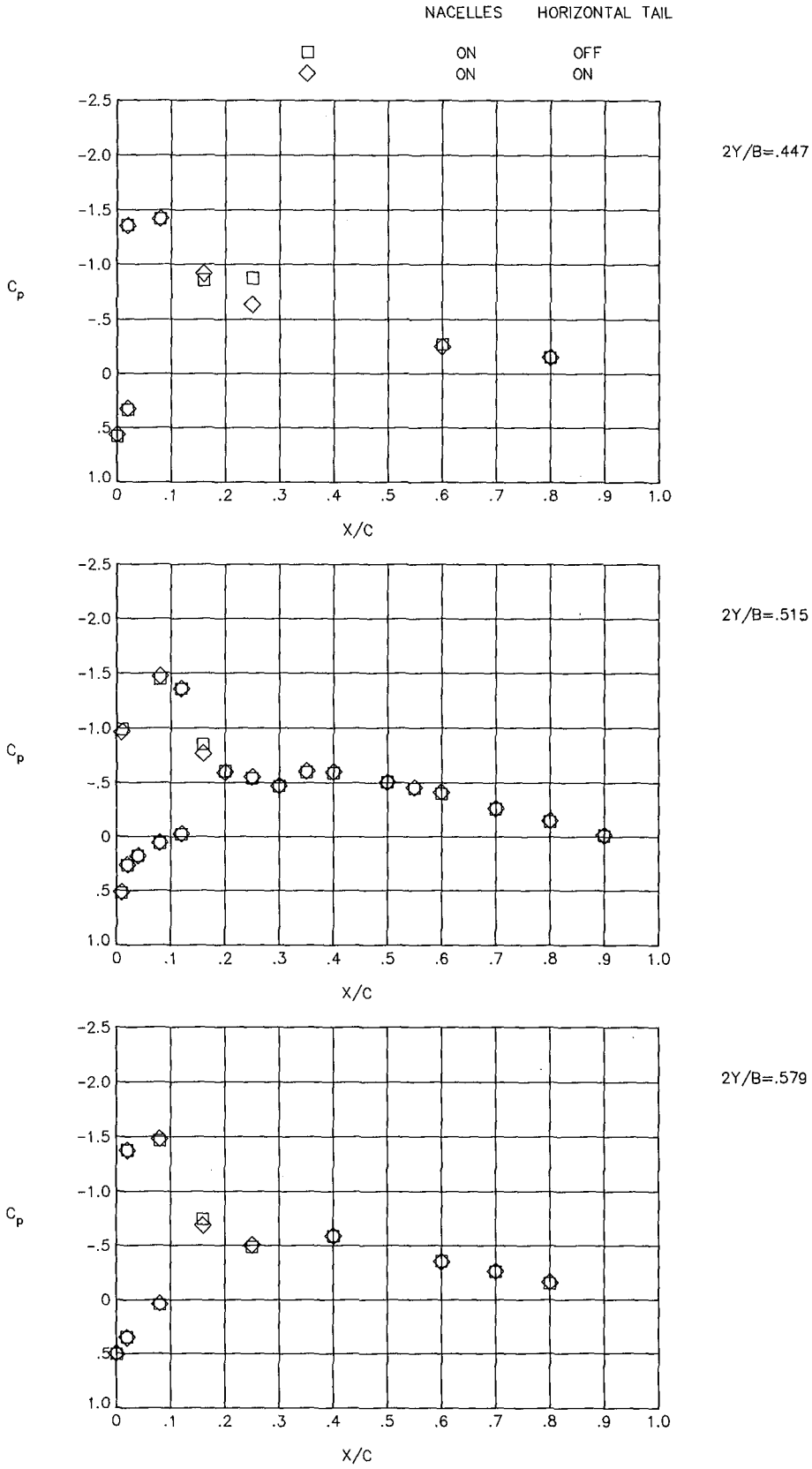

(c) α = 3.97.

Figure 19.- Continued.

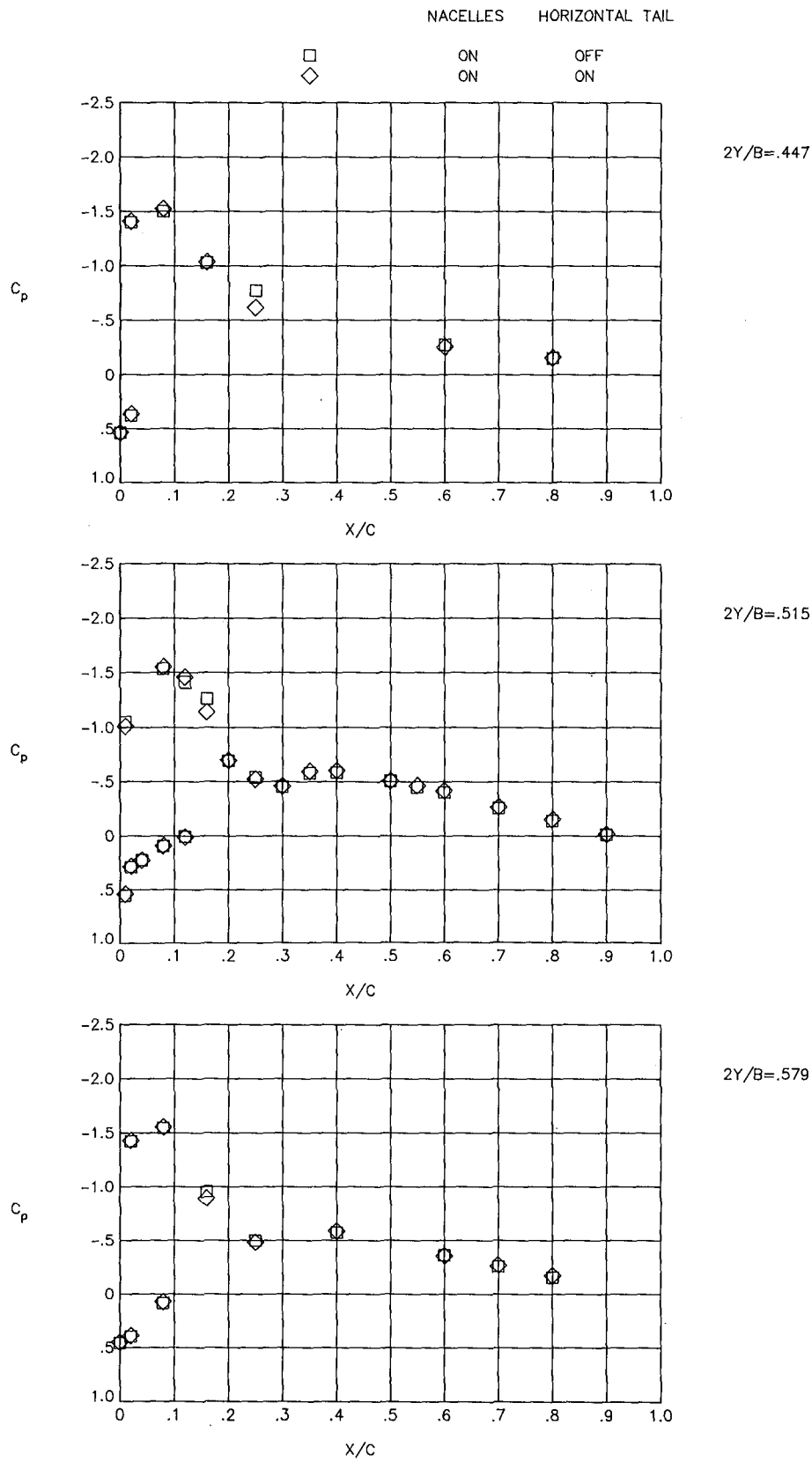

(d) α = 4.43.

Figure 19.- Continued.

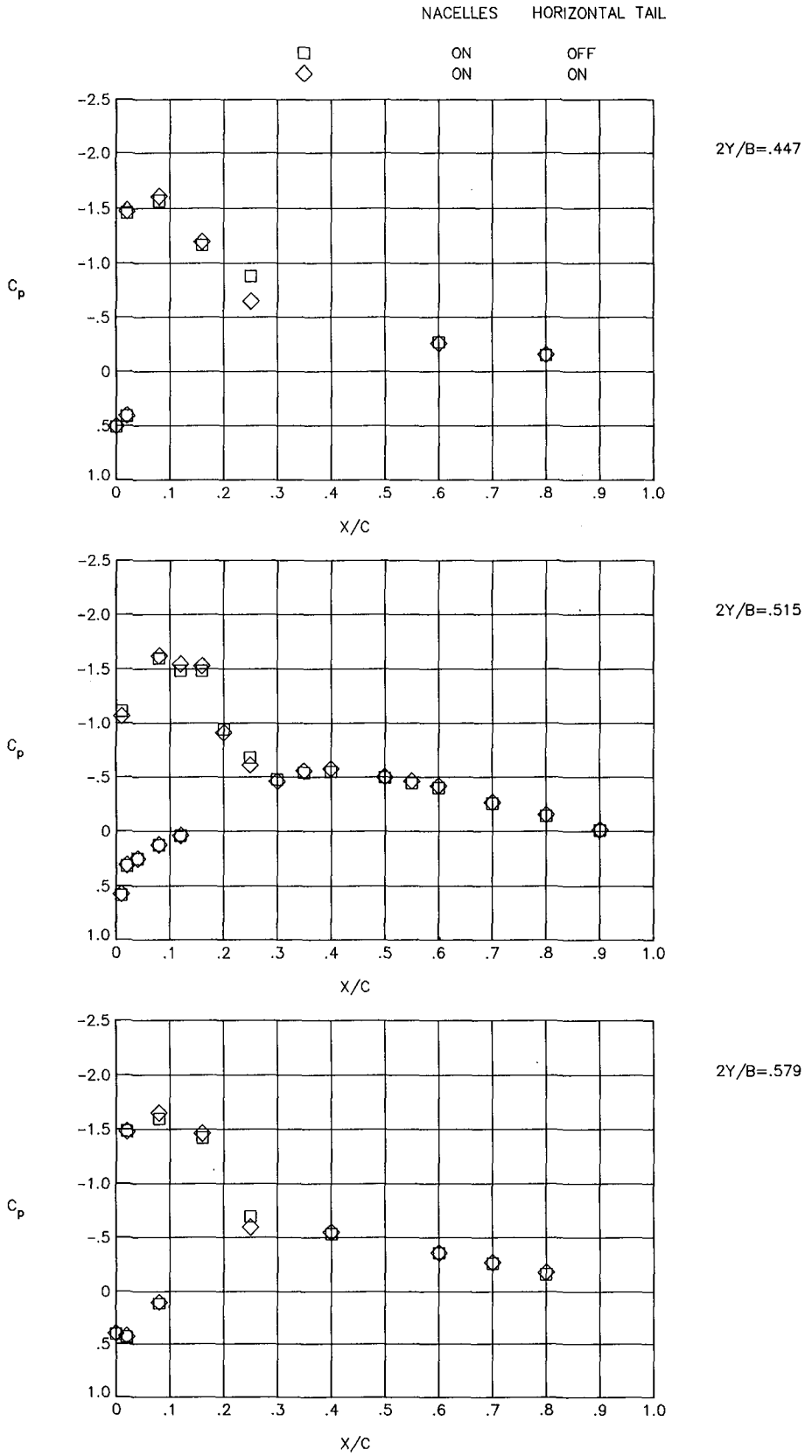

(e) α = 4.89.

Figure 19.- Concluded.

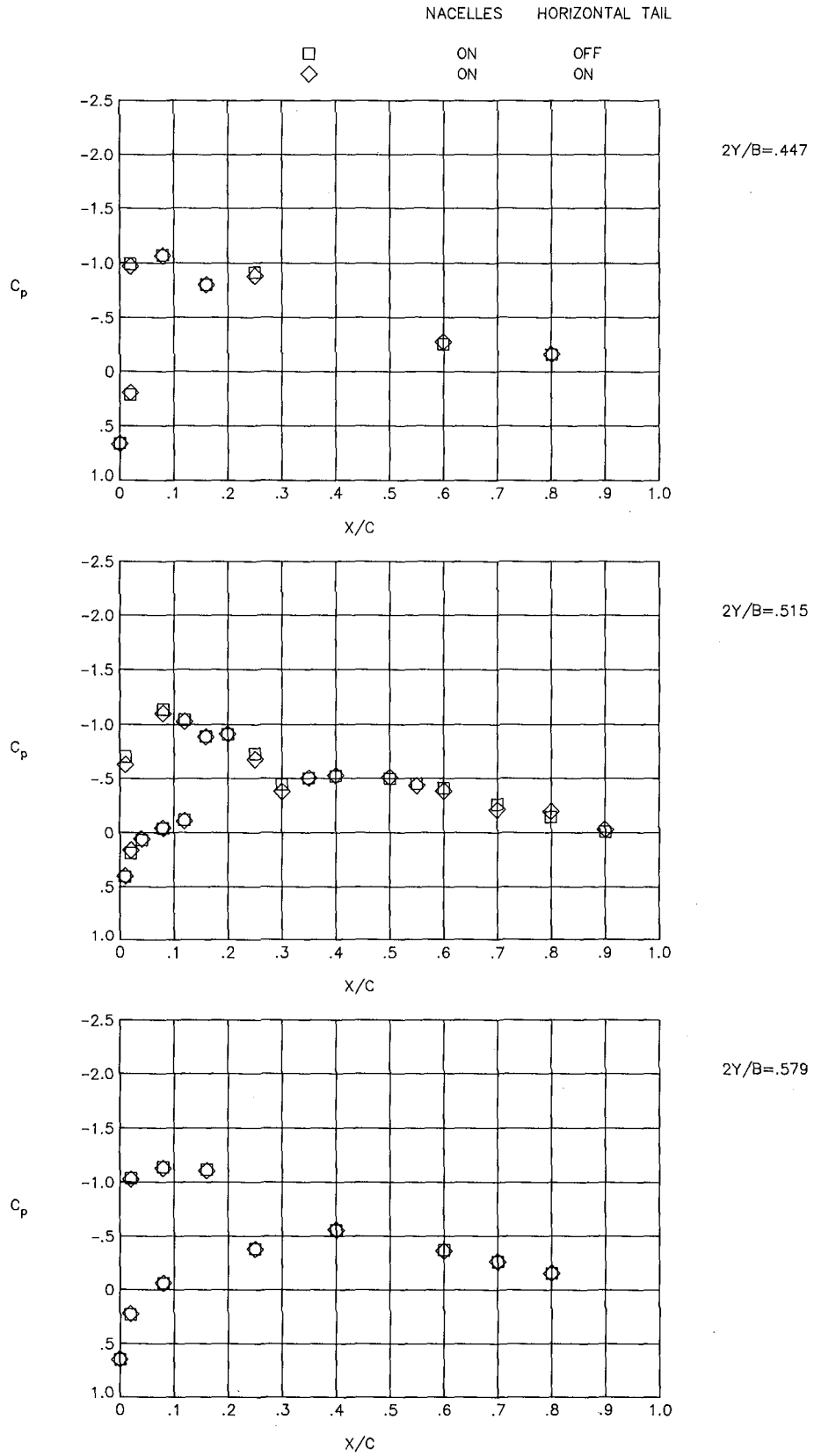

(a) α = 2.94.

Figure 20.- Effect of horizontal tail on wing pressure distributions at M = 0.80.

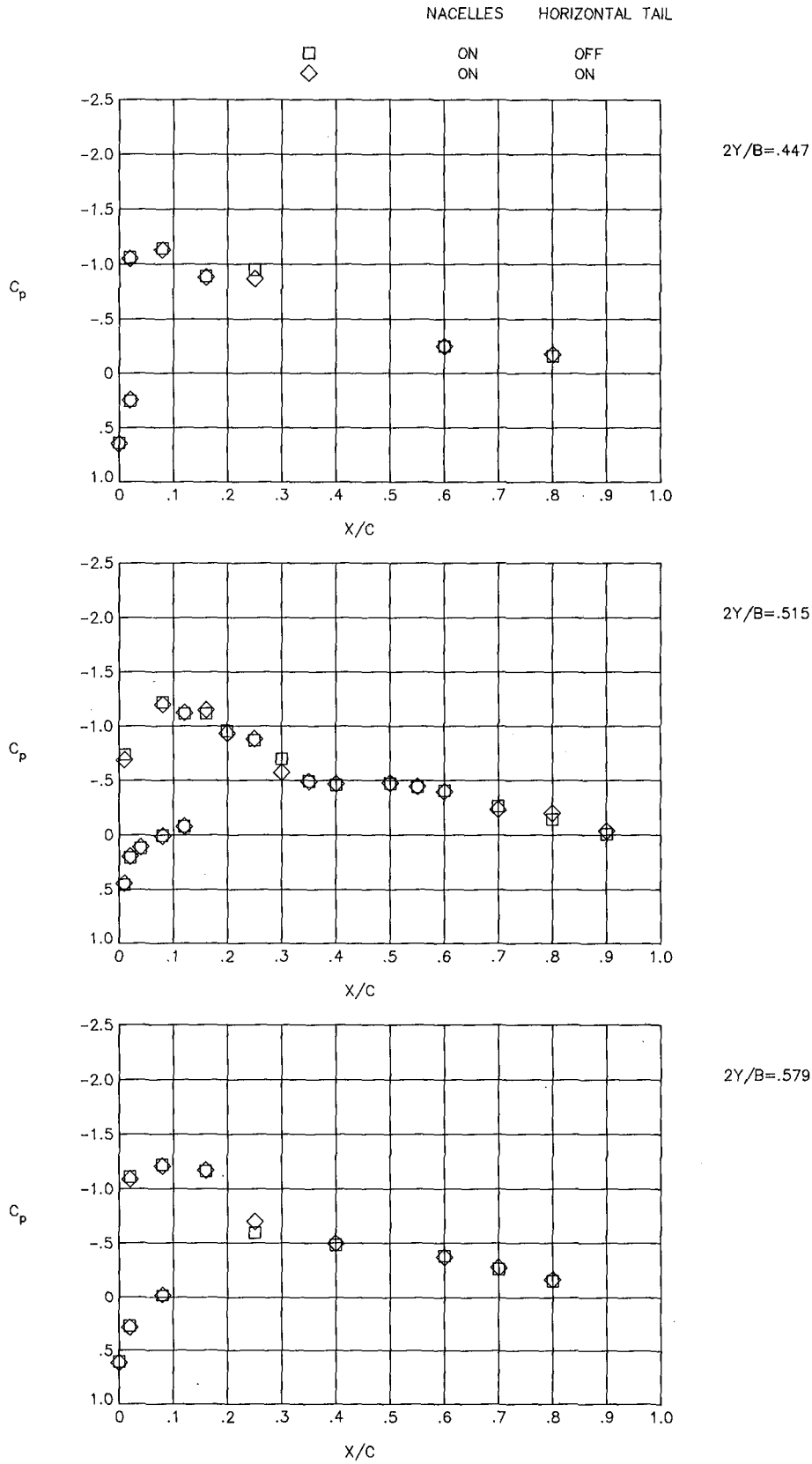

(b) α = 3.43.

Figure 20.- Continued.

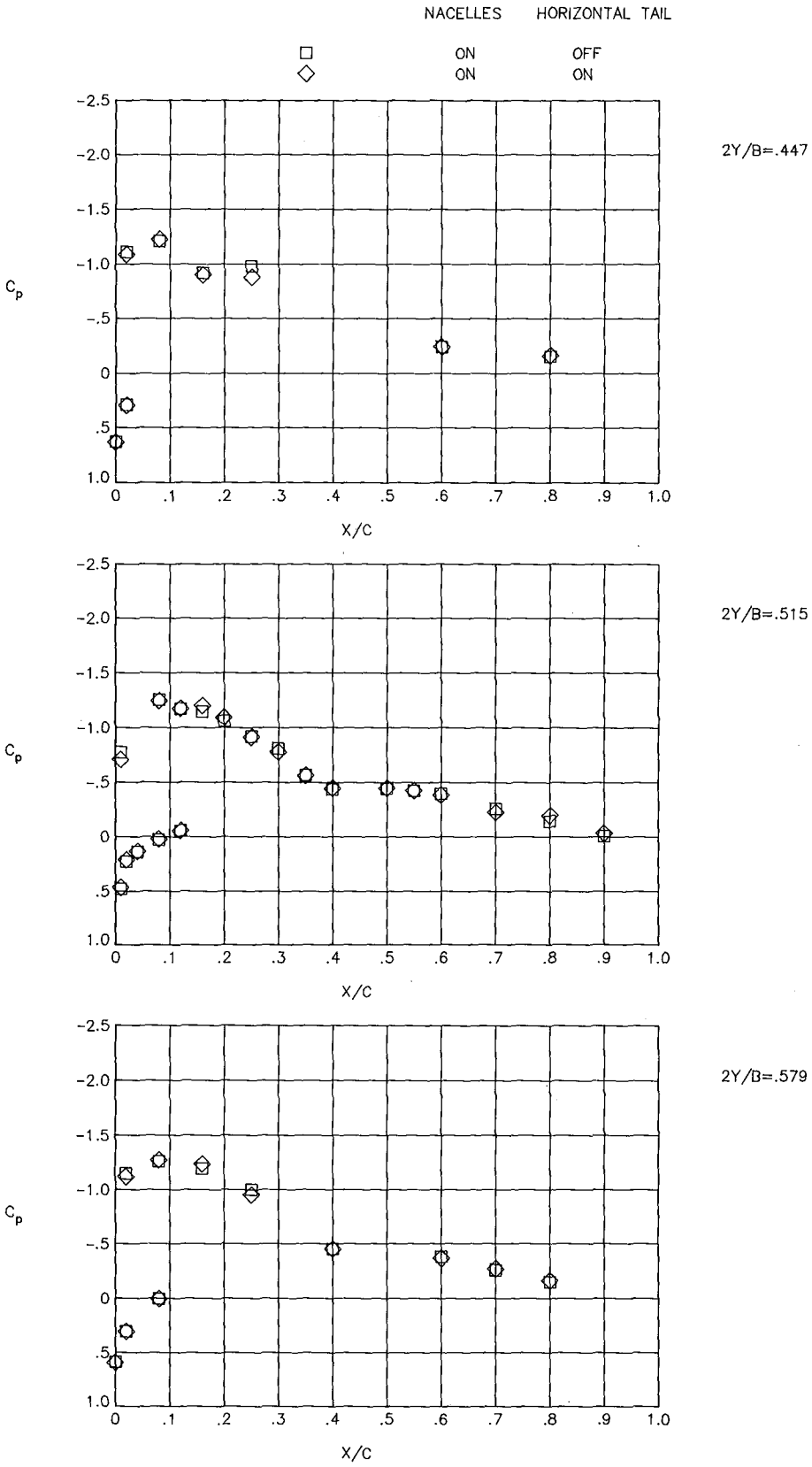

(c) α = 3.74.

Figure 20.- Continued.

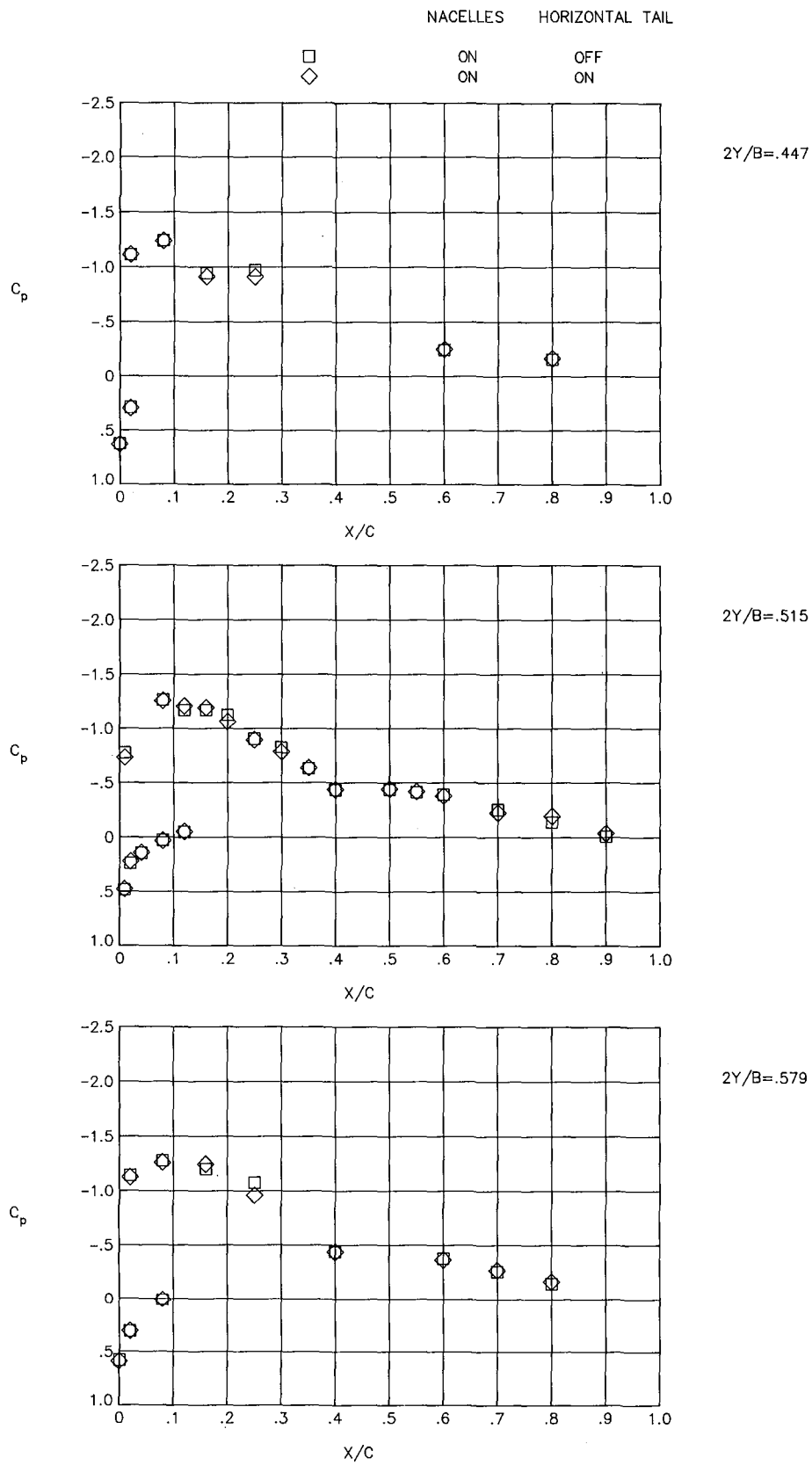

(d) α = 3.82.

Figure 20.- Continued.

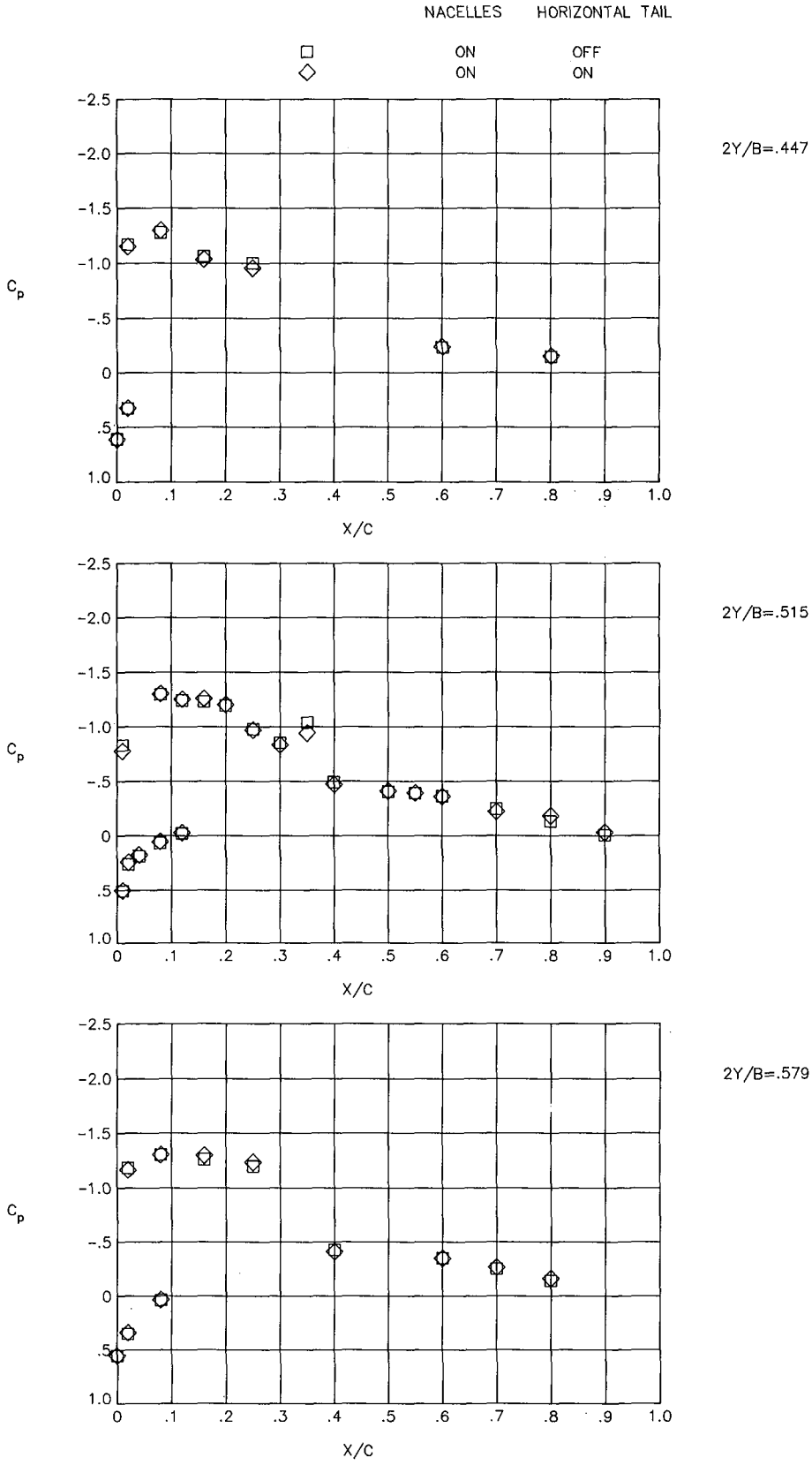

(e) α = 4.22.

Figure 20.- Continued.

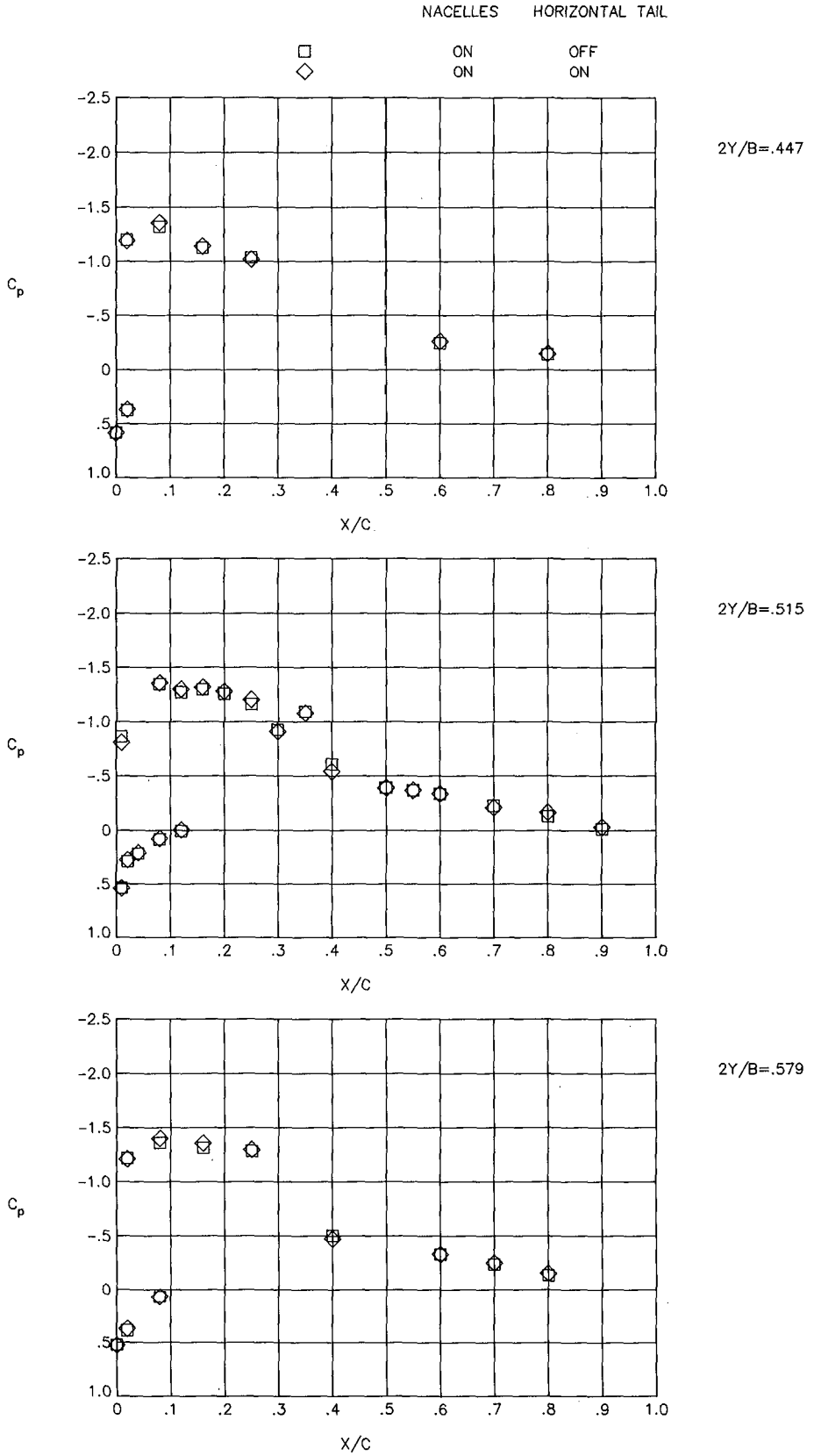

(f) α = 4.65.

Figure 20.- Concluded.

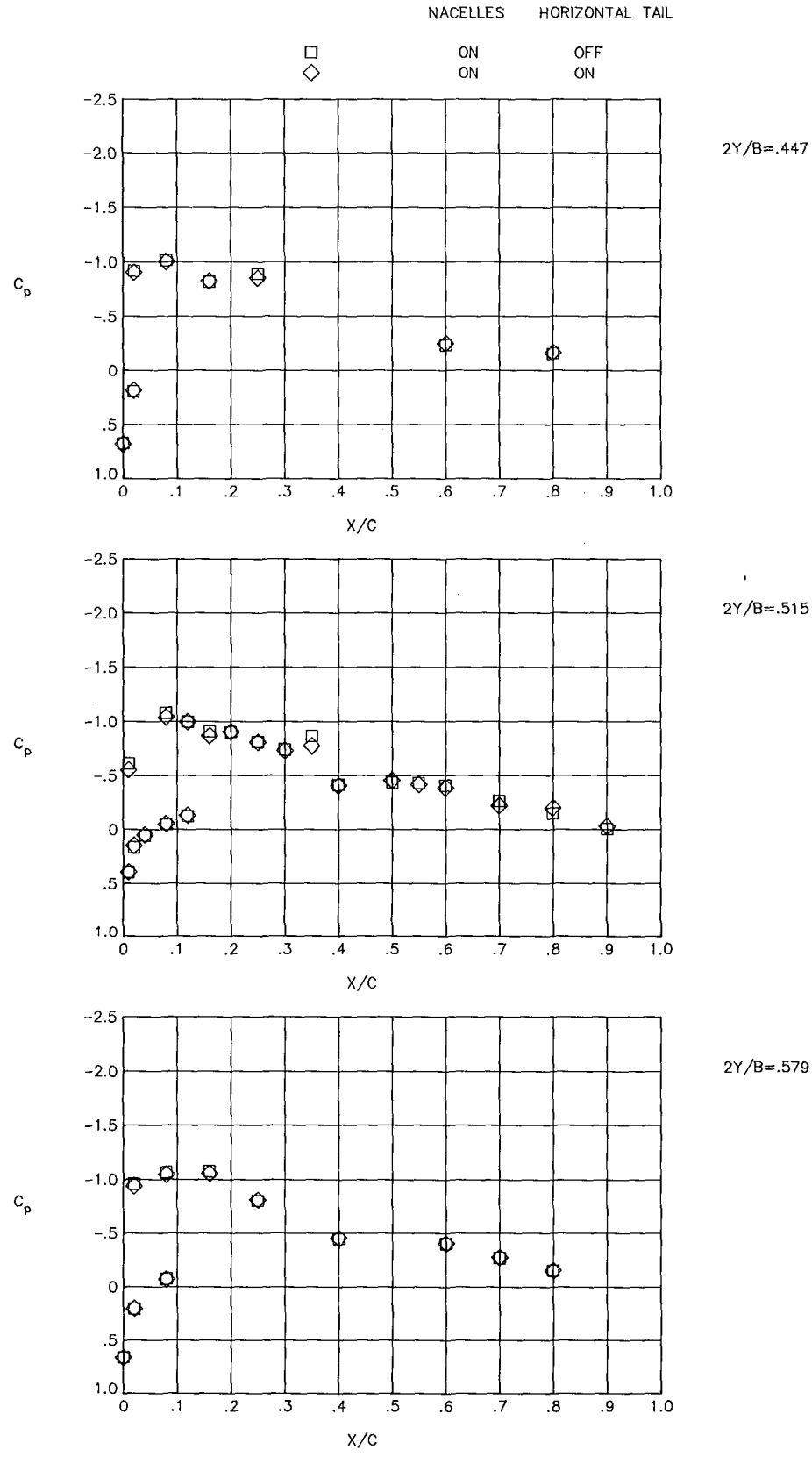

(a) α = 2.90.

Figure 21.- Effect of horizontal tail on wing pressure distributions at M = 0.82.

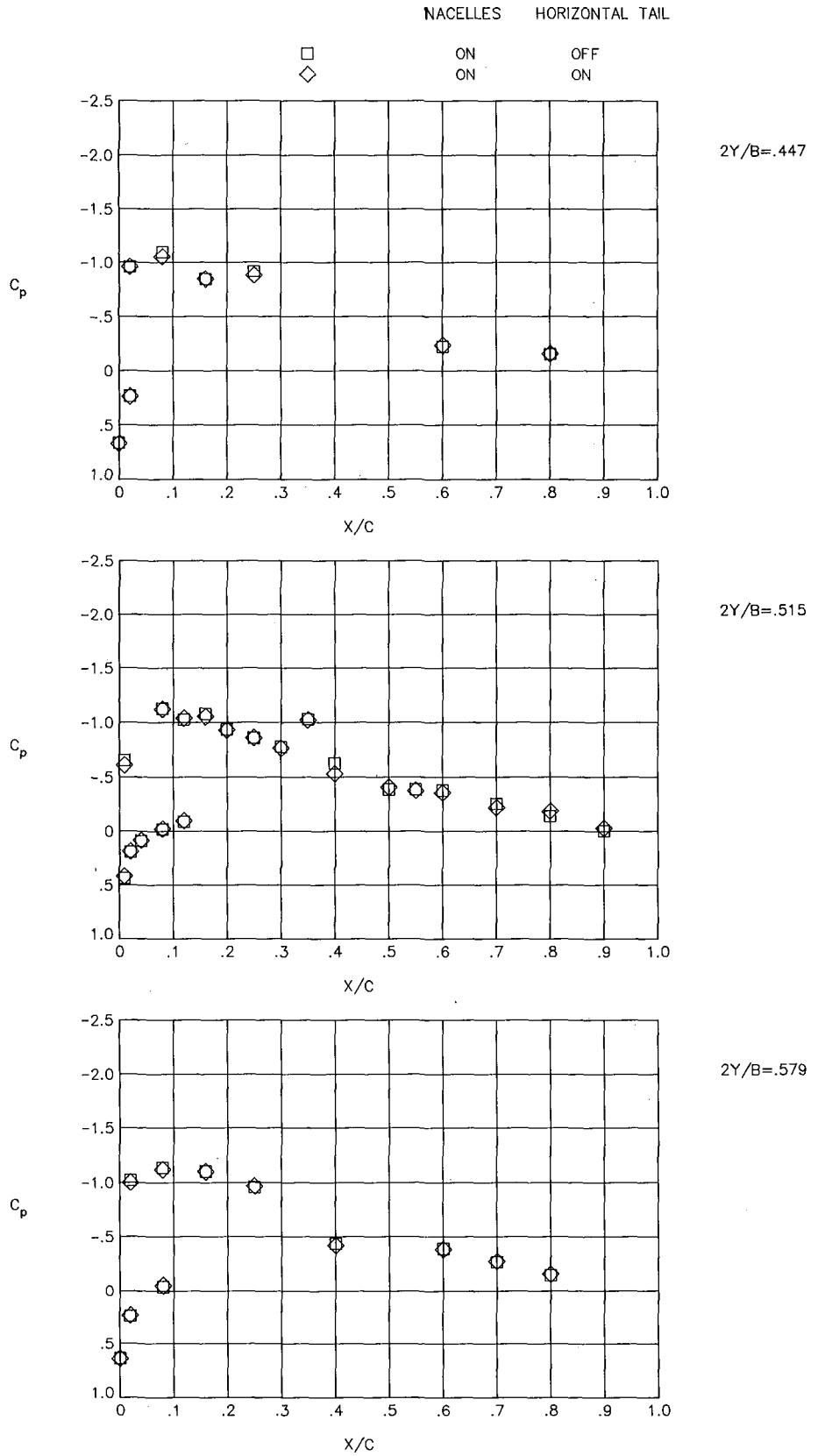

(b) α = 3.32.

Figure 21.- Continued.

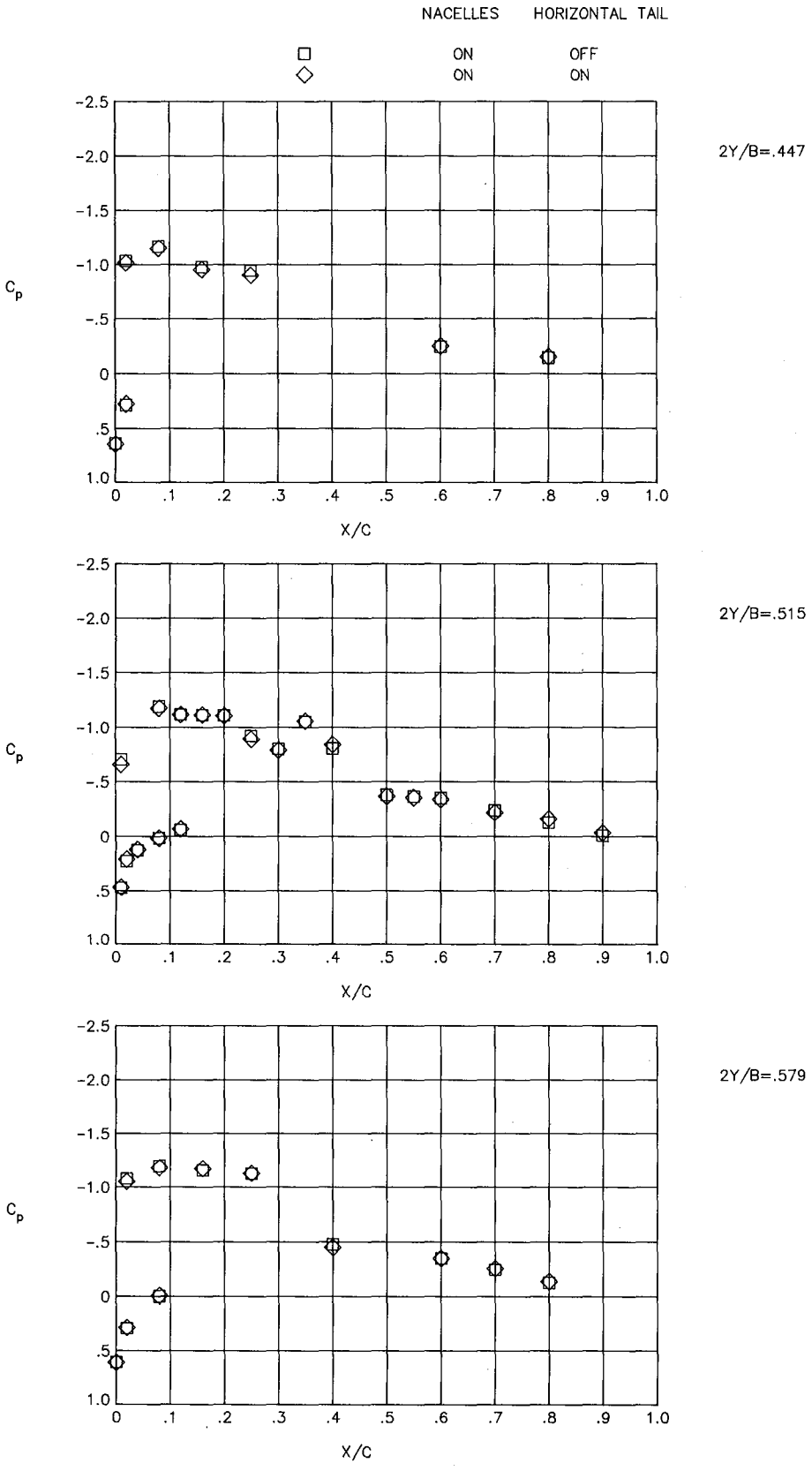

(c) α = 3.78.

Figure 21.- Continued.

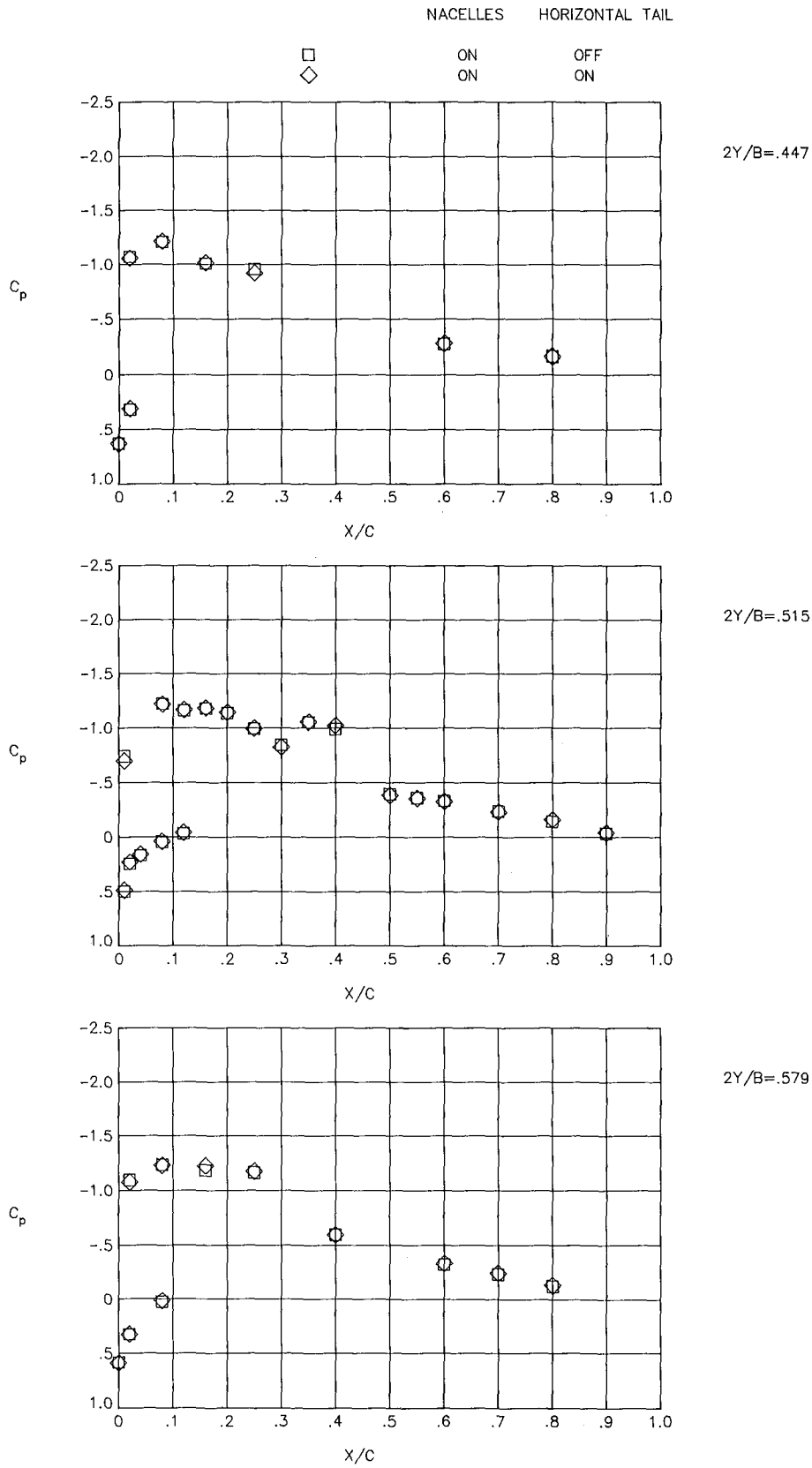

(d) α = 4.14.

Figure 21.- Continued.

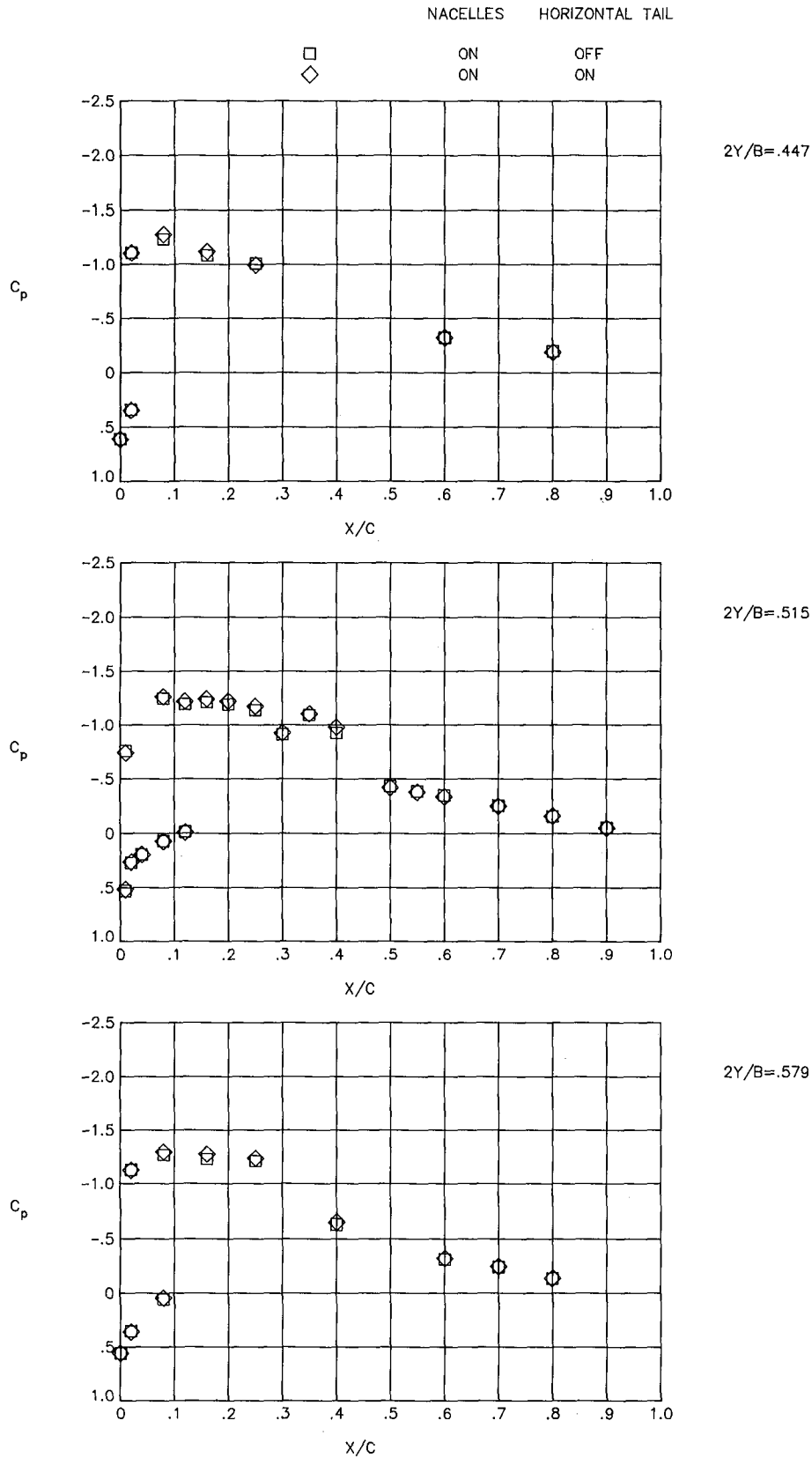

(e) α = 4.58.

Figure 21.- Concluded.

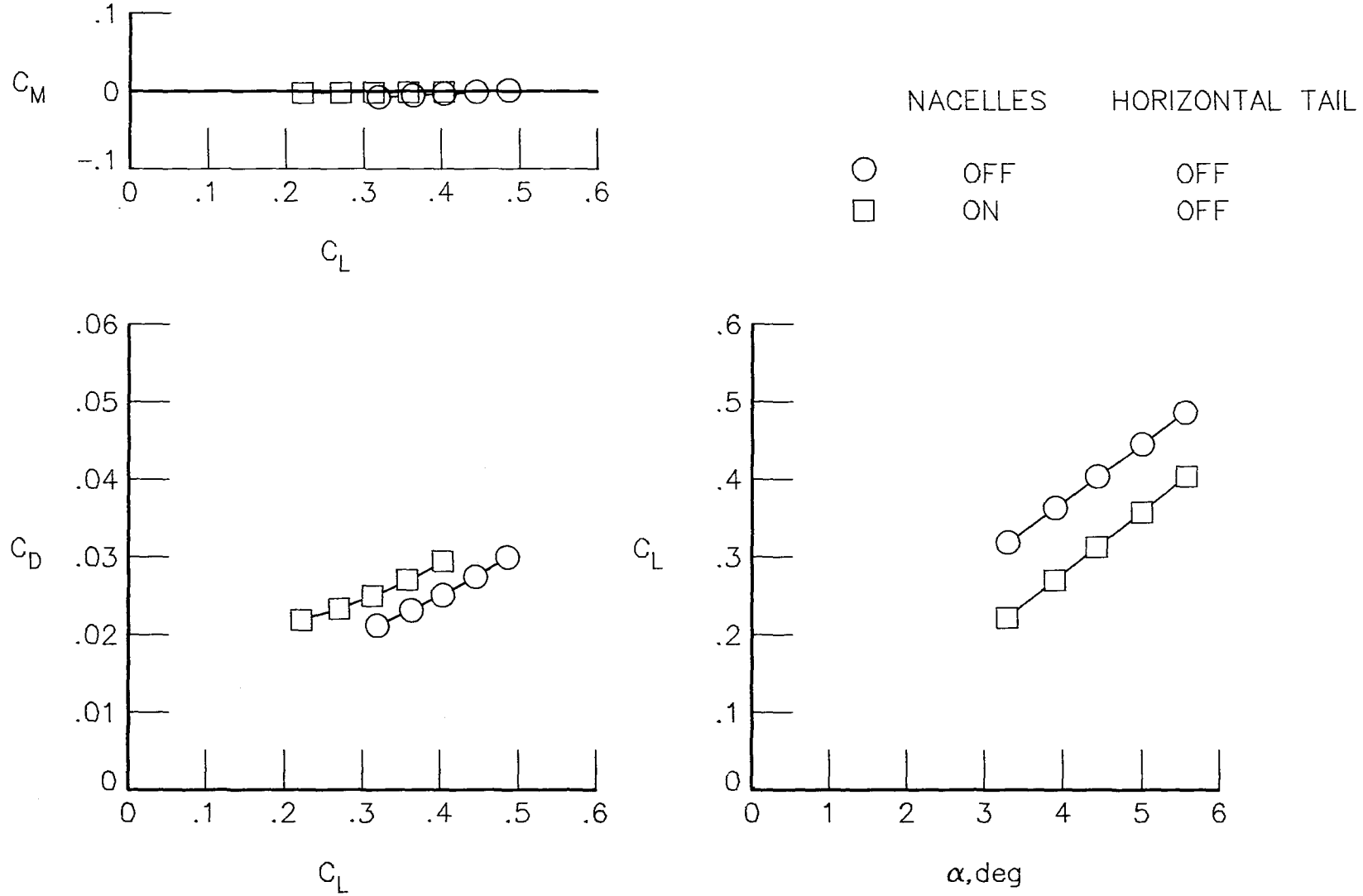

Figure 22.- Effect of nacelles on longitudinal aerodynamic characteristics at M = 0.40.

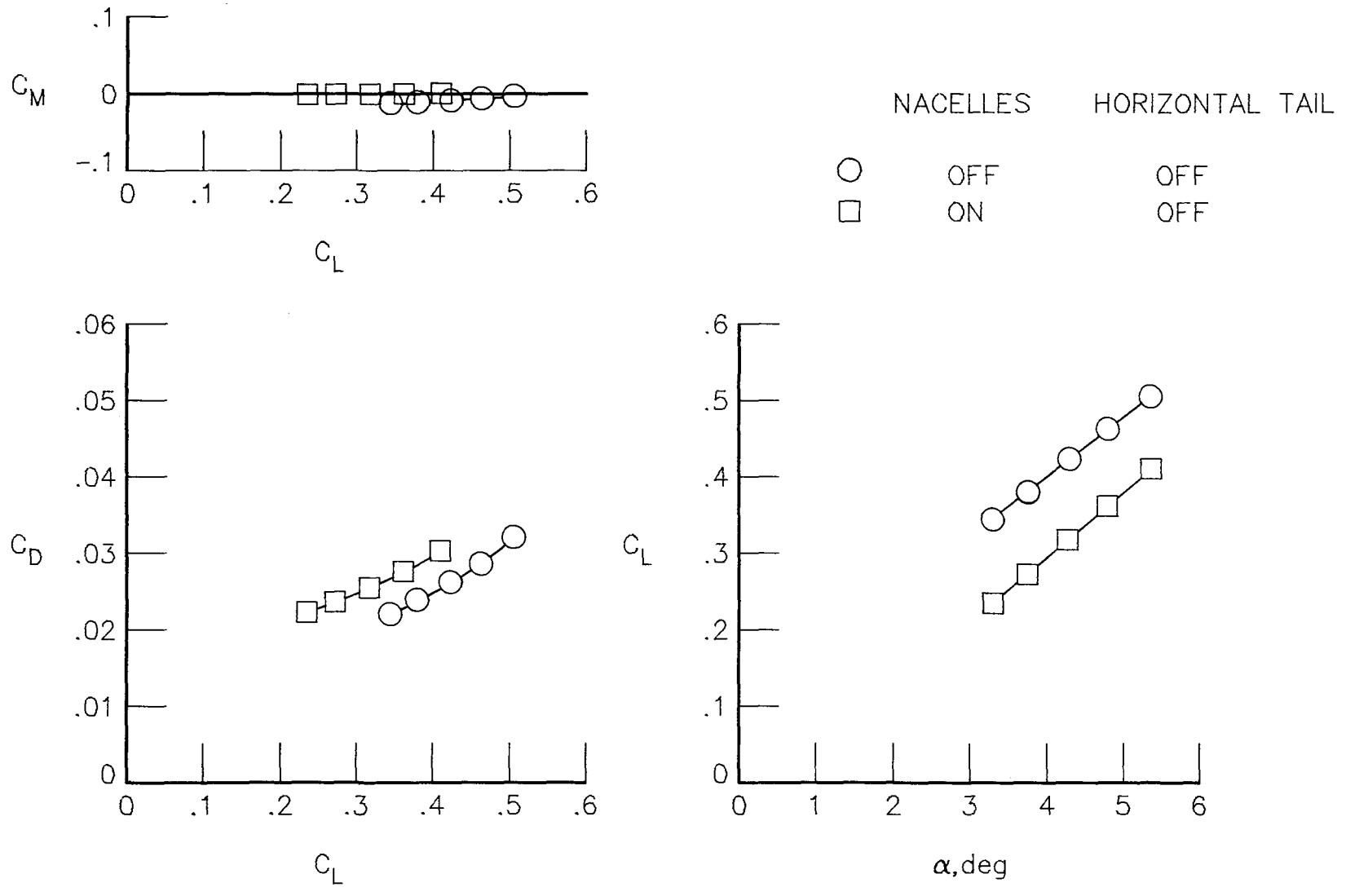

Figure 23.- Effect of nacelles on longitudinal aerodynamic characteristics at M = 0.60.

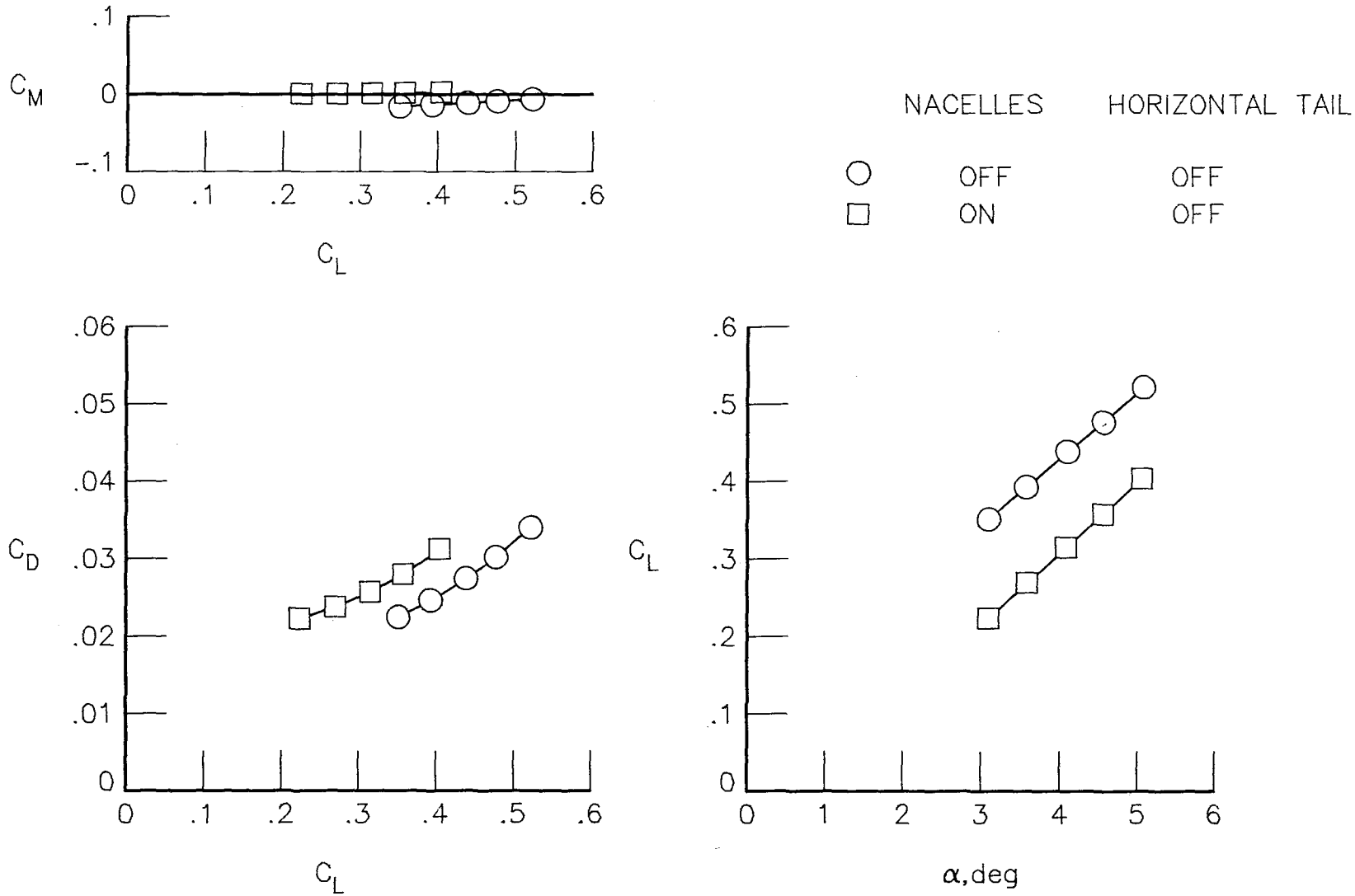

Figure 24.- Effect of nacelles on longitudinal aerodynamic characteristics at M = 0.70.

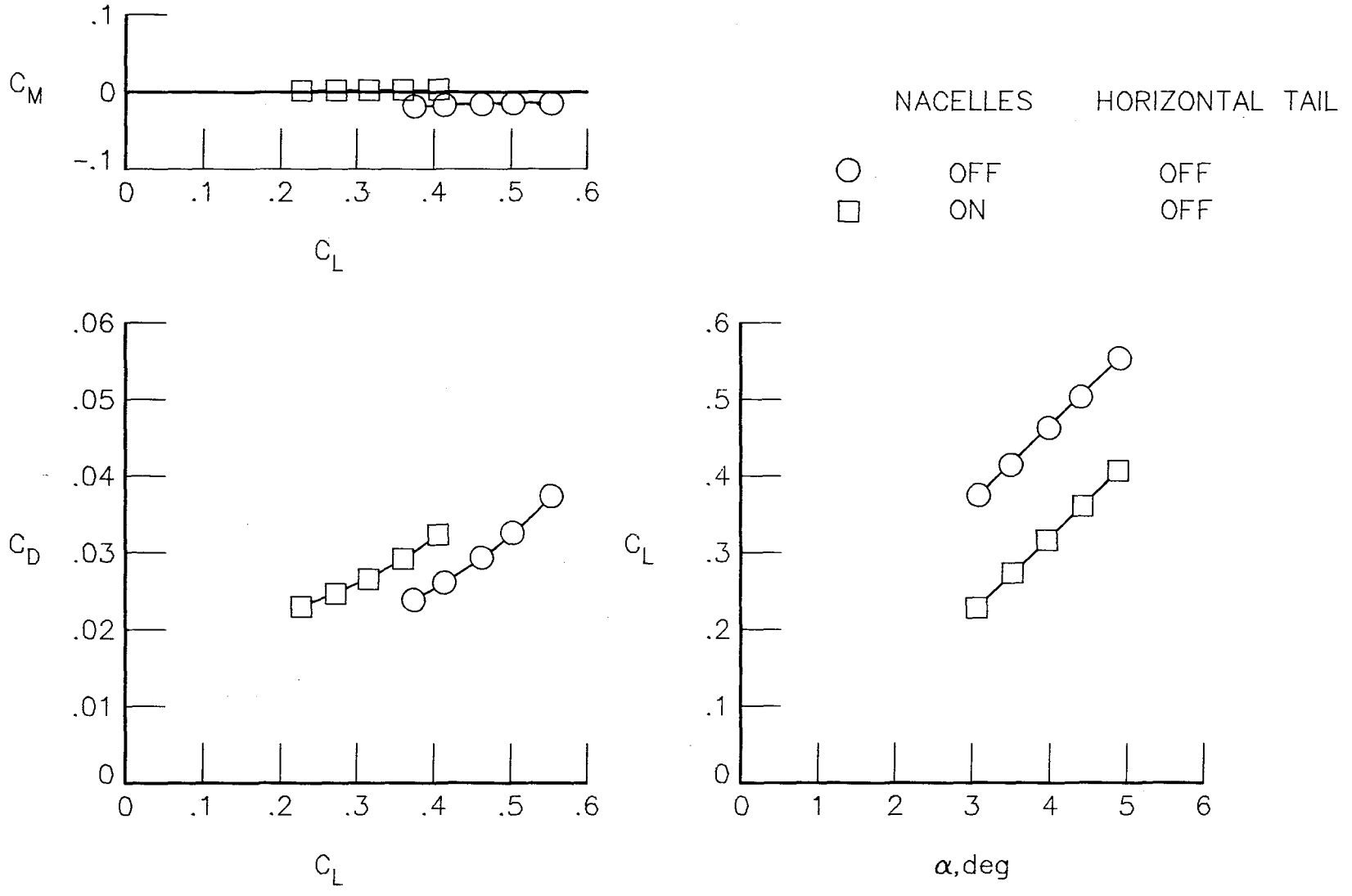

Figure 25.- Effect of nacelles on longitudinal aerodynamic characteristics at M = 0.75.

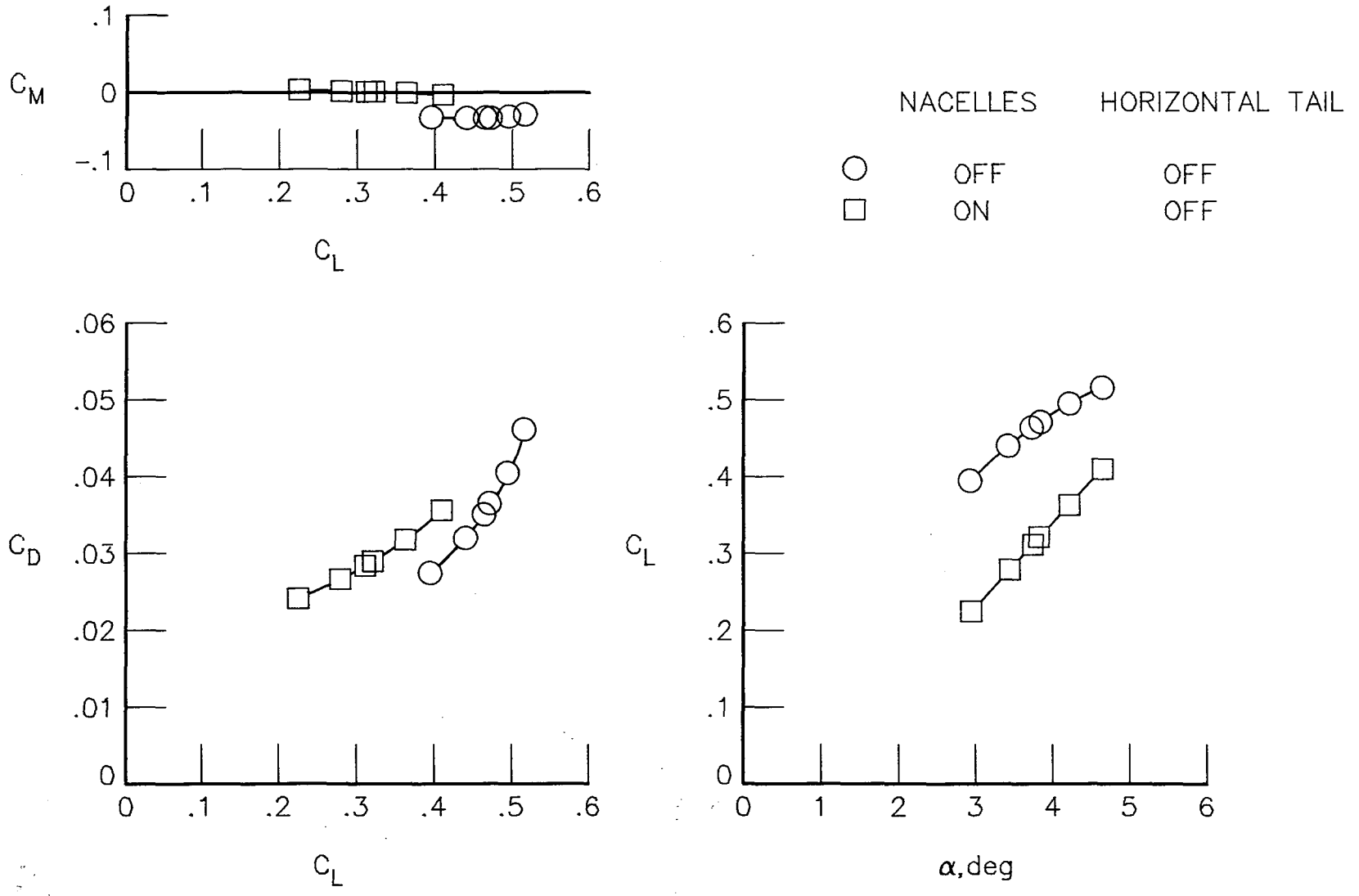

Figure 26.- Effect of nacelles on longitudinal aerodynamic characteristics at M = 0.80.

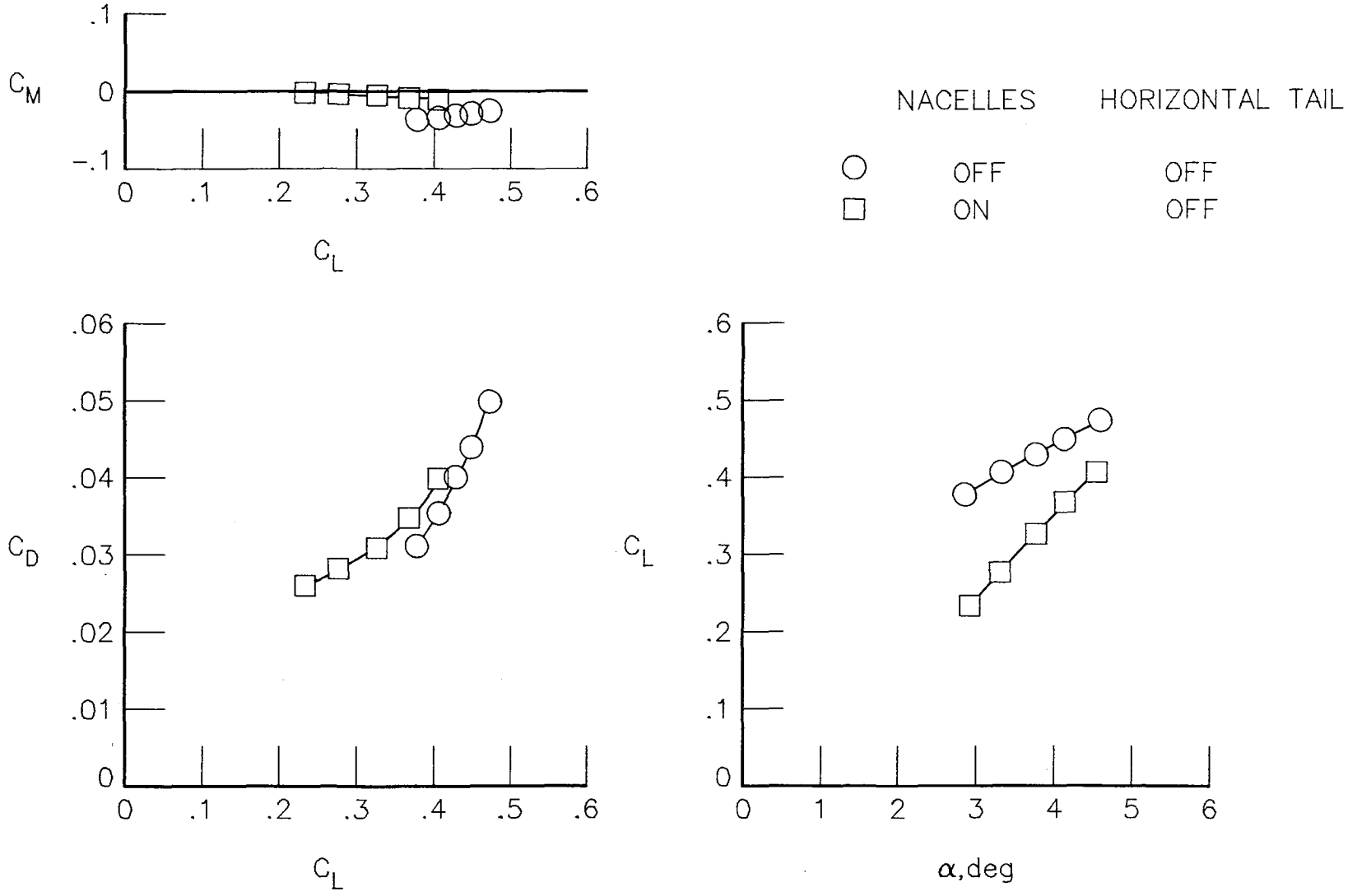

Figure 27.- Effect of nacelles on longitudinal aerodynamic characteristics at M = 0.82.

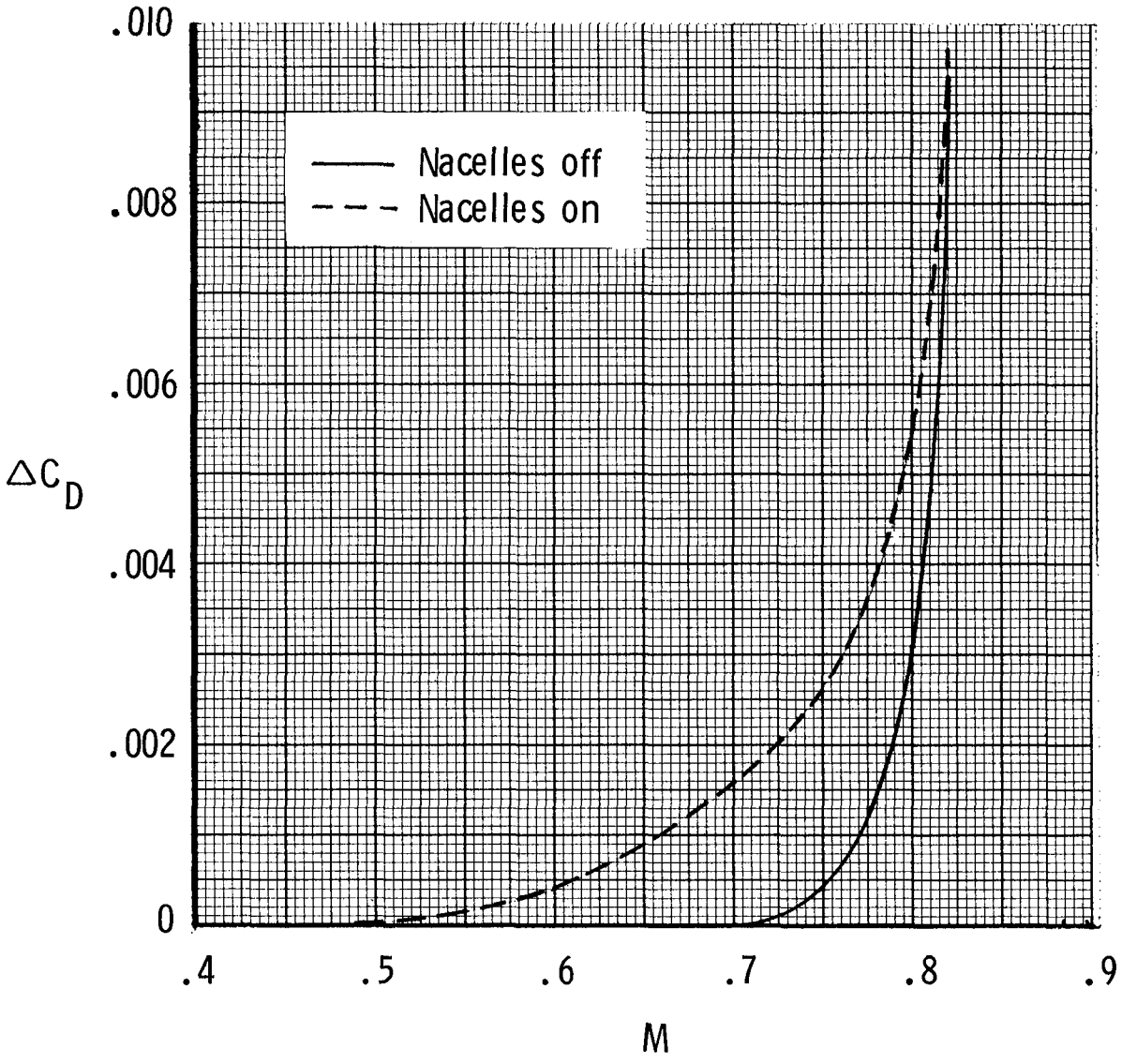

Figure 28.- Effect of nacelles on incremental drag as a function of Mach number $\left(\Delta C_D = C_D - C_D\big|_{M=0.40}\right)$ at $C_L \approx 0.4$ with horizontal tail off.

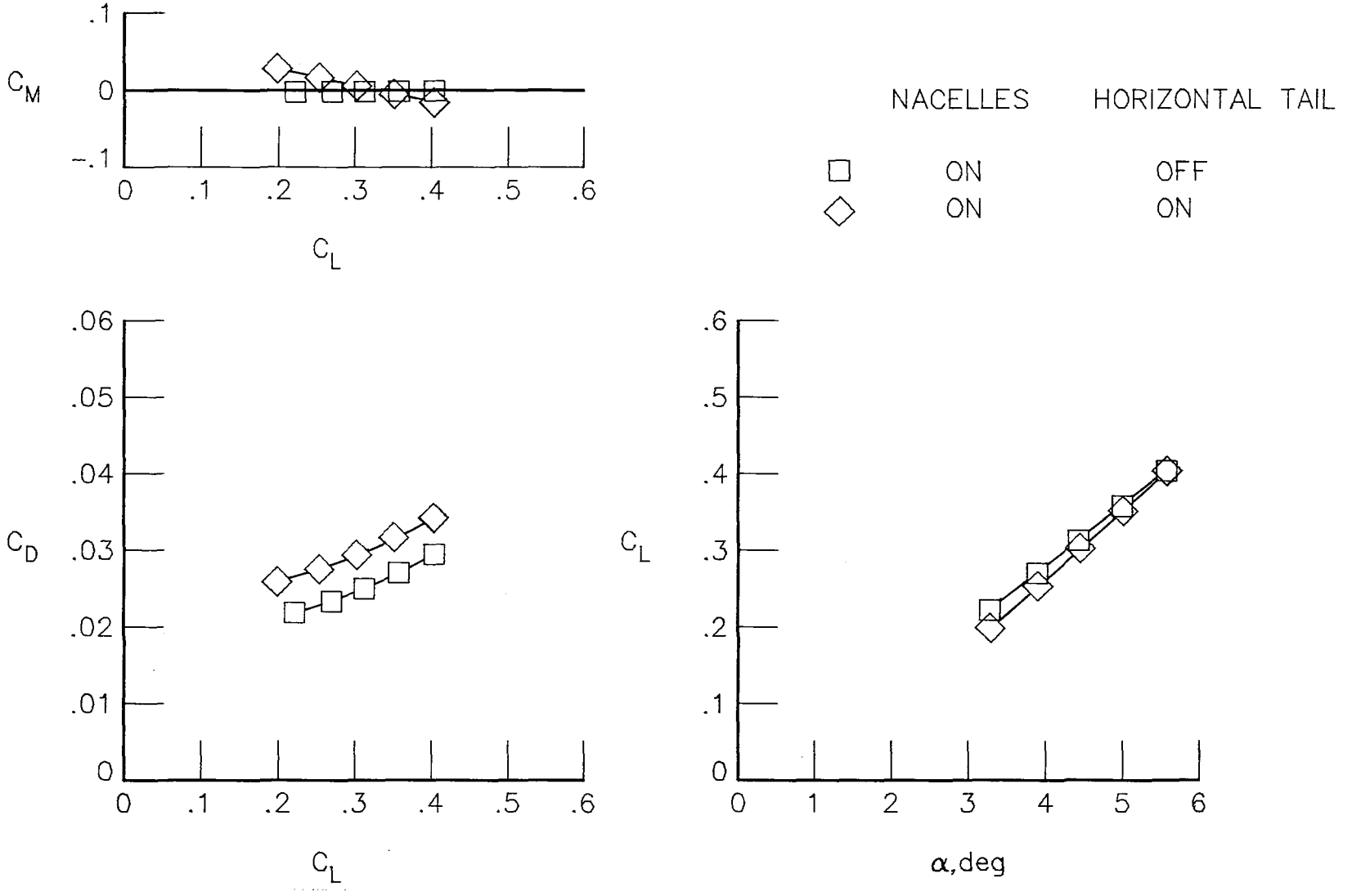

Figure 29.- Effect of horizontal tail on longitudinal aerodynamic characteristics at M = 0.40.

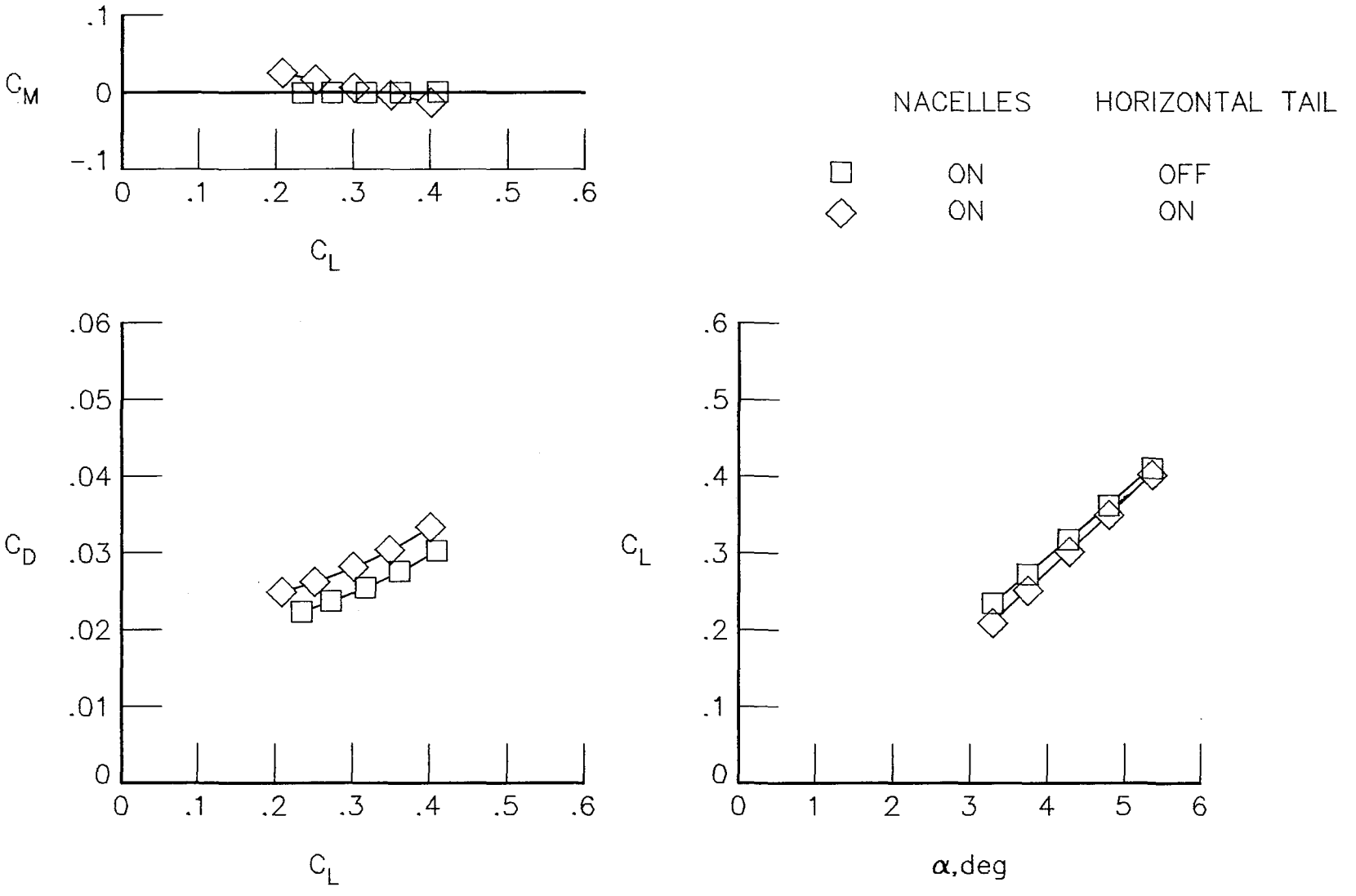

Figure 30.- Effect of horizontal tail on longitudinal aerodynamic characteristics at M = 0.60.

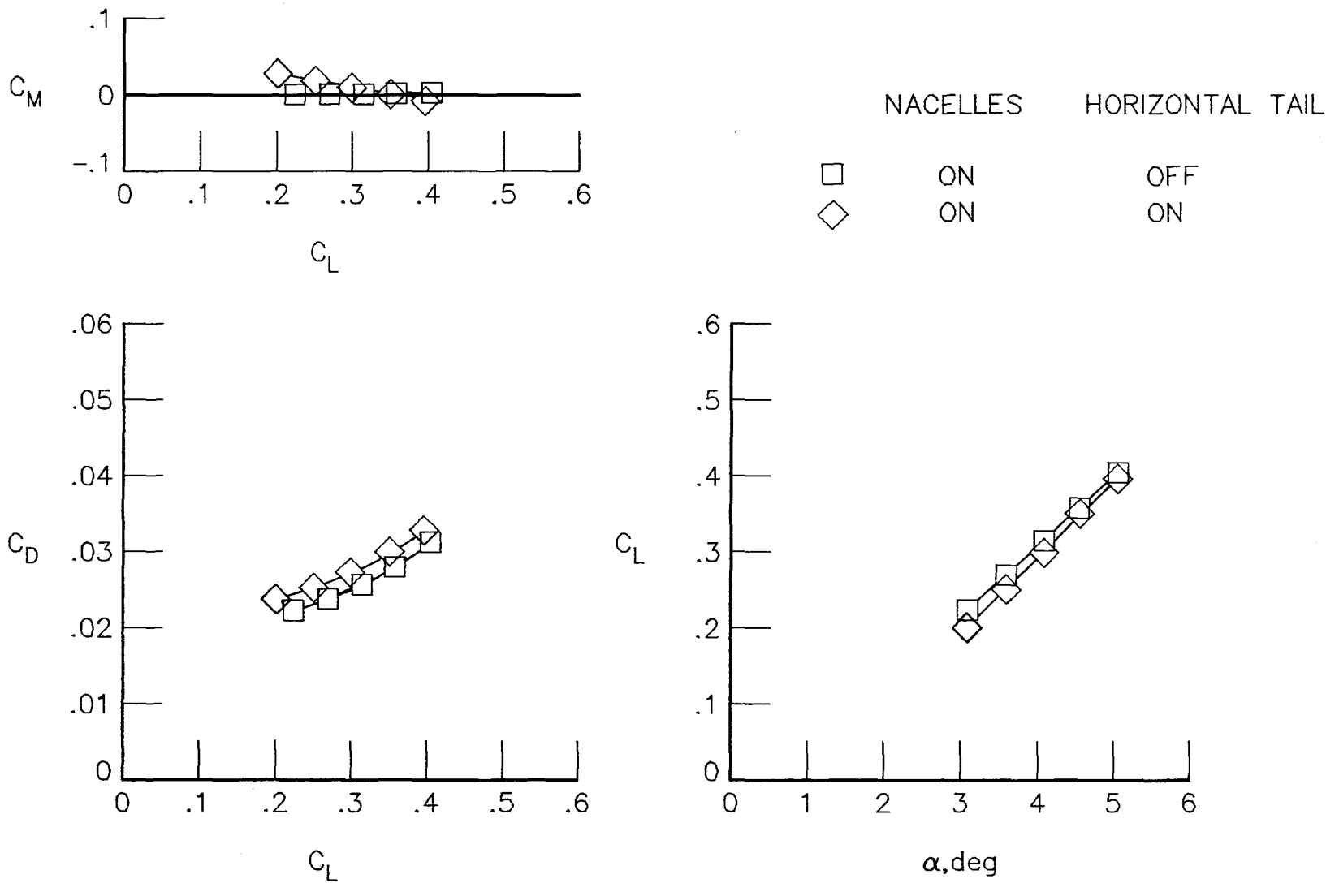

Figure 31.- Effect of horizontal tail on longitudinal aerodynamic characteristics at M = 0.70.

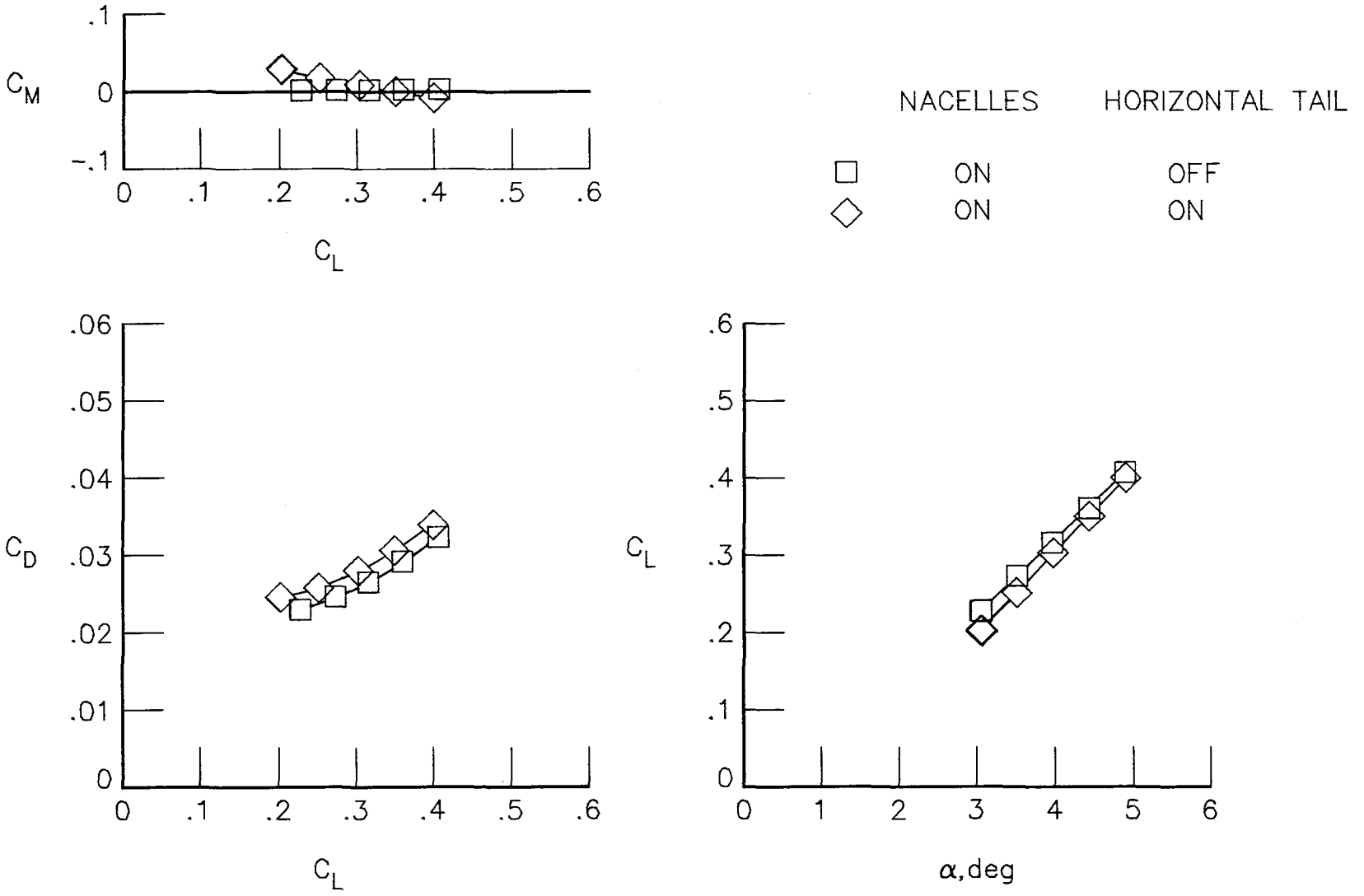

Figure 32.- Effect of horizontal tail on longitudinal aerodynamic characteristics at M = 0.75.

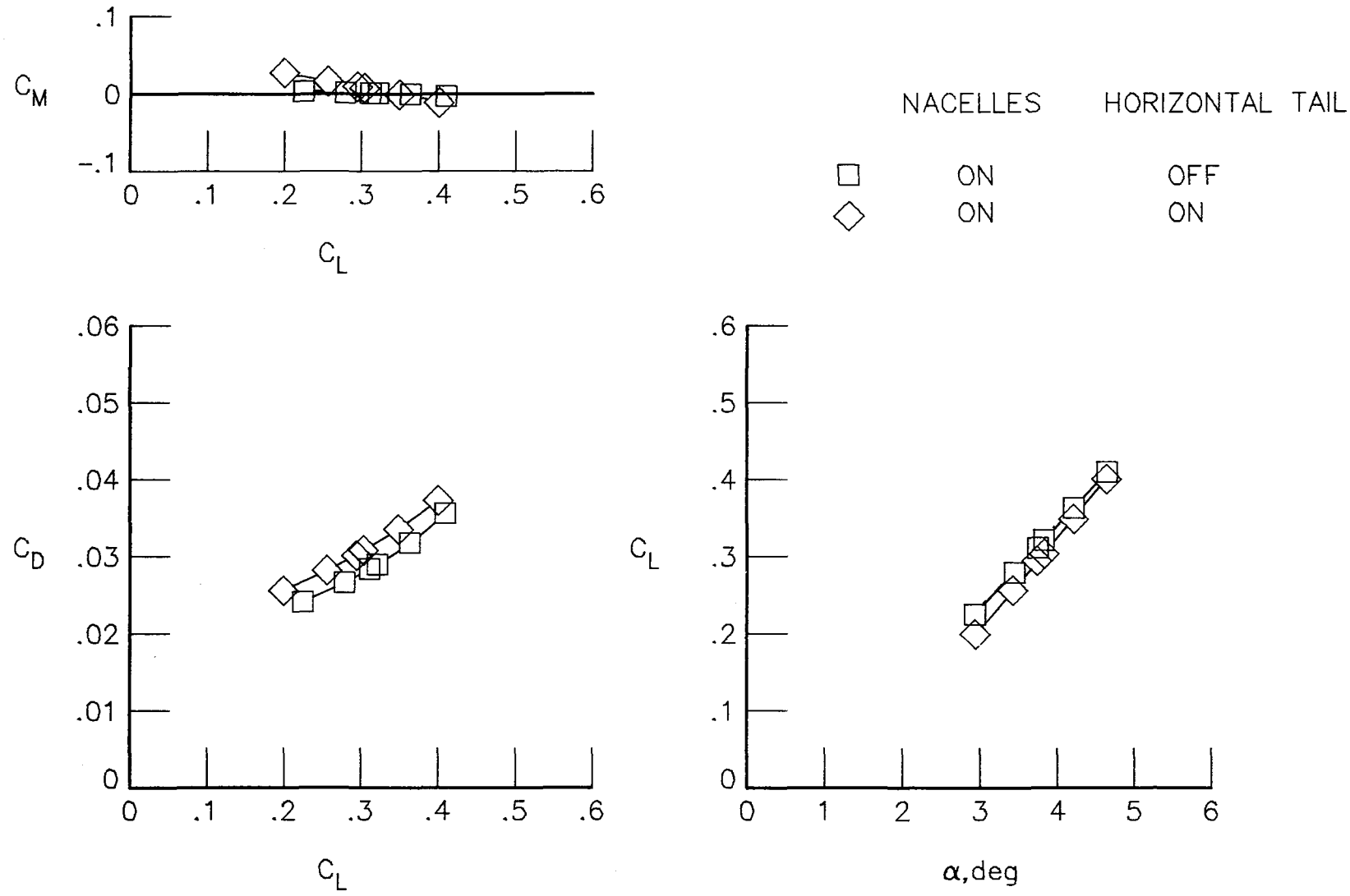

Figure 33.- Effect of horizontal tail on longitudinal aerodynamic characteristics at M = 0.80.

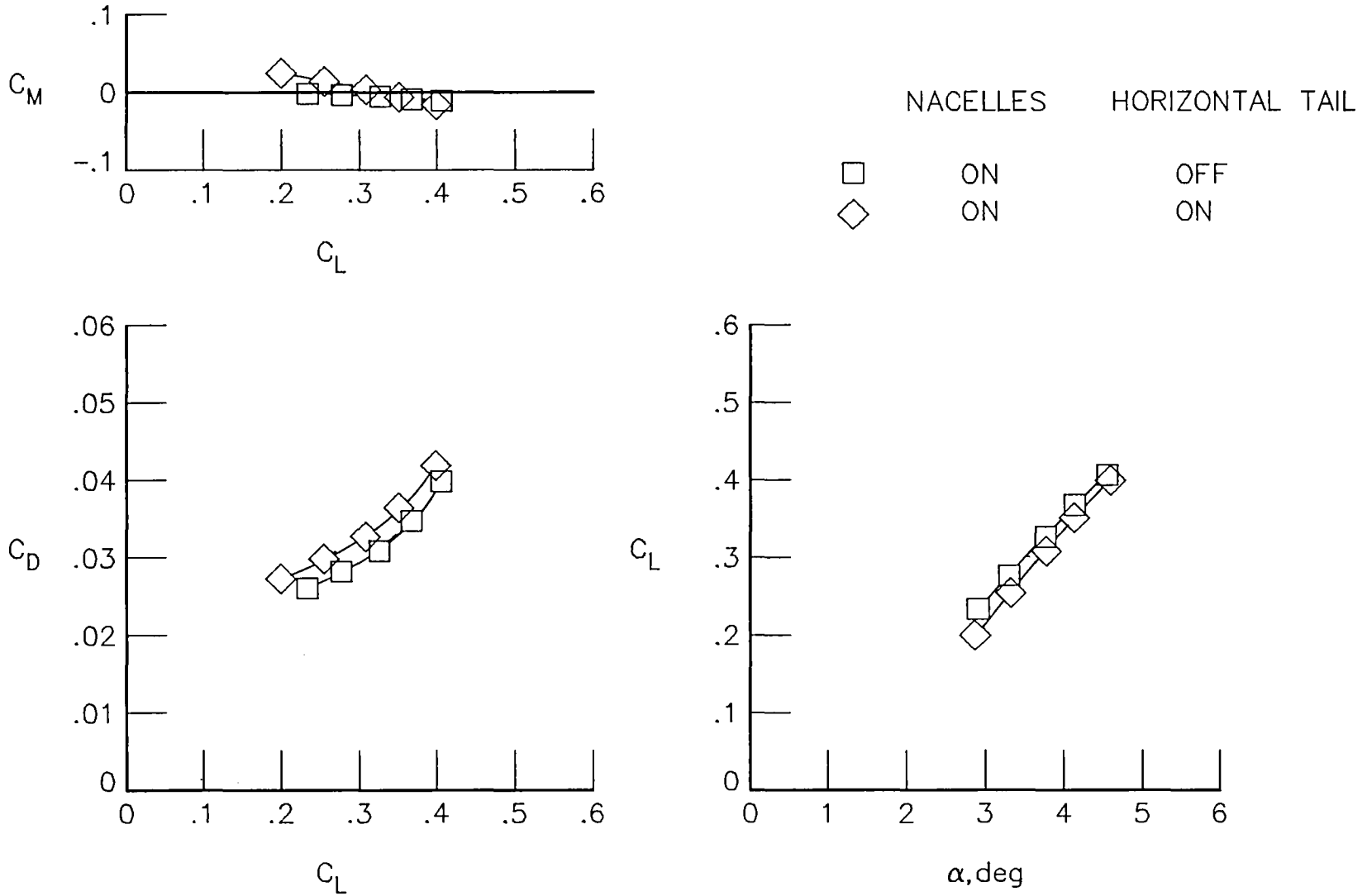

Figure 34.- Effect of horizontal tail on longitudinal aerodynamic characteristics at M = 0.82.

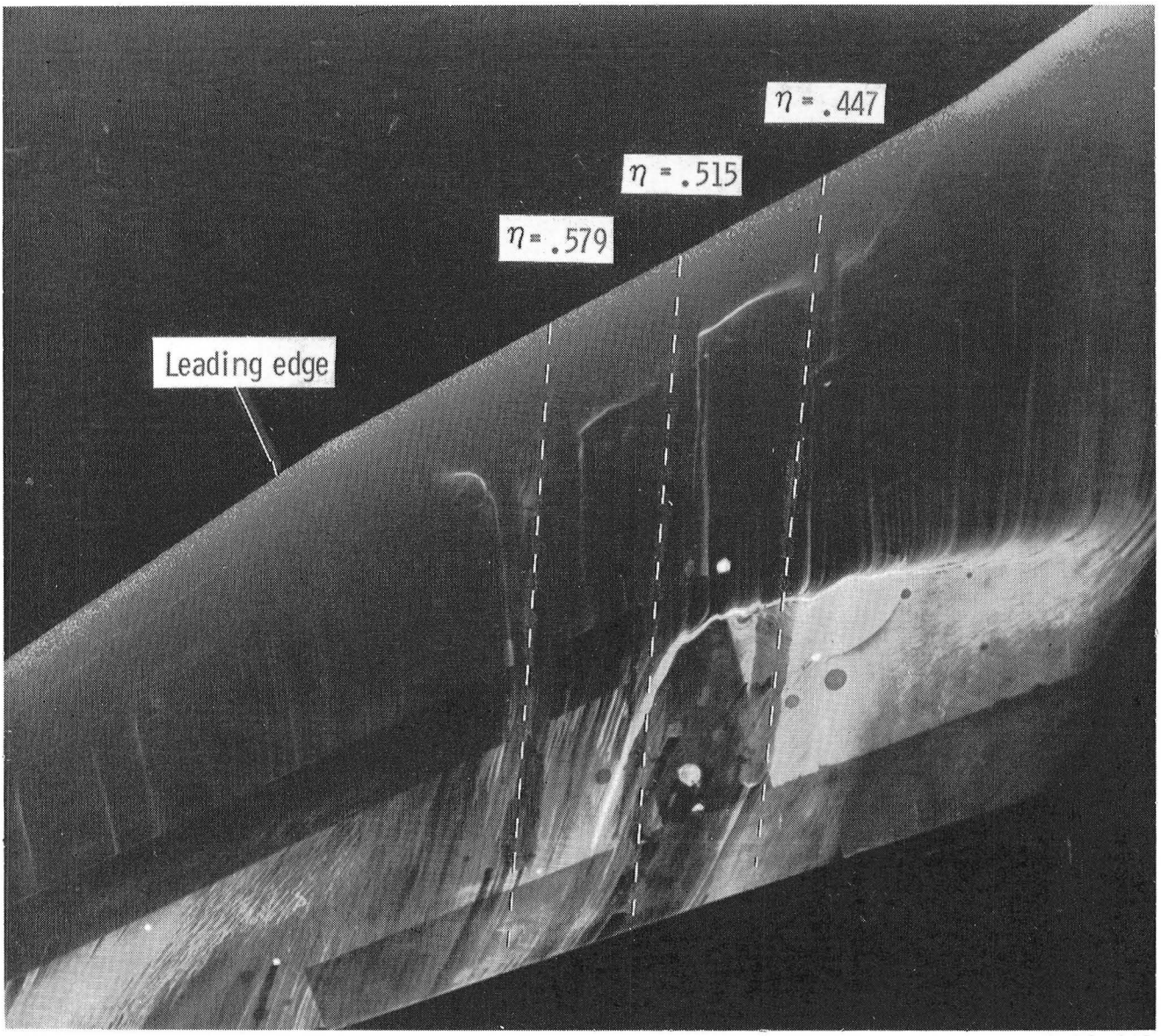

L-82-119

(a) Nacelles off.

Figure 35.- Wing oil-flow photographs of effect of nacelles at $M = 0.80$ and $\alpha = 2.9°$.

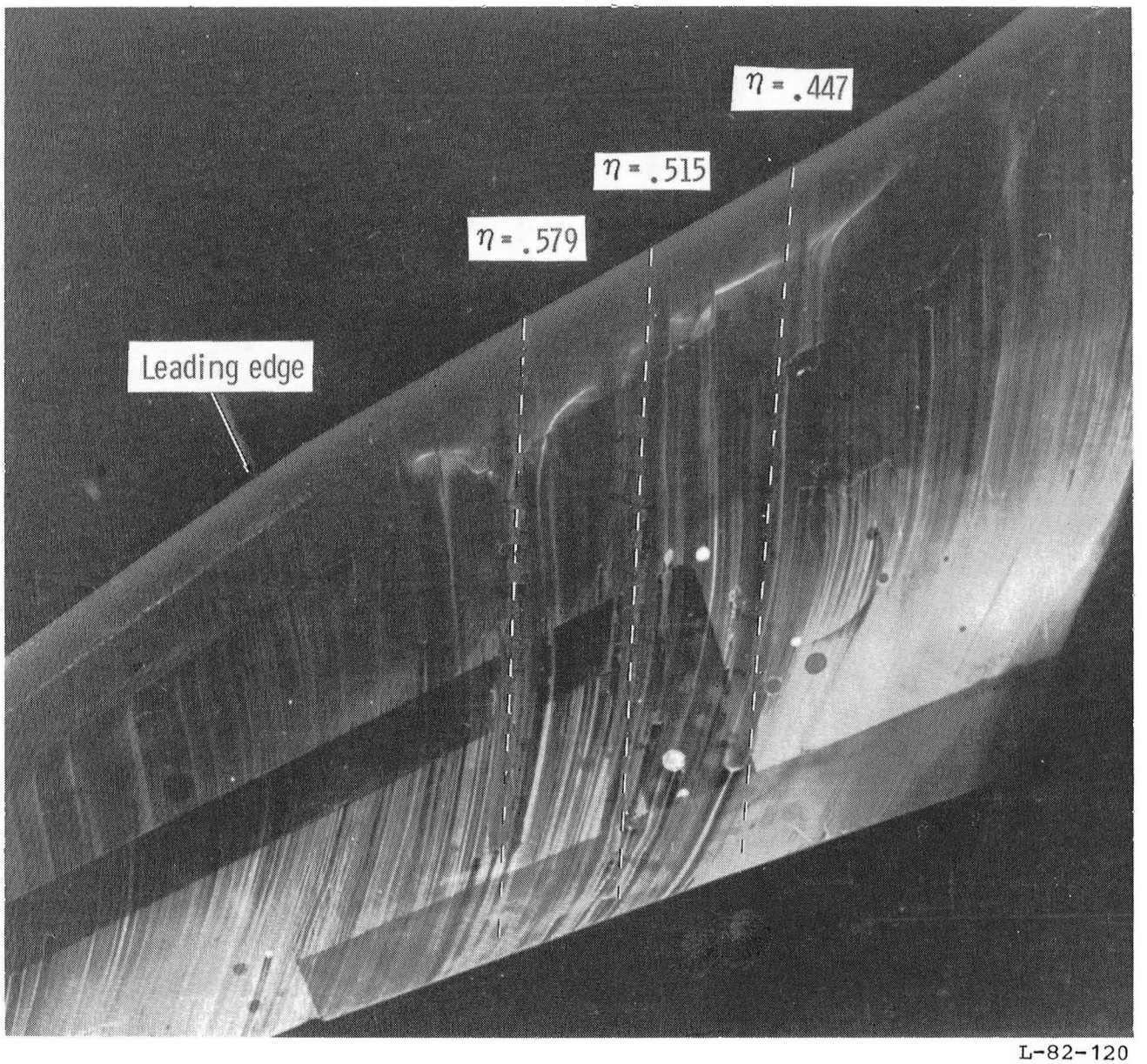

L-82-120

(b) Nacelles on.

Figure 35.- Concluded.

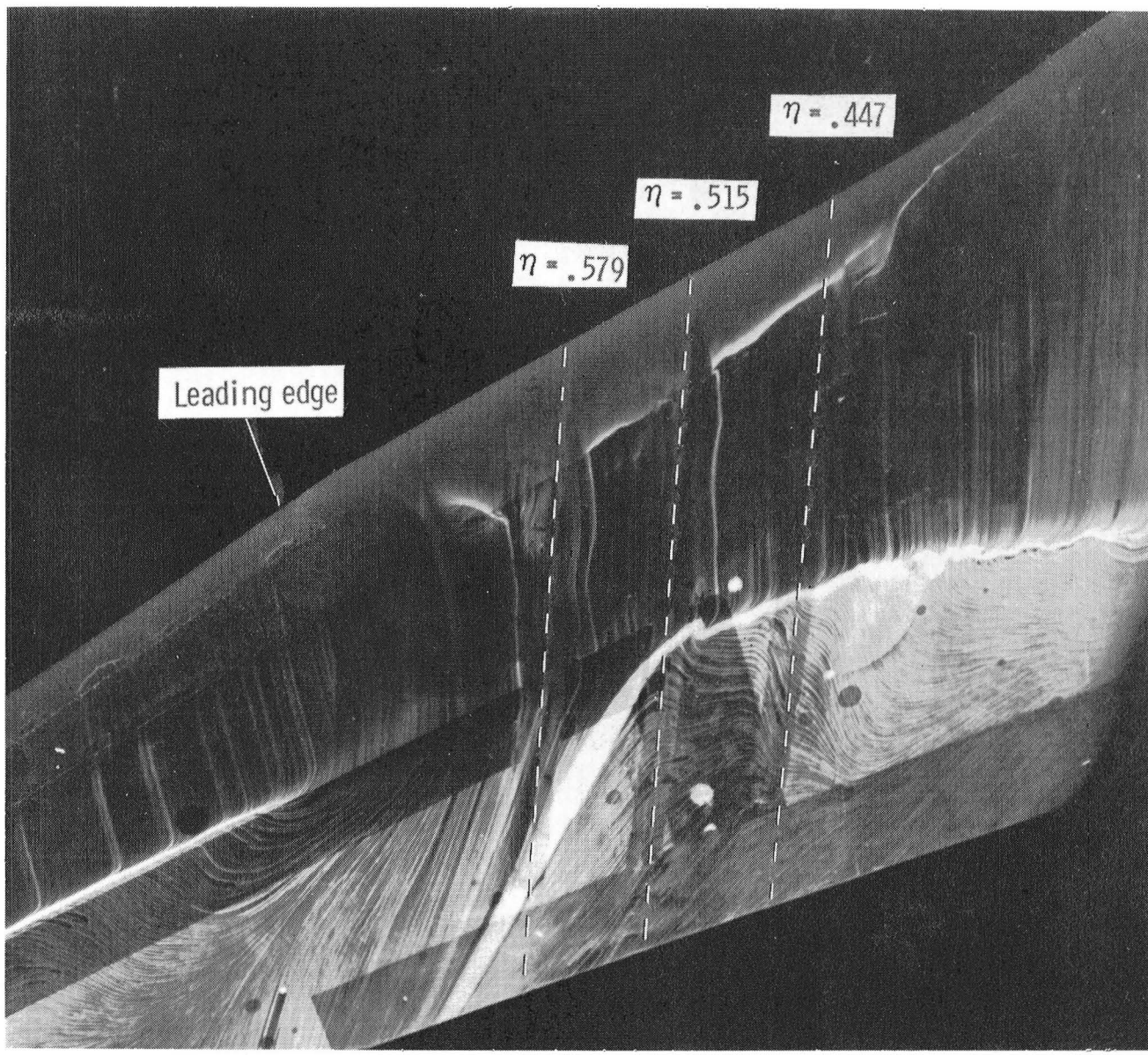

L-82-121

(a) Nacelles off.

Figure 36.- Wing oil-flow photographs of effect of nacelles at $M = 0.80$ and $\alpha = 3.8°$.

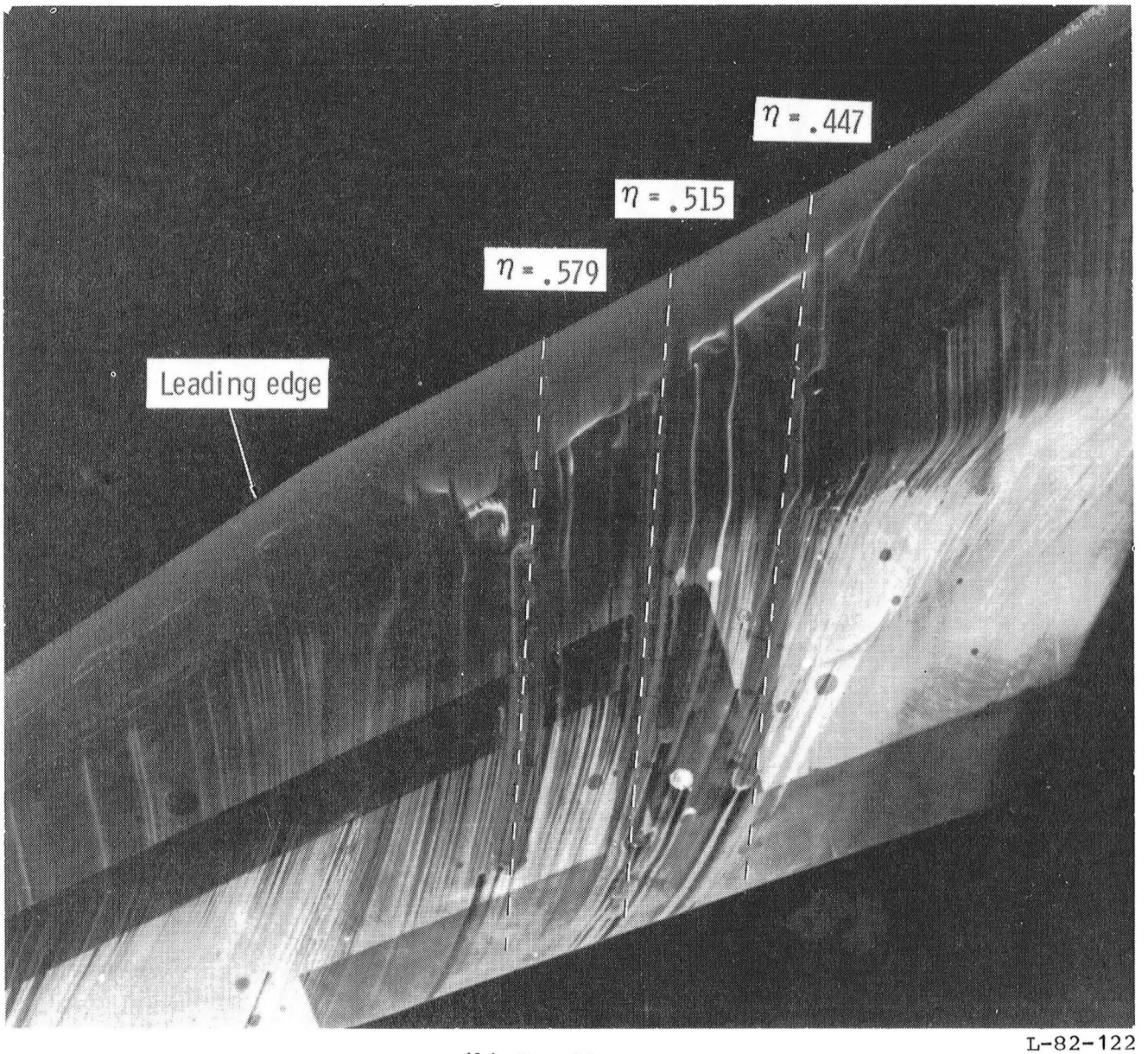

L-82-122

(b) Nacelles on.

Figure 36.- Concluded.

1. Report No.	2. Government Accession No.	3. Recipient's Catalog No.
NASA TM-83271		

4. Title and Subtitle	5. Report Date
EFFECT OF NACELLES ON AERODYNAMIC CHARACTERISTICS OF AN EXECUTIVE-JET MODEL WITH SIMULATED, PARTIAL-CHORD, LAMINAR-FLOW-CONTROL WING GLOVE	April 1982
	6. Performing Organization Code: 505-31-43-03

7. Author(s)	8. Performing Organization Report No.
Richard L. Campbell	L-14982
	10. Work Unit No.

9. Performing Organization Name and Address	11. Contract or Grant No.
NASA Langley Research Center Hampton, VA 23665	

12. Sponsoring Agency Name and Address	13. Type of Report and Period Covered
National Aeronautics and Space Administration Washington, DC 20546	Technical Memorandum
	14. Sponsoring Agency Code

15. Supplementary Notes

16. Abstract

Tests were conducted in the Langley High-Speed 7- by 10-Foot Tunnel using a 1/10-scale model of an executive jet to examine the effects of the nacelles on the wing pressures and model longitudinal aerodynamic characteristics. For the present investigation, each wing panel was modified with a simulated, partial-chord, laminar-flow-control glove. Horizontal-tail effects were also briefly examined. The tests covered a range of Mach numbers from 0.40 to 0.82 and lift coefficients from 0.20 to 0.55. Oil-flow photographs of the wing at selected conditions are included.

17. Key Words (Suggested by Author(s))	18. Distribution Statement
Laminar flow control Engine nacelles Transonic flow Executive jet Wing glove	Unclassified - Unlimited Subject Category 02

19. Security Classif. (of this report)	20. Security Classif. (of this page)	21. No. of Pages	22. Price
Unclassified	Unclassified	103	A06

For sale by the National Technical Information Service, Springfield, Virginia 22161

NASA-Langley, 1982

National Aeronautics and
Space Administration

Washington, D.C.
20546

Official Business
Penalty for Private Use, $300

THIRD-CLASS BULK RATE

Postage and Fees Paid
National Aeronautics and
Space Administration
NASA-451

NASA

POSTMASTER: If Undeliverable (Section 158
Postal Manual) Do Not Return